Syracuse University

SURFACE

Dissertations - ALL

5-30-2014

Effect of Confinement and Temperature on the Behavior of EPS Geofoam

Amsalu Birhan
Syracuse University

Follow this and additional works at: https://surface.syr.edu/etd

Part of the Engineering Commons

Recommended Citation

ABSTRACT

  EPS geofoam blocks underlying compacted soil and structural loads become subjected to multi-axial loading. Effects of confining pressure on the stress-strain behavior of EPS geofoam have been investigated in previous studies. Some studies found increases in confining stress lead to corresponding decreases in both modulus and compressive strength. Increasing confining stress has also been reported to result in higher compressive strength. Regardless of the sense and attributed significance of the effects of confinement on EPS geofoam behavior, the implied effects on performance are generally not considered in practice. A series of triaxial compression tests were conducted on EPS geofoams of different densities over a range of confining pressures. Results from the investigation indicate increases in confinement lead to decrease in yield stress and post yield compressive resistances, depending on the EPS density and range of confining pressures. The practical significances of confining stress effects are discussed. An approach for incorporating the more significant effects of confining stress on EPS geofoam behavior is considered.

  Evaluations of EPS-soil-structure interactions require reasonable representation of stress-strain relationships for numerical modeling. A method proposed in this work uses density of geofoam block and resin material properties to represent the stress-strain response of EPS geofoam. The stress-strain curves obtained from such representation are compared with results from laboratory tests and models by others. The stress-strain curves generated by the proposed method predict very well the relations especially for denser geofoams. A modified hyperbolic stress-strain relationships that can account for confining

stress effects is also proposed. The modified hyperbolic model only requires three parameters that can be obtained from triaxial tests. Prediction accuracy of this model is compared with data from triaxial tests which were not part of data sets used to obtain model parameters. Comparison is made with other models proposed by different authors and the stress-strain relationships obtained by this approach predict test data well.

Characteristics of inherent and stress induced anisotropy of EPS geofoam was investigated by triaxial tests conducted on pre-stressed EPS geofoam. Induced anisotropy was observed to reduce the modulus significantly.

A series of creep tests were performed on different densities of EPS geofoam with and without confining pressures. The results showed confining pressures can significantly affect the creep responses of EPS geofoam. Effects of confining pressures on creep deformations were more pronounced for lower densities.

Creep tests were performed in a temperature controlled chamber to evaluate effects of cyclic temperatures. Coupled effects of temperature and creep were studied for different stress levels. Comparisons were made to actual field observations and FLAC model results. Strains and induced stresses from seasonal temperature variations were relatively small.

EFFECT OF CONFINEMENT AND TEMPERATURE ON THE BEHAVIOR OF EPS GEOFOAM

by

Amsalu Birhan

B.Sc., Addis Ababa University, 2000

M.Sc., Addis Ababa University, 2005

Dissertation

Submitted in partial fulfillment of the requirements for the degree of

Doctor of Philosophy in Civil Engineering

Syracuse University

May 2014

ACKNOWLEGEMENT

TABLE OF CONTENTS

vi

LIST OF FIGURES

LIST OF TABLES

LIST OF SYMBOLS

ε_a Axial strain

σ_{c10} Axial stress at 10 % axial strain

σ_c or σ_3 Confining stress

ρ Density of EPS geofoam

$\Delta\sigma_{c10}$ Deviator stress at 10 % axial strain

m Dimensionless material parameter

n_F , m_F and σ_{eF} Dimensionless Findley material parameters

ε'_{oF}, σ_{mF} and σ_{eF} Dimensionless Findley material parameter

E_i Initial modulus of elasticity

ε_o Immediate strain when the stress is applied

E_p Post yield modulus

$\sigma_{f, av}$ Mean flexural strength of EPS

$\sigma_{t, av}$ Mean tensile strength of EPS

E Modulus of elasticity

ν Poisson's ratio

σ_{yo} Unconfined yield stress

γ Unit weight of EPS geofoam

ε_v Volumetric strain

ε_y Yield strain

σ_y Yield stress

1. INTRODUCTION AND RESEARCH BACKGROUND

Geofoam (expanded Polystyrene, EPS) refers to block or planar low density plastic foam solids when used as a light weight soil substitute or for thermal insulation in geotechnical applications(ASTM D6817 2013). EPS geofoam in common use has density of 15 to 30kg/m^3 having a comparable strength and stiffness as medium clay.

EPS is a very light weight material with good compressive strength, high water resistance and excellent cushioning properties. Most of these characteristics are affected by the density and fusion of the molded foam material.

The closed cell structure of EPS results in excellent insulating characteristics that remains stable over the life of the material. There is no thermal drift associated with blowing agent migration and hence assures that the insulating performance will not deteriorate as long as the material is correctly installed and maintained. The insulation properties of the foam do not change significantly for temperatures up to 167 ^{o}F (75 ^{o}C) under long term temperature exposure with virtually no low temperature limit(Greeley 1997).

The use of EPS geofoam in different civil and environmental engineering applications such as embankments, retaining walls, slopes, etc. is frequent especially in very soft soils. In many applications, EPS geofoam is subjected to compressive loads either from the dead load-surcharge or transient live loads.

Time dependent strains and residual deformations of structural systems are important design considerations for EPS geofoams. Creep deformations are minimized or essentially avoided in most design procedures by limiting allowable loads or surcharge pressures to

well below the prescribed compressive strengths of the EPS geofoam (usually 30 % of the strength at 5 or 10 % strain).

A number of investigations were carried out towards the evaluation of the salient properties of EPS geofoam including density, compressive strength, modulus of elasticity, yield strength, Poisson's ratio, flexural strength, tensile strength, shear strength, creep deformation and thermal conductivity, etc. Among these properties, density, compressive strength, modulus of elasticity, creep properties and thermal conductivity are most commonly used in evaluating the performance of EPS geofoam in different geotechnical applications. With the exception of thermal conductivity, other properties were evaluated by performing short term and long term unconfined compression tests. Nevertheless, EPS geofoam is used in areas where loading condition may be multi axial. For example confining pressure may result in multi axial loadings. Confining pressure on EPS geofoam may result from lateral pressures due to soil or hydrostatic pressure. Some studies have also shown that increase in confining stress will reduce strength (Preber et al. 1994; Sun 1997)]. Anasthas et al. 2001 performed triaxial tests on cylindrical samples of two different densities to investigate effect of confining stress on compressive resistance. Different confining stress levels and duration of confinement showed that compressive resistance of EPS geofoam reduced with increasing confining stress especially at confining stress levels closer to its unconfined compressive strength. This reduction in strength may make the applied stress in excess of the allowable load to result in increased creep deformation. However, the compressive strength of EPS geofoam tested at small confinement pressures (0 to 20 kPa) have shown that the strength increased as the confining stresses increased(Zou and Leo 2001). But the strength increase noted was very small.

Chun et al. 2004 tested the ultimate compressive strength of EPS geofoam samples of 50mm diameter and 100 mm height of different densities (15, 20, 25, and 30 kg/m^3). Confining pressures of 0, 20, 40, and 60 kPa were used with axial load applied perpendicular to the direction of fabrication at a loading rate of 1 %/minute. It was observed that the ultimate strength increased as the confining pressure increased but the effect of confining stress was small.

Thus, effect of confinement on the strength of EPS geofoam is uncertain. Tests with different cell pressures followed by application of deviatoric stresses at 1 or 10 % per minute can be made. Effect of duration of confinement before application of shear can be studied as well. Significance of confining pressure effect on the existing design approaches will be discussed.

Creep behavior of geofoam has been studied for unconfined axial compression(Anasthas 2001; Sheeley 2000; Srirajan et al. 2001; Sun 1997). No study is available to date on effect of confining pressure on creep behavior of EPS geofoam. Creep due to confinement can be investigated by conducting a series of tests under biaxial loading.

In addition to confining stresses, the mechanical behavior of EPS is also affected by factors like material density, strain rate and temperature(Atmatzidis et al. 2001; Chun et al. 2004; Duškov 1997a; Elragi et al. 2001; Preber et al. 1994; Wong and Leo 2006; Zou and Leo 1998).

EPS geofoam has been used above ground and temperatures can go up to 40 ^{o}C. Hence, effects of temperature on the properties of this material should be investigated. The effect of temperature on the strength of EPS geofoam was studied by different researchers(Yeo and Hsuan 2009; Zou and Leo 2001). Generally, the compressive strength was observed to

decrease with increase in temperature. As a rule of thumb, in the range of –5 °C to 60 °C, the compressive stress at 10 %/ minute compression decreases by about 7 % of the value at 20 °C for each 10 °C rise in temperature. The cellular materials have a correspondingly higher compressive strength at temperatures below 20 °C, but the increase is less than 7% at temperatures below –5 °C. However, the cellular material does not become brittle even at –196 °C(BASF 1998). Effects of low temperatures on properties of EPS geofoam were also studied by Duškov (Duškov 1997a) by performing compression tests on cylindrical EPS20 samples at temperature ranges of -8.6 to -12.9 °C and found low temperatures did not change mechanical behavior of EPS.

Creep tests for different axial stresses were made and replicated at different temperatures in order to study the combined effect on EPS geofoam samples so as to understand its field behavior under similar circumstances. For testing, daily and seasonal temperature change effects were modeled by cycling the temperature in a temperature controlled chamber.

Triaxial tests were carried out to study confining stress effects on short and long term deformation behavior of EPS geofoam. Volumetric and axial strain relationship was studied. Volumetric deformation, axial deformation and applied load were measured respectively with differential transducer, LVDT and load cell. Tests were modeled in FLAC, finite difference based computer modeling software, and outputs were compared. Two cylindrical samples of different sizes were used. The first group was cylindrical EPS samples of 102 mm diameter and 203 mm height. The second group was 64 mm diameter and 127 mm height. Samples were precision cut to required dimensions in a factory. Densities of 16, 20 and 32 kg/m^3 were considered. Different axial strain rate of loading

4

were used. Tests were conducted at approximately constant room temperature and humidity. Tests were performed to investigate temperature induced changes of confining pressure and associated creep deformations. Samples were placed in a chamber where temperature was set to desired values and deformation and temperature were recorded and subsequently compared with FLAC outputs.

Scope of this research were put in to five main sections: (1) studying effect of confining pressure on compressive strength, yield stress and elastic modulus of EPS geofoam (2) characterizing stress-strain relations of geofoam in the presence of confinement by using modified hyperbolic relationship (3) studying effect of induced anisotropy on stress-strain behavior of geofoam (4) examining effect of confining pressure on the creep behavior of EPS geofoam and (5) studying effect of seasonal temperature variations on long term performance of EPS geofoam.

Derivatives of this research were extracted as articles. One article was reviewed and accepted to be part of ASCE geotechnical special publication and two journal papers are submitted for review, other three are in preparation for submittal.

Organization of this dissertation is as follows. The first chapter is general introduction and research background. The second chapter covers literature review. Chapter three discusses lab tests and lab procedures followed. Test results, constitutive and FLAC modeling are discussed in detail in chapter 4. Finally in the fifth chapter, outcomes from this research are summarized with recommendations for further studies.

2. LITERATURE REVIEW

2.1 Production of EPS Geofoam

EPS geofoam is manufactured by pre-expanding polystyrene beads which are moulded and fused in block-moulds using dry saturated steam. Generally three main stages exist in the manufacturing process of EPS geofoam: pre-foaming; maturation; and moulding blocks before cutting into predetermined dimensions (BASF 1993). The polystyrene beads themselves are produced by the polymerization of styrene monomer in an aqueous suspension. During the polymerization process a blowing agent, normally pentane is absorbed by the expandable polystyrene beads to enable expansion in the later production phase. Pentane is contained in petroleum and styrene is a petroleum derivative. Both are pure hydrocarbons, i.e. they consist solely of carbon and hydrogen. Expandable polystyrene (EPS) is product of polymerization of monostyrene by adding small amount of pentane, Figure 1.

Styrene C_8H_8 $\longrightarrow$ $\bigcirc$ $\longleftarrow$ Pentane C_5H_{12}

Polymerization

$$\left[\begin{array}{c} CH_2-CH \\ \bigcirc \end{array} \right]_n$$

EPS
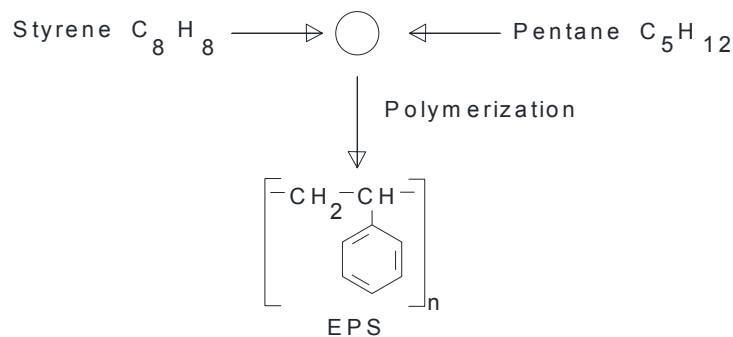
Figure 1. Schematic presentation of polymerization (BASF 1998)

After completion of polymerization, the beads are separated from the water by centrifuging and drying. The dry expandable polystyrene beads are distributed with respect to their size by sieving. The beads are then coated to optimize the later conversion processes such as expansion and moulding. The average diameter and volume of these polystyrene resin beads is 1.0 mm and 0.52 mm^3, respectively. Expandable resin beads are the raw materials that are supplied by chemical companies to geofoam manufacturers. Resin beads are supplied in different grades for producing foams of different applications like for general block and shape molding operations, leak resistance containers and packaging foams.

In geofoam manufacturing plants, the polystyrene resin beads are pre-expanded with steam at a temperature of about 100 - 110 °C. Pre-expanded beads are formed as the temperature softens the beads and pentane gas expands up to 50 times or more to create enlarged cellular structures within the pre-puffs. The density of the final foam block is governed by the degree of expansion, temperature, and duration of steam exposure during pre-foaming stage. This stage is relatively controllable and thus the density of the block is controlled with a certain precision. The pre-expanded beads or pre-puffs are cooled to mature and stabilize. After maturating, during which time air diffuses into the newly formed cells, this pre-foam is moulded and fused in shape or block-moulds, again under the influence of dry saturated steam. Some amount of recycled expanded polystyrene can be shredded and mixed with the pre-puffs just before molding. Figure 2 is a schematic representation of EPS manufacturing processes. Typical block sizes produced and commercially available in the United States are 0.61m x 1.22m x 2.44m (2 ft x 4 ft x 8 ft)

and may go up to 0.6m x1.25m x 8.0m (Negussey and Jahanandish 1993). Around 140

geofoam manufacturing plants exist in the United States (Elragi 2000).
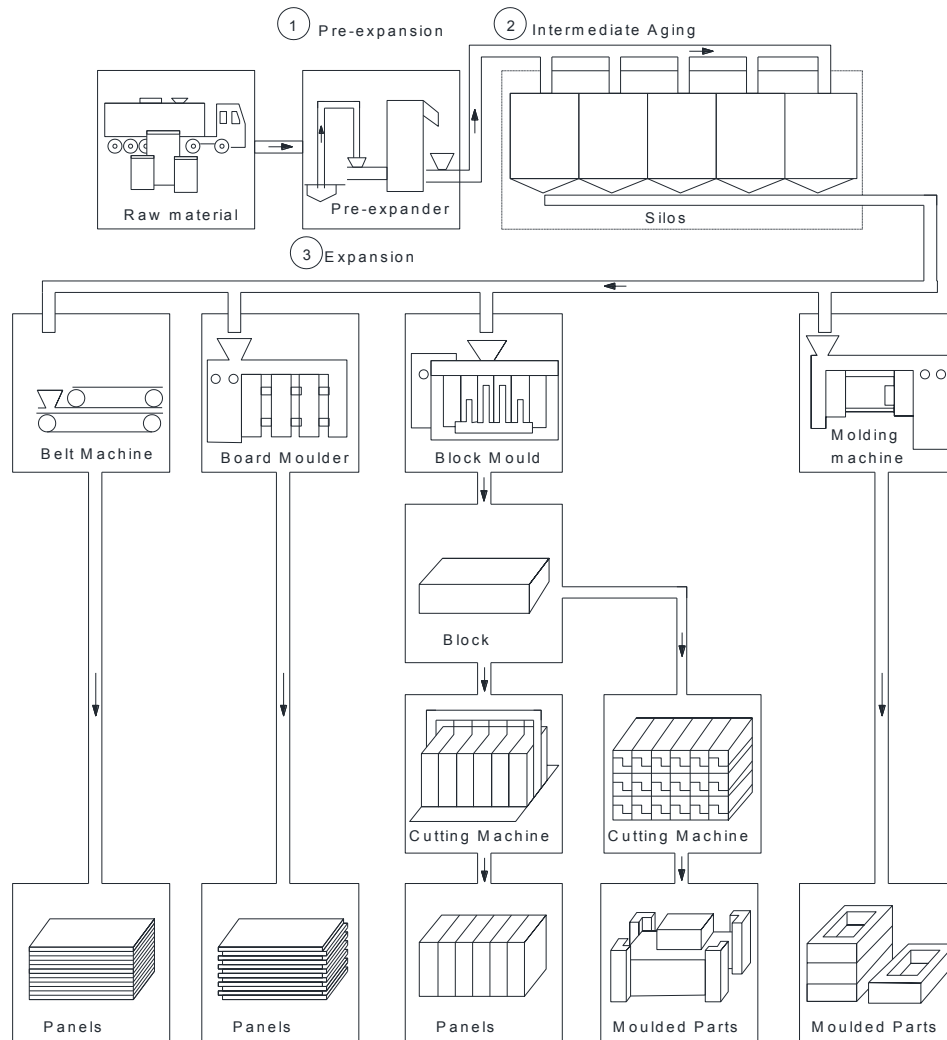
Figure 2. Schematic representation of EPS production (BASF 1998)

The resulting geofoam consists of many hexagon-shape microcells containing air. The cell

walls and air inside the microcells play a significant role in the compression properties of

the geofoam. The solid density of polystyrene-1030 kg/m^3 produces cellular solid densities

in the range of 15 to 35 kg/m^3, depending on the type of resin beads. High air content of

foam and the closed cell structures result in very low thermal conductivity and density, two main EPS geofoam characteristics. Expanded polystyrene is a thermoplastic material. In the absence of oxygen it will soften when heated and eventually becomes viscous and changes to liquid form and hardens when cooled (Koerner 2005).

2.2   Properties of Geofoam

2.2.1 Density

The density of EPS geofoam is considered as the main parameter for characterizing compressive strength, stiffness, creep and other mechanical properties. EPS geofoam has a unit weight approximately 50 to 100 times lighter than conventional fill materials. Table 1 provides unit weights of some light weight materials used in practice. Geofoam of different densities can be fabricated with application-specific properties; spanning from insulation to light weight construction purposes. The ranges of standard geofoam densities commonly vary between 16 kg/m^3 to 32 kg/m^3 (1pcf to 2pcf). Higher density blocks of up to 64 kg/m^3 can be produced. Light weight fill applications commonly use 20 to 30 kg/m^3 and for insulation purposes 30kg/m^3 or above are used to obtain optimum insulation properties(van Dorp 1988). Density of EPS geofoam is determined as per(ASTM D1622 2008). The cost of EPS geofoam blocks is generally proportional to density.

EPS geofoam classifications based on density are commonly used by manufacturers and designers. For instance, ASTM standard D-6817 presents the types, physical properties, and dimensions of rigid cellular polystyrene (RCPS) intended for use as geofoam (ASTM

9

D6817 2013). Similarly C-578 is ASTM standard specification that covers types of rigid

cellular polystyrene (RCPS) thermal insulations(ASTM C578 2011).

Table 1. Light weight materials(Miki 1996)

Material	Density (kg/m^3)	Remarks
Volcanic ash soil	1200 - 1500	Natural material
Fly ash	1100	
Light clay (Leca)	800 - 1000	
Tire chips	700 - 900	Usually used above ground water level; cover soil layer of at least 0.9m is required
Wood chips	700 - 1000	Usually to be used below ground water level; anti leaching measures needed
Expanded beads mixed light weight soil	700 or more	Variable density; similar compaction and deformation characteristics to soil
Air foamed mortar and air foamed light weight stabilized soil	500 or more	Adjustable density; flow able; self hardening
EPS geofoam	14 – 32	Ultra light weight

2.2.2 Compression Strength

Information on the compression behavior of EPS geofoam is necessary for appropriate design of infrastructures which use EPS geofoam. The compressive strength of EPS geofoam is usually taken as the stress at which the axial strain reaches 5 or 10 %. Differences between strengths at 5 % (σ_{c5}) and 10 % (σ_{c10}) strain are relatively minor and both the 5 and 10 % strain criteria have been used in factored strength design procedures (Negussey 2007).

Unconfined compression tests on small sample sizes (50 mm cubes) are commonly used to obtain most of the available design parameters(ASTM D1621 2010). Compressive strengths increase with increasing sample size, but this increase is small (Atmatzidis et al. 2001; Elragi et al. 2001). Results from unconfined compression tests adequately represent the mechanical behavior of EPS geofoams in applications where applied normal stresses remain well below yield stress or conceptual elastic strain limit. Shape, size and aspect ratio of EPS geofoam samples tested in unconfined compression have relatively insignificant effects on measured compressive strength at 10 % strain (Atmatzidis et al. 2001; Eriksson and Tränk 1991).

Density of the EPS geofoam has a significant effect on the values of the compressive strength. The strength increases as the density of the geofoam increases (Negussey 2007). The compressive strength depends on the strain rate (Abdelrahman et al. 2008) as well as the temperature (Yeo and Hsuan 2009; Zou and Leo 2001). An increase in strength is observed when there is an increase in strain rate. However the strength decreases with temperature for temperatures above room temperature (BASF 1998; Yeo and Hsuan 2009).

2.2.3 Modulus of Elasticity

The initial modulus of elasticity, E_i (slope of the initial linear segment of the stress-strain curve), the compressive strength, σ_{c10} (usually defined as the axial stress at 10 % axial strain) and the yield stress, σ_y (point of intersection of the initial linear segment and a post yield linear segment of the stress-strain curve) are used to characterize the stress stain curves obtained from the unconfined compression tests (Preber et al. 1994). Initial tangent modulus, Young's modulus and modulus of elasticity are interchangeably used to define the initial linear portion of the stress-strain curve. The stresses are linear for smaller values of strains, usually up to 1 % axial strain (Abdelrahman et al. 2008; Horvath 1998).

Values of initial tangent modulus vary with density. Different authors have suggested empirical relations for E_i as a function of density. In all relations listed below E_i and density have units of MPa and kg/m^3.

(Magnan and Serratrice 1989)	$E_i = 0.479\,\rho - 2.875$	(1)
(Eriksson and Tränk 1991)	$E_i = 0.0097\rho^2 - 0.014\,\rho + 1.8$	(2)
(Horvath 1995)	$E_i = 16.431 - 1.645\,\rho + 0.061\,\rho^2$	(3)
(Duškov 1997b)	$E_i = 0.45\,\rho - 3.0$	(4)
(Elragi 2000)	$E_i = 0.3554\,\rho - 2.0827$	(5)
(Anasthas 2001)	$E_i = 0.008\rho^2 + 0.152\,\rho + 0.015$	(6)

Young's modulus values for geofoam are commonly determined by testing 50mm cube samples in accordance with(ASTM D1621 2010; LST, EN. 826 1998)]. But results from conventional 50 mm cube samples significantly underestimate Young's modulus values for EPS geofoam (Duškov 1997b; Elragi 2000). Modulus values that are obtained from these small size laboratory samples are about half of the values that were estimated from field

observations and should be increased for design applications(Negussey 2007). The initial tangent modulus value depends on the loading rate. Higher strain rates resulted in higher modulus values (Abdelrahman et al. 2008; Elragi 2000).

2.2.4 Tensile Strength

The tensile strength of EPS geofoam is highly dependent on the degree of fusion of the expanded polystyrene beads. Tensile and flexural tests are useful indices as they imply how well the beads fused during manufacturing of EPS. Compared to the flexural and shear strength, tensile strength is highly affected by processing conditions (BASF 1998). For a given density, the mean value of tensile strength increases linearly with density. The mean value is given by the following expression which was obtained from data provided in (BASF 1998).

$$\boldsymbol{\sigma_{t,av} = 14.557\,\rho - 7.2456} \tag{7}$$

where $\sigma_{t,av}$ is the mean tensile strength in kPa and ρ is EPS geofoam density is in kg/m^3.

2.2.5 Flexural Strength

The flexural strength of EPS geofoam is mostly used as quality control test. It also increases linearly with density. The fusion affects the ductility of the foam and is reflected in the degree of deflection. The magnitude of deflection gets less as the density increases. The mean value of the flexural strength is given by the following expression which was obtained from data provided in (BASF 1998).

$$\boldsymbol{\sigma_{f,av} = 19.655\,\rho - 95.996} \tag{8}$$

where $\sigma_{f,\,av}$ is the mean flexural strength in kPa and ρ is EPS geofoam density is in kg/m^3.

2.2.6 Poisson's Ratio

Assuming EPS geofoam to be homogenous, isotropic and linear elastic; only two parameters, modulus and Poisson's ratio, would be required for analysis. The Poisson's ratio of EPS geofoam is reported to be a function of density in addition to confining stresses (Chun et al. 2004).

Table 2. Values and expressions for Poisson's ratios

Author	Poisson's ratio expressions or values	Remarks
(Eriksson and Tränk 1991)	0.05	
(Duškov 1997a),	≤ 0.15	
(Yamanaka et al. 1996)	0.075	
(Sanders 1996)	0.05 - 0.20	
(Horvath 1995)	$v = 0.0056\rho + 0.0024$	ρ = density (kg/m^3)
(Preber et al. 1994)	$v = 0.20 - 0.5\dfrac{\sigma_3}{62kPa}$	σ_3 = confining stress (kPa) $0 \leq \sigma_3 \leq 62$ kPa
(Chun et al. 2004)	$v = 0.0967+0.00308\rho - 0.0023\sigma_3$	ρ = density (kg/m^3) σ_3 = confining stress (kPa)
(Wong and Leo 2006)	≤ 0.15	
(Negussey and Sun 1996)	0.09 and 0.33	
(Momoi and Kokusyo 1996)	0.5	

Generally Poisson's ratios are reported to be very small positive values for small strains and zero or negative values for large strains (Atmatzidis et al. 2001; Wong and Leo 2006; Zou and Leo 1998). Table 2 is a summary of values or expressions for Poisson's ratios of EPS geofoams. Poisson's ratio values tend to be underestimated due to non uniformity and end effects in the proximity of the rigid loading platens (Elragi et al. 2001).

Broad range of variability and uncertainty in the values of Poisson's ratio exist and hence factors that are perceived to affect the Poisson's ratio determination need a more detailed study.

2.2.7 Creep Behavior

EPS geofoams under service loads develop creep deformations. Live loads such as due to traffic and the associated deformations are generally transient. Post construction creep deformations of geofoam mainly depend on the level and duration of dead loading. Creep deformations are the main concern in the design of geofoams rather than shear failure. Creep is considered negligible if the initial strain does not exceed 0.5 % (Frydenlund and Aabøe 2001). The thickness of EPS geofoam will not change much over a long period of time if the initial compression is less than 1.5 % (BASF 1998).

Working stress values are selected so as to limit creep deformations to acceptable levels over the service life of the facility. A design approach developed in Norway is most commonly used and it is based on limiting the allowable surcharge load over geofoam to 30% of the compressive strength at 5 % strain as determined by laboratory testing of small size samples at a strain rate of 10 % per minute (Frydenlund and Aabøe 1996).

Creep tests were conducted on 50 mm geofoam cubes using nominal stress levels of 30, 50 and 70 or 80 % of the compressive strength (Anasthas et al. 2001; Sheeley 2000; Srirajan et al. 2001; Sun 1997). Results have shown that creep deformations can be considered negligible for stress levels less than 30 % of compressive strengths at 5 % strain, see Figure 3. (van Dorp 1988) and (Duškov 1997a) also reported that if geofoam is exposed to loads greater than 50 % of the compressive strength at 5 % strain, larger creep deformations occur. At working stress levels of less than 50 % of the yield, geofoam is found to have insignificant creep deformation (Negussey and Jahanandish 1993). At yield and post yield stress levels, time dependent deformation will be of appreciable amount.
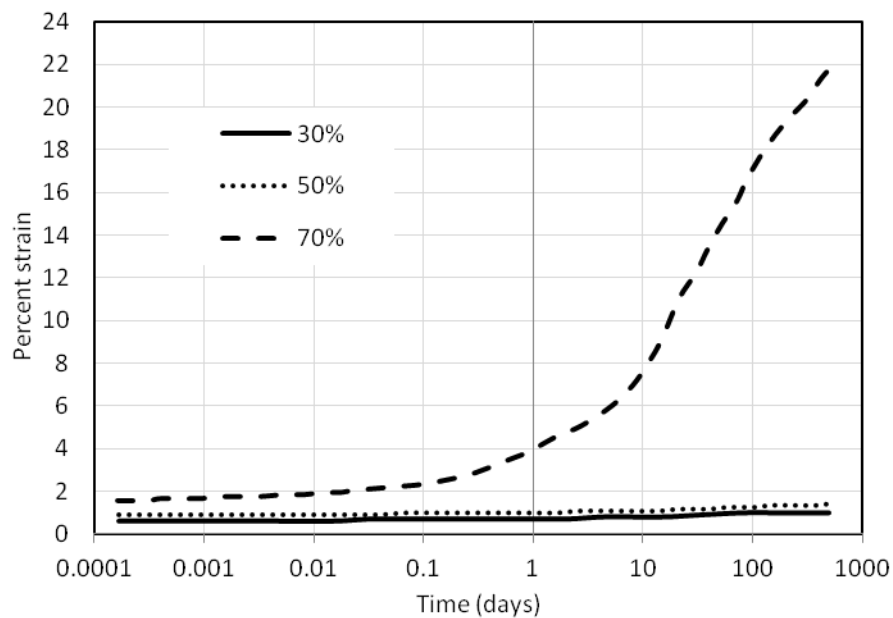
Figure 3. EPS geofoam creep behavior under different stress levels (Sheeley 2000)

(Srirajan et al. 2001) have shown that creep behavior of EPS geofoam is affected by sample size and density. Larger samples experienced less creep deformation over a given time period and equivalent loading. Small samples overestimate creep deformation of EPS

geofoam due to end effects and more pronounced seating error (Elragi et al. 2001; Negussey 2007).

Density is reported to have an effect on the creep behavior of EPS geofoam. Denser samples experienced less creep at the same level and duration of loading, Figure 4. But density had little or no influence on immediate strains for larger samples tested at equal stress levels of 50 % of compressive strength and lower (Srirajan et al. 2001).
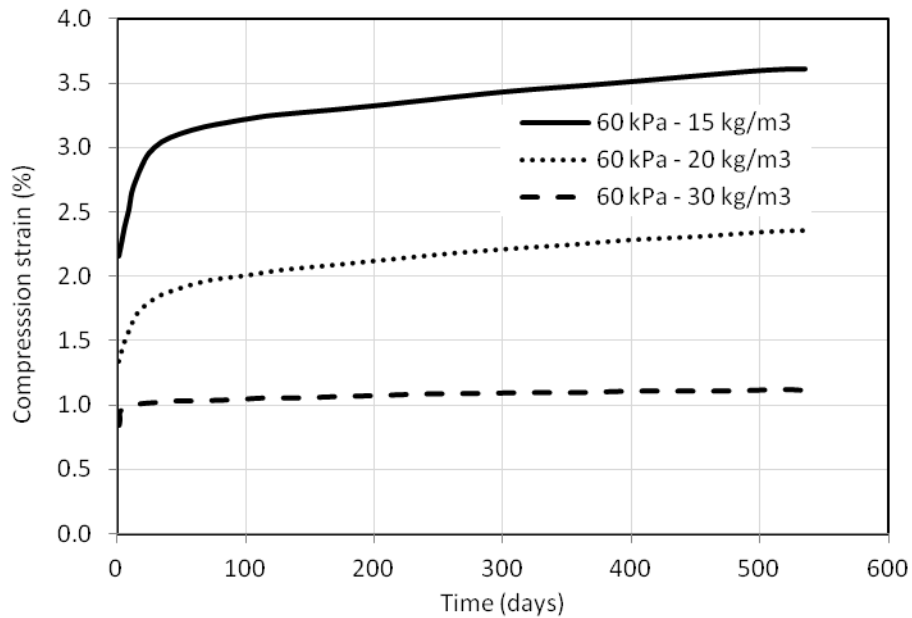
Figure 4. Density effect on creep of EPS geofoam (BASF 1998)

Two series of creep tests were conducted on cylindrical EPS geofoam by Duškov(Duškov 1997b). In the first series, samples of 100 mm diameter and 200 mm high EPS20 were exposed to 20 kPa axial stress. In the second series both EPS15 and EPS20 samples of 150 mm diameter and 300 mm height were exposed to 10 and 20 kPa stresses to represent light and heavy pavement structures. Observations of total strains over 400 days, resulted in 0.2 % total strain for the first series of tests of which 35 % (i.e. 0.07 %) occurred in the

17

first day. For the second series of tests a total strain of 0.50 and 0.25 % for 20 and 10 kPa

stresses respectively resulted and about 50 % of each happened in the first day. No

significant differences were observed in EPS15 and EPS20 samples. ASTM - D6817 2013

provides 70 and 110 kPa as the strength at 10 % axial strain for EPS15 and EPS20. Hence

the axial stresses used in the above tests represent utmost 28.5 % of the strength for

EPS15.

EPS samples of 50 mm cube and 18.4 kg/m^3 density were tested for creep(Sun 1997).

Axial loads of 6.6, 10.8, and 15.2 kgf which correspond to 30, 50, and 70 % of the

unconfined compression strength at 5 % strain were used. The respective total axial strains

were 0.8, 3.0 and 14.4 % respectively after 461 days. Strain recoveries of 0.7, 1.5 and 3.3 %

were observed after 252 days past load removal.

Creep tests were done on 21 kg/m^3 nominal density and 50 mm cube EPS geofoam

samples by Sheeley,(Sheeley 2000).These samples had 98 kPa as the unconfined

compressive strength at 5 % axial strain. The axial stresses were set as 30, 50 and 70 % of

98 kPa. Axial strains were recorded for over 500 days and 0.95, 1.35 and 22 % axial strains

were observed for the respective stresses. Out of which 66 and 68 % of the total axial

strains were observed in the first day for 30 and 50 % loads respectively. Samples loaded

with 70 % stress level continued to show increasing strains to 500 days.

Srirajan et al. 2001 reported creep tests on EPS geofoam of five different sample sizes of

50, 64, 100 and 300 mm cubes and 300x300x600 mm blocks for 12 to 30 kg/m^3 densities.

Axial stress levels of 30, 50 and 80 % of the unconfined compressive strength at 5 % strain

were used. The smaller sample sizes developed more creep deformation than the larger

samples for the same level of loading and time. Different densities were tested for one

stress level and sample size. The results showed low density geofoam experienced more strains than high density geofoam. Most of the strains for all samples and tests occurred in the first day.

The amount of strains depends on the magnitude of stresses, sample size, density and duration of loading. For the same sample size, density and duration of loading, (Srirajan et al. 2001) and (Duškov 1997b) reported values of strains which were in direct proportion to the magnitude of stress levels for stress levels up to 50 % of the unconfined compressive strength at 5 % strain.

(Srirajan et al. 2001) noted that the practice of limiting the design stress to 30 % of unconfined compressive strength at 5 % strain was conservative. Hence, use of 50 % of the unconfined compressive strength at 5 % strain as a working stress was suggested. A large scale laboratory creep test was conducted on an EPS geofoam fill made from 1x1.5x0.5 m blocks having an unconfined compressive strength of 100 kPa (Aabøe 1993). The plan dimensions of the fill were 4mx4 m and 2mx2 m at the base and top respectively. With average side slopes of 2:1, the 2 m high fill had four layers of blocks. Surcharge of 52.5 kPa applied for 1270 days developed a total strain of about 1.187 %, out of which 64 % occurred in the first two days.

(Kutara et al. 1989) reported anisotropic behavior of EPS geofoam may affect the deformation characteristics of the material. Loading perpendicular to the direction of fabrication has shown higher deviatoric stresses at failure. But similar observation has not been confirmed by others.

In creep tests conducted to date, effects of confinement and changes in volumetric strain have not been considered. This study examines these effects and associated practical implications in analysis and design of EPS geofoam.

2.2.8 Interface Friction

The interface friction between EPS geofoam blocks can be high (Negussey et al. 2001; NRRL 1992) and is comparable to the internal friction angle of sand (Negussey 1997). The interface friction between geofoam and other materials is given in Table 3. The effect of density on the interface friction is small.

Table 3. EPS geofoam interface friction factors (after Sheeley and Negussey 2001)

Interface	Peak factor	Residual factor
Foam – Foam, 20 kg/m^3 (dry)	0.85	0.70
Foam – Foam, 20 kg/m^3 (wet)	0.80	0.65
Foam – Foam, 30 kg/m^3 (dry)	0.85	0.65
Foam – Foam, 30 kg/m^3 (wet)	0.75	0.65
Foam – Foam, 20 kg/m^3 (dry)	0.85	0.70
Foam – cast in place concrete	2.36	1.00
Foam – Textured HDPE membrane	1.00	1.00
Foam – Smooth HDPE membrane	0.29	0.23
Foam – Smooth PVC membrane	0.70	0.40

(Sheeley and Negussey 2001) studied the practical significance of metal binders which have been used in the field to attach foam blocks and increase shear resistance. The binders did not provide increased shear resistance in one directional loading; instead they decreased the resistance in reverse loading and reloading.

2.2.9 Thermal Property

More than about 98 % of the volume of EPS geofoam is air. This large air volume is divided into smaller volumes enclosed within cells and resulted in reduced convection currents. EPS geofoam has small thermal conductivity due to small amount of solid material and the air within smaller cells result in less heat transfer. Thermal conductivity is greatly affected by bulk density (BASF 1998). In Figure 5, minimum value of thermal conductivity is attained when density gets close to 30 to 40 kg/m³. As density increases further, thermal conductivity increases about linearly to a value of 0.13 W/ (m K) at 1050 kg/m³ (compact polystyrene). (van Dorp 1988) also reported that the thermal resistance, R- value of geofoam, reaches maximum at about 35 kg/m³ density. R-value is expressed as the inverse of thermal conductivity.
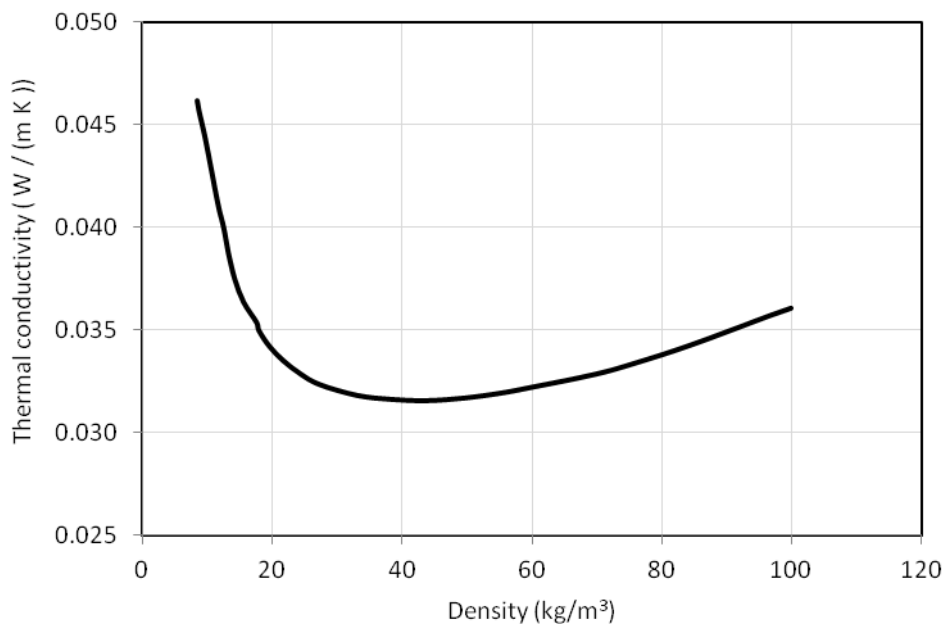
Figure 5. Thermal conductivity as a function of bulk density at 10 ºC (BASF 1998)

Low thermal conductivity of EPS geofoam makes it an excellent insulation material. The performance of highway pavements and airport runways can be improved when geofoam is used as subgrade insulation in colder climates. It has also been used in the construction of slab-on-grade and shallow foundations where geofoam is employed as thermal insulation so as to minimize or avoid frost heave(NAHB 2004).

Thermal conductivity of EPS geofoam is affected by the amount of moisture which diffused in to the cells(Negussey 1997). Nevertheless, even in an extreme exposure to moisture the thermal conductivity of EPS geofoam is about 20 to 40 times less than that of soil (Horvath 1994).

2.2.10 Effects of Moisture

EPS geofoam absorbs minute proportions of water(BASF 1998). The amount of absorption depends on factors like density, duration of moisture exposure and level of fusion of beads during production. High density, good fusion and smaller exposure result in less moisture absorption and vice versa. The absorbed moisture has a tendency to increase density and thermal conductivity. van Dorp (van Dorp 1988) reported about 10 % moisture absorption by volume for EPS geofoam in a roadway after 12 years of service. However the water absorbed by EPS geofoam has negligible effect on the mechanical properties (BASF 1998).

2.2.11 Chemical Properties

EPS geofoam is resistant to water and aqueous solutions of salts, alkalis, and acids. However adhesives, paints, and organic solvents may damage the foam. Table 4 is a summary of effects of different chemicals.

Table 4. Resistance of EPS to chemical agents (after BASF 1998)

Source of attack	EPS resistance* to attack
Salt solutions (sea water)	Resistant
Soaps solutions and wetting agents	Resistant
Bleaching solutions, such as hypochlorite, chlorine water, hydrogen peroxide solutions	Resistant
Dilute acids	Resistant
35 % hydrochloric acid, nitric acid up to 50 %	Resistant
Anhydrous acids, (e.g., fuming sulfuric acid, glacial acetic acid, 100 % formic acid)	Non Resistant
Sodium hydroxide, potassium hydroxide and ammonia solution	Resistant
Organic solvents such as acetone, ethyl acetate, benzene, xylene, paint thinner, trichloroethylene	Non Resistant
Paraffin oil, Vaseline	Limited Resistant
Diesel oil , Motor gasoline	Non Resistant
Alcohols (e.g., methanol, ethanol)	Limited Resistant
Silicone oil	Resistant
* Resistant = the foam remains unaffected even after long exposure Limited Resistance =the foam may shrink or suffer surface damage on prolonged exposure Non Resistant = the foam shrinks more or less rapidly and is dissolved	

2.2.12 Properties Considered During Design and Construction

a) Buoyancy: Uplift forces are main design concerns when EPS geofoam is installed
below the ground water level or placed above the ground water table with potential
flooding and groundwater rise. Thus, every design should assure an adequate
surcharge either from the overburden pressure on top of the EPS blocks or from
uplift resisting anchors. Use of EPS in dry condition is preferred and regulation of
ground water table can be considered.

b) Concentrated loads: Under concentrated loads EPS geofoam will puncture easily.
Load distribution concrete slab is commonly employed. The slab significantly
attenuates the load on the EPS (Nishi et al. 1996). Placement of the EPS blocks under
adequate soil cover is an alternate solution.

c) Chemical attacks: Table 4 gives summary of substances which can dissolve EPS
geofoam. Soils adjacent to EPS might also be contaminated and have solvents that
can attack the EPS. Geotextile membranes or plastic covers will help to protect the
EPS. Besides load distribution, concrete slab on top of the EPS fill can protect the
EPS against gasoline or other solvent spills during construction or while in service.
In general, tests are recommended if EPS geofoam is to be used in contact with
substance of unknown composition (BASF 1998).

d) Flammability: Geofoam is a combustible like other organic materials. Care should be
taken during storage and construction. EPS geofoam produced with fire retardants
is more difficult to ignite and has slow spread of flame but is more expensive.

e) Insect Infestation: Thermal insulation property of geofoam makes it suitable place
for insects to inhabit, deposit their eggs and store their food. Coating vulnerable

surfaces with cement slurry may help prevent insects temporarily. EPS geofoam with additives can also be manufactured making it resistant to insect attack.

f) Ultraviolet degradation: Prolonged, direct exposure to UV from the sunlight degrades EPS geofoam surface and results in discoloration and dust. A reduction in peak interface friction is observed on such degraded geofoam (Sheeley and Negussey 2001). Prolonged direct sunlight exposure should be avoided by covering with opaque sheeting.

g) Differential icing: When EPS geofoam is used as thermal insulation or fill under road pavements, ice may form during winter. Whereas the adjacent section of the rod without EPS geofoam may not form ice due to the geothermal heat. Such phenomenon on road where some portion is icy and the other ice free is called differential icing. Differential icing due to placement of EPS geofoam under a road way is dangerous as compared to those occurring in bridges and girder supported pavements because drivers may not be ready for such unexpected instances. Increased thickness of granular base coarse above EPS geofoam fill reduces the magnitude of differential icing (Frydenlund and Aabøe 2001).

h) Moisture absorption: When EPS geofoam absorbs some amount of moisture (maximum of about 10 % by volume), its density and thermal conductivity increase and should be accounted in design. For example if 20 kg /m^3 foam absorbs 10 % by volume water, its density will approximately increase to 120 kg/m^3.

i) Durability: EPS geofoam is highly durable even when used in manure (fertilized earth with phosphates, acid rain etc).

j) Sliding: The interface between EPS geofoam blocks is high as long as there is adequate normal load. However sliding may occur during construction due to lateral loads from backfilling as the normal loads for the mobilization of friction resistance are not in place. Care must be taken to avoid such sliding.

k) Block alignments and transition zones: Continuous vertical and horizontal joints between EPS blocks should be avoided by staggering the blocks so as to increase integrity of fill. Side slopes of EPS layers should be stepped in order to make a transition zone between geofoam and earth fill which will reduce problems of differential settlement.

l) Environmental friendliness: Toxic fumes and water contamination are not expected when EPS geofoam is under fire. Chlorofluorocarbons (CFCs) and hydrogenated chlorofluorocarbon (HCFCs) are not released to the environment during production, processing and use of EPS, simply because they are not used in manufacturing. In addition alpha, beta, gamma radiations and radon were not detected in EPS geofoam. EPS geofoam is insoluble in water and does not contaminate ground water and does not affect plant and animal life (BASF 1998).

2.3 Use of EPS Geofoam and Case Histories

Geotechnical engineering applications of EPS geofoam is enjoying wide acceptance especially in soft ground conditions due to a better understanding of its properties. EPS geofoam was introduced in 1950s as a light weight construction material (BASF 1998). Since then it is used in the construction industry of different countries for the first time,

Table 5. It has been used as lightweight fill, compressible inclusion, thermal insulation and small amplitude wave damping (ground vibration and acoustic)(Horvath 1997).

Table 5. Historical first use of EPS geofoam

Country	First time use	Project type	Reference
Germany	1960	Frost protection in pavement	(Hillmann 1996)
	1995	Highway embankment	
Norway	1965	Insulation	(Sanders et al. 1994)
	1972	Embankment	(Frydenlund and Aabøe 2001)
Japan	1985	Embankment	(Miki 1996)
United States	1960	Light weight fill	(Monahan 1993)

2.3.1 Light Weight Fill

EPS geofoam was first used as a light weight fill in Norway, in the reconstruction of the approach fill to Flom Bridge, near Oslo(Frydenlund and Aabøe 1996). One meter ordinary fill was replaced by EPS blocks in the embankments adjoining this bridge in order to reduce settlements. The embankments were resting on 3m thick peat above 10m soft, sensitive clay layer. It has then been used as light-weight fill in many civil engineering applications like in road embankments, bridge abutments, retaining walls etc (Duškov 1997a; Elragi et al. 2001; Murphy 1997).

The Utah Department of Transportation (UDOT) and the Utah Transit Authority (UTA) have made extensive use of EPS embankment for several major interstate, light rail, and commuter railway embankments in Salt Lake Valley, Utah. Constructed between 1998 and 2001, the Interstate 15 Design Build Reconstruction Project involved the widening of interstate embankments within a 27 km narrow corridor and limited right-of-way. Approximately, 100,000 m^3 of EPS fill was placed at various locations to minimize post-construction settlements of deep, compressible lake deposits (Negussey et al. 2001). A typical section of an embankment where EPS geofoam is used as a light weight fill is shown in Figure 6. Settlement problems can be reduced or avoided as the stress increments from EPS geofoam is much less than conventional earth fill. Steep side slopes up to 2:1 or more can be employed with EPS geofoam (Elragi 2000; Sun 1997).

EPS geofoam can also be used as a light weight fill at the back of retaining walls and bridge abutments in weak soils. It has double purposes. First smaller vertical stresses will help in minimizing or avoiding settlements in the back fill and hence avoid elevation difference between approach road and bridge deck. Secondly the lateral stresses on the wall are smaller as a result of smaller density, higher interface friction or interlocking and higher compressibility of EPS geofoam. The settlement in a bridge abutment was highly minimized by employing 9m EPS geofoam fill (Ishihara et al. 1996). About 28,000m^3 EPS geofoam was used as a fill next to outside perimeter of basement of Carousel Mall, Syracuse, NY with the intention of decreasing settlement of edge of the building (Stewart et al. 1994).
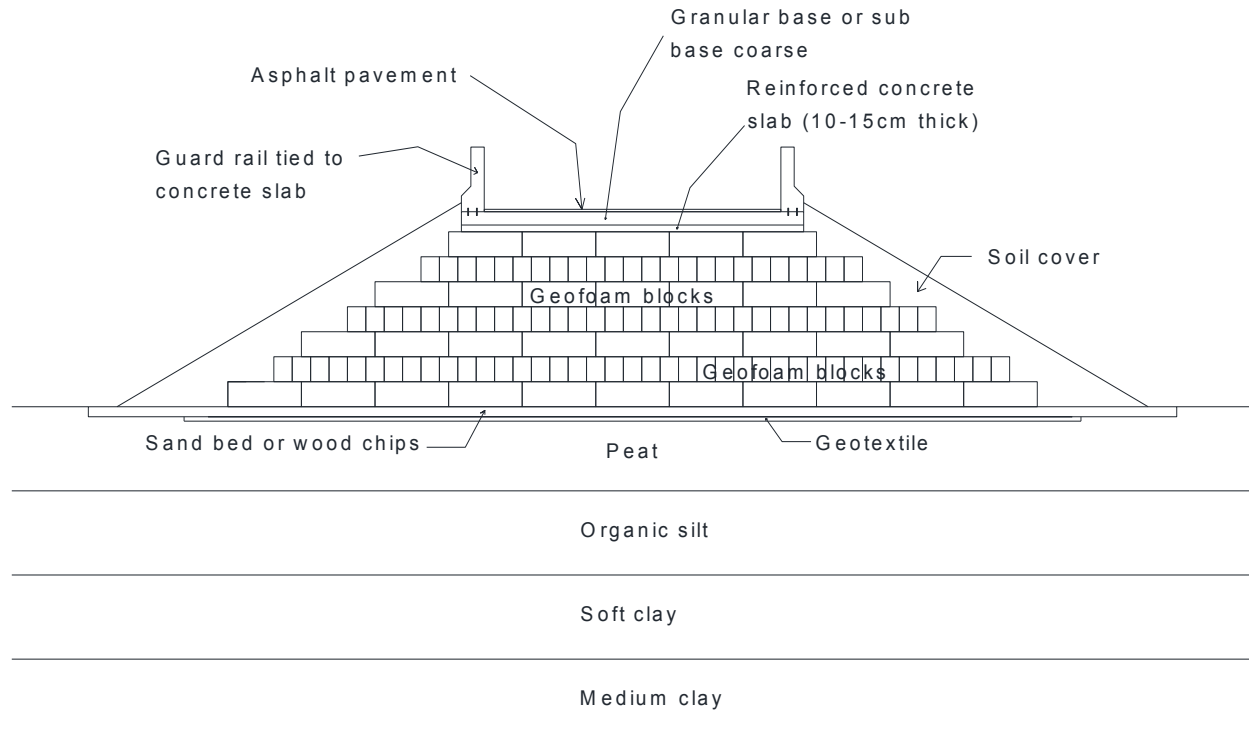
Figure 6. Typical embankment section with EPS geofoam fill

2.3.2   Compressible Inclusion

As a first documented use of EPS geofoam as a compressible inclusion, it was applied on a rigid concrete basement wall retaining approximately 10 m of sand and gravel fill (Partos and Kazaniwsky 1987).

(Negussey and Sun 1996) showed that use of EPS geofoam in the active zone of basement wall significantly reduced the earth pressures on the walls. EPS is used as a compressible inclusion aiming at reducing the lateral pressure (Horvath 1992, 1997; Zarnani and Bathurst 2007). EPS geofoam is being used as a construction material of interest under conditions where its mechanical property like contraction under deviatoric loading can be used advantageously to lower lateral loading below normal earth pressures (Wong and Leo

2006). A strip of 0.5 m thick EPS geofoam utilized behind 14m high abutment highly

reduced lateral pressure and overall bending moment (Matsuda et al. 1996).

Studies have also shown that vertical EPS panels used as buffers reduced the seismic earth

pressures against rigid non-yielding basement retaining walls, bridge abutments, etc

(Athanasopoulos et al. 2007; Hazarika 2001; Pelekis et al. 2000; Trandafir et al. 2010;

Zarnani and Bathurst 2009).

EPS geofoam can be used as a compressible inclusion on top of buried culverts. A very

small compression of EPS causes portion of the fill over the culvert to move down; what is

called negative arching. Shear stresses will mobilize on the sides and vertical earth

pressure on the culvert reduces as part of the pressure is carried by neighboring ground,

Figure 7. Up to 50 % vertical earth pressure reduction (Ooe et al. 1996; Vaslestad et al.

1993) and up to 30 % cost reduction were obtained (Vaslestad et al. 1993). The stresses

due to the seasonal heave and shrinkage of expansive soils can also be relieved by utilizing

EPS geofoam as a compressible inclusion.
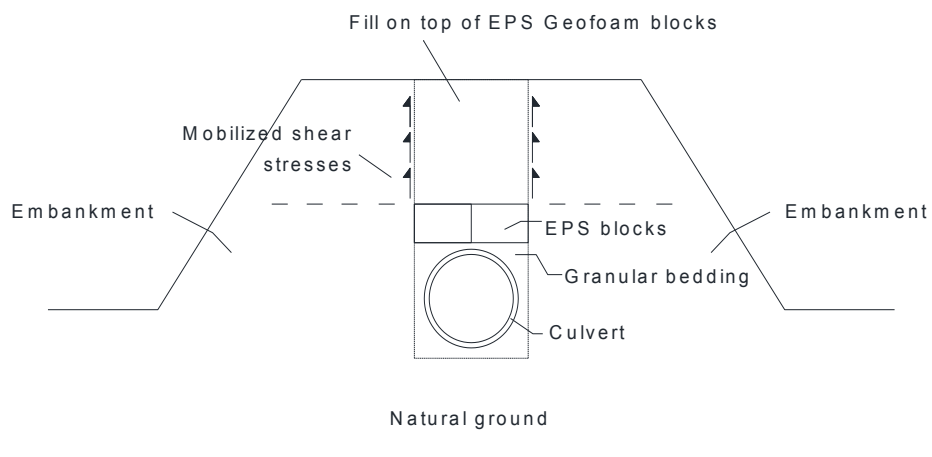
Figure 7. EPS as a compressible inclusion mechanism of arching

30

2.3.3 Slope Stability

Light weight characteristic of EPS geofoam was also employed to improve the factor of safety of slopes(Elragi 2000; Sheeley 2000). Even though the density of EPS geofoam is about 100 times less than the density of compacted-fill, its price can be about five times that of the cost of compacted soil of equal volume. Studies were done by (Negussey et al. 2001) on the most effective placement of the geofoam with respect to volume and location so as to reduce costs.

A failed road embankment on US 160, Colorado, used about 648 m^3 EPS geofoam as a fill in the crest of the slope to improve the factor of safety (Yeh and Gilmore 1992). About 1834 m^3 EPS geofoam was employed for 104 m long road embankment on a steep hill side (Suzuki et al. 1996). It was a cheap and fast solution.

2.3.4 Thermal Insulation

Cold regions with seasonal ground freezing and potential frost heave demand shallow foundations to be placed below the depth of frost penetration(IBC 2006). EPS geofoam can be systematically employed as an insulation material in order to decrease the depth of frost penetration and hence allowing design and construction of shallow foundations called frost protected shallow foundations (FPSFs) (NAHB 2004). Shallower frost penetration depth results when the soil is warmed up by both the building heat and geothermal heat with placement of vertical and horizontal insulations, Figure 8. The insulation also minimizes heat lose from the building.

31
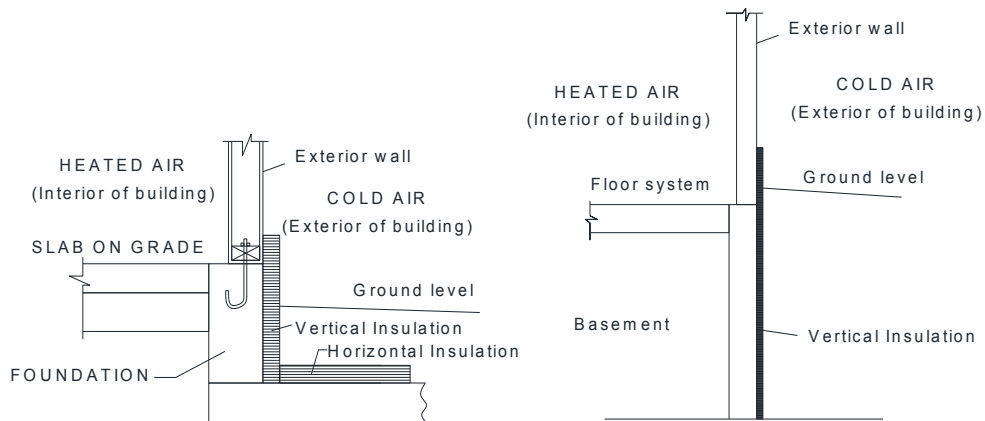
Figure 8. EPS application as a vertical and horizontal insulation

EPS geofoam is also used as insulation in highway pavements and airport runways so as to improve their performances by minimizing seasonal ground freezing and frost heave effects. To avoid problems of differential icing, the thickness of granular material above the EPS should be adequate. NRRL also suggested a minimum pavement thickness of 80 cm above geofoam to minimize icing possibility (NRRL 1992). Figure 9 is a cross section through a typical pavement where EPS geofoam is used as insulation.
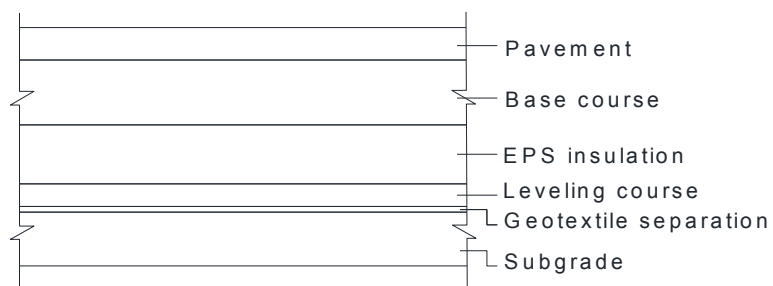
Figure 9. EPS application as pavement insulation

32

In 1985, Colorado Department of Highway successfully used geofoam as an insulation material in the reconstruction of subgrade of I-70 highway damaged by frost heave. XPS with thickness of 51 mm (2 in) and compressive strength of 276 kPa was employed (Upright 1989).

Generally in most geofoam applications a granular base is provided in order to allow drainage and minimize buoyancy problems. It also helps in creating a level surface for placement of the geofoam.

3. LABORATORY TESTS

3.1   Introduction

In order to investigate the properties of EPS geofoam, a number of tests with different densities and sample sizes are done. The main focus of this investigation is study and understanding of confining pressure effects on the most important and commonly used parameters in the design and analysis of EPS geofoam. Compressive strength, modulus of elasticity, yield strength, Poisson's ratio and creep deformation are studied and evaluated in the presence of different levels of confinement. Most of these parameters can be obtained by conducting short and long term unconfined compression tests. Existing design methodologies on EPS geofoam are solely based on unconfined compression tests. A number of unconfined short and long term tests are also done as a basis of comparison with results obtained from compression tests in the presence of confinement. Effect of temperature on behavior of EPS geofoam was studied by doing different tests inside a controlled chamber. Effect of cyclic temperature was also investigated.

Laboratory tests conducted in this research are classed under four main sections and are summarized in Table 6.

1) Short term compression tests: These compression tests were done using a strain rate of 10 % per minute on EPS samples of different densities. Confining stress levels of 0 to 250 kPa were used. Fewer tests were done for axial strain rate other than 10 % per minute. Most tests were done at room temperature but some were tested at other temperatures. Finally compression tests were done in order to study

34

the effect of mechanical anisotropy on the compression characteristics of EPS geofoam.

2) Isotropic compression tests: EPS geofoam samples of different densities and sizes were acted upon by isotropic compression where the isotropic pressure was varied at different rates. The bulk modulus and Poisson's ratio were determined.

3) Creep tests: Axial and volumetric deformations of EPS geofoam samples were obtained when samples of different densities and sizes are acted by different levels of confining pressure. The constant axial stress levels were also varied.

4) Thermal tests: Temperature was varied in a controlled chamber and short and long term compression tests were done. Creep tests with cyclic temperature variation were done to simulate seasonal temperature variation effects.

Table 6.Summary of tests

Test type	Density (kg/m^3)	Sample sizes	Confining pressure kPa
Compression tests	16, 20, 32	50 mm cube, 64 mm &102 mm diameter	0 to 207
Isotropic compression	16, 20, 32	64 mm &102 mm diameter	0 to 103
Creep	16, 20, 32	50 mm cube, 64 mm &102 mm diameter	0 to 103
Thermal	20	50 mm cube, 64 mm &102 mm diameter	0

3.2   Sample Preparation

EPS geofoam cylindrical samples of 64 mm and 102 mm nominal diameter and 127 mm and 203 mm nominal height, respectively, were supplied by Shelter Enterprises Inc. The samples had nominal densities of 16, 20 and 32 kg/m^3. Some of these samples were shortened to have an aspect ratio of 1:1. Block samples were also provided from which cubic samples were cut using hot wire cutter.

The samples supplied by the manufacturer and those cut in the lab were weighed using a sensitive balance $\pm$ 0.01g and their dimensions were measured to a scale sensitive to 0.01mm. The densities were calculated and are summarized in Table 7.

Table 7. Summary of average calculated densities of different samples

	Density (kg/m^3)	
No. of Samples	Calculated	Nominal
14	15.11 ($\pm$ 0.33)	16
14	19.20 ($\pm$ 0.55)	20
17	29.14 ($\pm$ 1.16)	32

3.3   Testing System and Procedures

GeoJac testing systems were used for most of the tests in this research. GeoJac testing systems use interconnected modules, power supplies and AD converters connected to a computer by a serial (COM) port. The computer exchanges reliable information (commands and data) with each module at high speeds, as high as 115200bits/sec (Trautwein 2004). The following are the three modules which are interconnected.

a) TestNet modules- regulate the flow of commands and data between the computer and the load frame

b) AD-IO modules - provide channels of analog data acquisition and excitation voltage for the sensors. Data rate of 80 readings per second (80Hz) was possible.

c) SERVO modules –control the GeoJac actuators with commands to control the velocity and direction of movement of the actuators.

8900N (2000lbf) capacity GeoJac automated load actuators were employed.

The sensors used in the tests include load cells, linear variable differential transducers (LVDTs), pressure transducers, and differential pressure transducers.

All the sensors were calibrated and cross checked for accuracy and stability. LVDTs were used to measure the vertical deformation of the EPS geofoam sample. They have sensitivity of $\pm$ 0.025 mm (0.001 in) and a working range of 76.2 mm (3in).

The load cells were used to measure the vertical loads applied directly to the sample either using a loading platen alone or a piston rod attached with a platen in the case of triaxial tests. They can accurately measure a load as low as 0.5N (0.01lbf) and have capacities of 444.8 N (100lbf) to 8896.4 N (2000lbf).

During triaxial testing, the pressure in the cell was monitored using a pressure transducer having sensitivity of $\pm$ 0.1 kPa (0.01psi) and working capacities of 1379 kPa (200psi). Volume accumulators were custom made in the workshop at Syracuse University. It has two pipes of diameters 19 mm (0.75in) and 63.5 mm (2.5in) from which de-aired water was supplied to the sample. The supply source was controlled by four way valves to allow recharge of emptied pipes.

The differential pressure transducer of sensitivity $\pm$ 0.01 kPa D (0.0014psi D) and capacities 6.9 kPa D (1psi D) to 34.5 kPa D (5psi D) were used to measure the differential pressure in the pipes. Differential pressures were calibrated with the volume change in the pipes.

In the short term compression tests, the axial stresses were applied by the vertical actuator at a predefined strain rate which in most cases was 10 percent per minute. For the long term compression or creep tests, a pre set constant value of axial stress was applied. The cell pressure for the confined triaxial tests was supplied from either pipe in the volume change measuring device. Regulated air pressure supply was introduced to the top of both pipes of the volume change measuring device. The air regulator was able to regulate up to 137.9 kPa (20 psi) with $\pm$ 0.001psi. Surge tank was also attached to the system in order to have a regulated air pressure supply.

Triaxial tests were done by using a triaxial cell which is commonly used for soil testing. The base and the top plates were of the same diameter as tested samples. The top plate was connected to a rod and the load cell during testing. The sample was covered by a rubber membrane and tied at the base and top plates with O-rings so as to prevent water.

When cell pressures were applied into the cell, there was some expansion of the acrylic triaxial cell wall. The volume of water taken to compensate for this expansion was subtracted from the total volume of water pushed into the cell so as to isolate the volumetric deformation of the EPS sample. For this effect, system calibration was made to provide compliance corrections for volume change readings during testing EPS geofoam samples. Hence, the volume expansion of the cell totally filled with de-aired water was measured for different cell pressures. A graph showing the relationship between measured

38

volume increase and the corresponding pressure level is shown in Figure 10. For a comparison, the radial strain due to the pressure is computed for the acrylic cylinder so as to have the new internal diameter of the cylinder. The volume increase with pressure was evaluated from the computed radial strain. The acrylic cylinder has an internal diameter of 114.3 mm (4.5 in); cell wall thickness of 6.4 mm (0.25 in), and height of 273.1 mm (10.75 in). The result from the theoretical computation agrees very well with the measured volume changes as shown in Figure 10. Cell pressure values of up to 206.8 kPa were used and a volume measurement error of up to 0.5 % could have been taken as sample deformation had the compliance correction not been done. High pressure resistant stiff tubes were used in all the connections in order to minimize the system compliance.
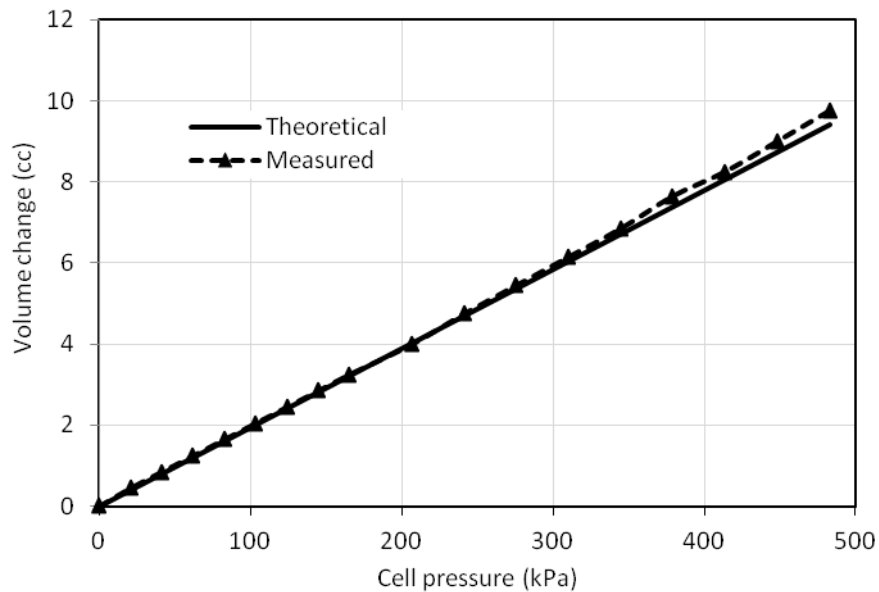
Figure 10. Volume change vs. cell pressure plot

3.4   Short Term Compression Tests

Unconfined and triaxial compression tests were done by using the GeoJac testing system. Vertical deformation of the sample was measured with LVDT attached to a rod. The rod is attached to top plate over the EPS geofoam sample. The displacement of the vertical actuator after being in contact with the sample can also be used to calculate the sample deformation. Load cell was used to measure the vertical load applied on the sample. In triaxial tests, the pressure inside the cell was monitored with a pressure transducer to make sure that the sample is acted upon by the applied cell pressure. The volume accumulator assembly and the differential pressure transducer were used to track volumetric deformation of the sample. The dry (low) side of the differential transducer was connected to the two pipes at the top using a T-connection. The wet (high) side was attached to the two pipes at the bottom also using a T- connection. Four-way valves were used to control connection of the wet side of the differential transducer to either the big or the small pipe. Flow to the triaxial cell was exposed to the wet side of the differential transducer.

The differential pressure measured is the head of water in the pipe connected to the wet side. Measurement of head difference at two different time periods enabled computation of volume of water pushed into the cell and hence volumetric deformation of the sample after compliance correction.

Finally axial strain, axial stress, cell pressure and volumetric strain were obtained at any stage of the test. Data collected by all sensors were logged in the central data acquisition system. Figure 11 shows the test set up for most of the tests conducted in this study.
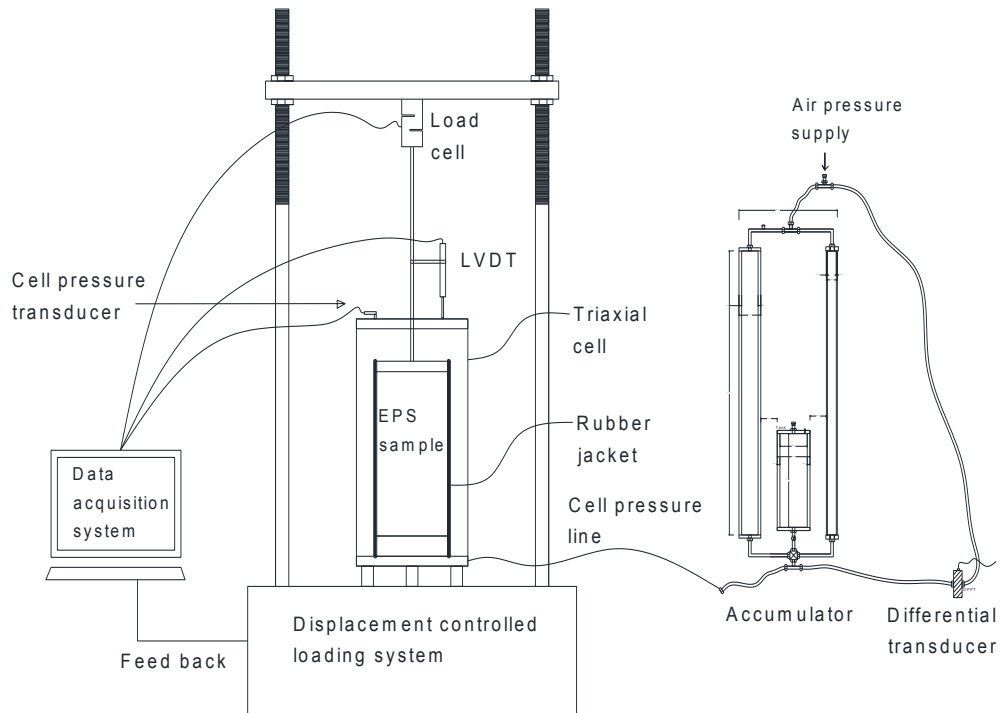
Figure 11.Test setup for triaxial testing

In the triaxial tests, cylindrical EPS samples placed inside rubber membranes and tied at the top and bottom with O-rings were placed at the center of the cell. The cell was assembled and filled with de-aired water by making sure all air bubbles in all tubes were expelled out and replaced with de-aired water. A loading rod was threaded into the top plate seated on the sample. The free end of the rod had a load seat. The load cell was suspended from the vertical actuator that was mounted on a rigid loading frame. This arrangement avoided uplift on the rod when the cell pressure was applied.

Application of cell pressure and axial loading were started at the same time in most of the triaxial tests. However, for comparison some samples were allowed to deform due to cell pressure alone for two weeks before the axial load was applied at 10 percent per minute

displacement. Such effect of consolidation on the stress-strain relations was found to be negligible.

3.5 Creep Tests

Long term compression tests were done by monitoring the deformation over a longer period of time under a constant axial stress. Unconfined and confined creep tests were done on cylindrical samples of EPS geofoam. For comparison purposes, unconfined creep tests were done on 50 mm cube samples. A similar test set up as explained above was used for creep tests. However the software controlling the closed loop system was different. The test was stress controlled where a preset axial stress was applied throughout the test duration. Axial stresses of 30 and 50 % of the unconfined compression strength at 10 % axial strain were used as constant axial stresses. Confining pressures were applied at the same time as the constant axial stress. Axial deformation, volumetric deformation, axial load, and cell pressure were recorded at preset intervals.

4. TEST RESULTS AND DISCUSSIONS

Test procedures and methods of data collection were discussed in the previous sections. Collected data were analyzed thoroughly and are presented in this section. Procedures followed in the data analysis are discussed as necessary. Test data are summarized in tables, figures and charts. The test results are discussed, compared and contrasted with reference to available published results, if there are any. Practical relevancies of outputs are also discussed.

4.1 Short Term Compression Tests

Both unconfined and confined compression tests were conducted by using EPS samples of 2 in cubes and cylindrical samples of nominal diameters 64 mm and 102 mm. Height of these cylinders were 127 mm and 203 mm, respectively. Sample densities of 16, 20, and 32kg/m³ were used. Axial strain rate of 10 %/min was used unless indicated otherwise. Confining pressures 0 to 207 kPa were used. Confining pressure was applied at the same time as the axial compression unless indicated otherwise.

4.1.1 Unconfined Compression Tests

Average axial strains and stresses were determined from axial deformations and axial loads registered by LVDT and load cell. A typical unconfined compression test result is plotted as stress vs. strain curve as shown in Figure 12. The initial portion of the curve usually has seating error as the sample might not be cut smoothly and the loading platen might not be just touching the sample during the initiation of axial loading. Seating error correction was made by extending the straight portion of the curve downwards and

moving the whole curve to the left to make the curve start at the origin in accordance with (ASTM D1621 2010).
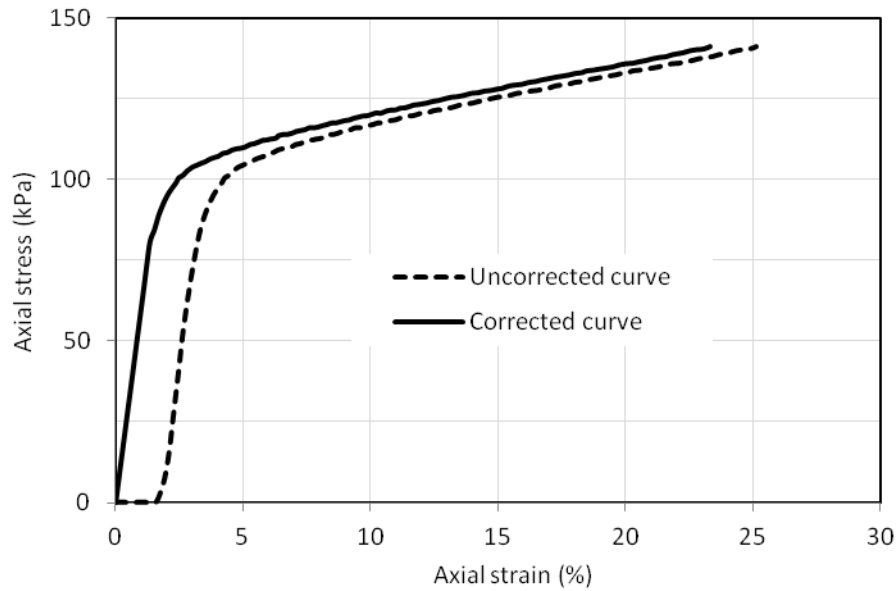
Figure 12.Stress vs. strain curve (64 mm diameter and 20 kg/m³)

The stress-strain curves are used to obtain different parameters. Definitions for most of these parameters are common. However their definition and notations as used in this study are included and shown in Figure 13.

Initial elastic modulus, E_i: is the slope of the initial straight part of the curve.

Post yield modulus, E_p: is the slope of the straight portion of the curve beyond the elastic yield.

Unconfined compressive strength, $\sigma_{c10\%}$: is the compressive stress corresponding to an axial strain of 10 %.

Yield strength, σ_y: is the value of the axial stress corresponding to the intersection point of the initial straight part of the curve and the straight line part beyond yielding. The corresponding axial strain at this intersection is the yield strain, ε_y.

44
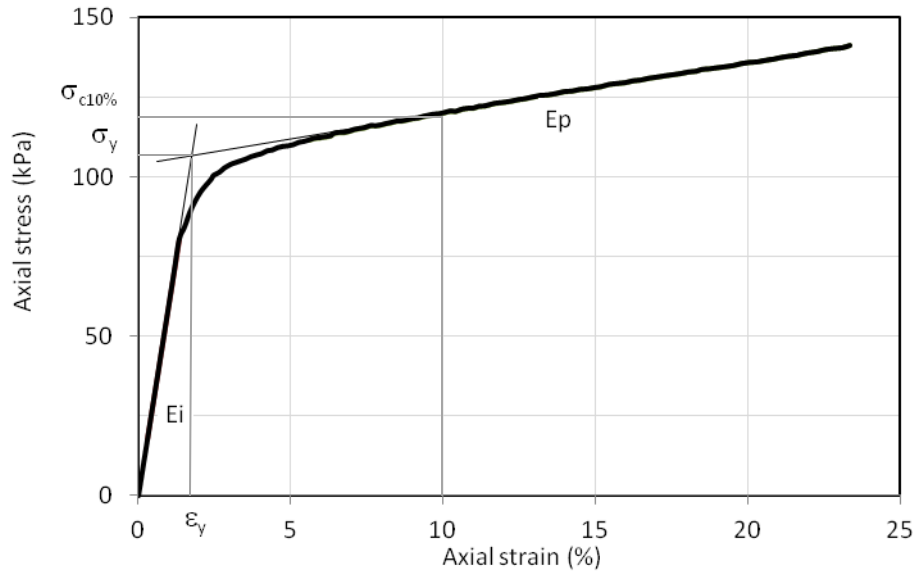
Figure 13. Notations and definition of parameters

Figure 14 shows stress-strain curves for unconfined compression tests with different strain rates, densities, and sample sizes. Values of elastic modulus, compressive strength and yield strength are higher for denser EPS geofoams, Figure 15. Axial strain rate and sample size effects on the initial elastic moduli were minimal for a given density. Nevertheless the compressive strength obtained on tests done with smaller axial strain rates were less than those obtained from tests done with higher axial strain rates. This difference has increased as the density increased, Figure 15.
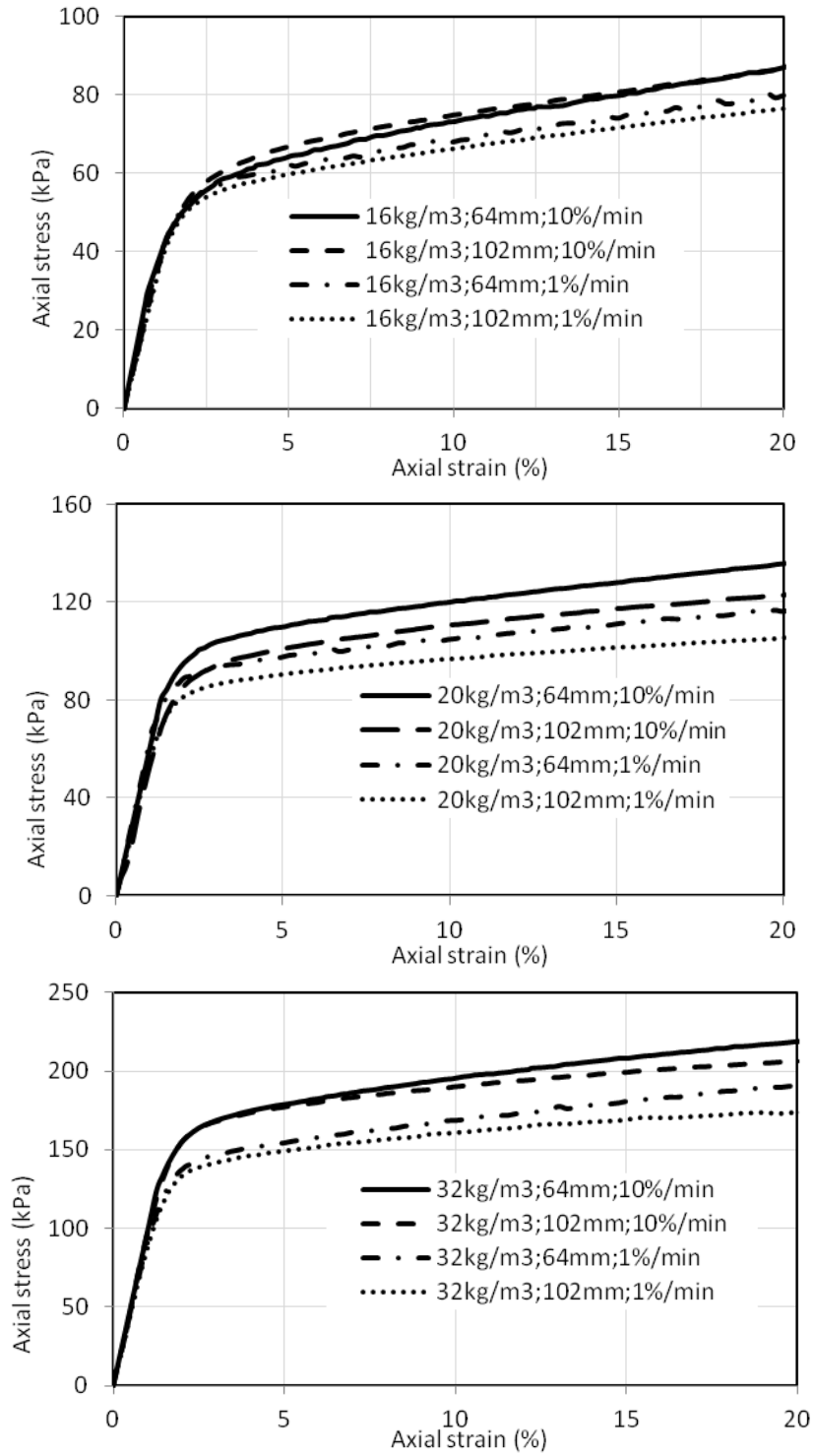
Figure 14. Stress vs. strain curves for unconfined compression
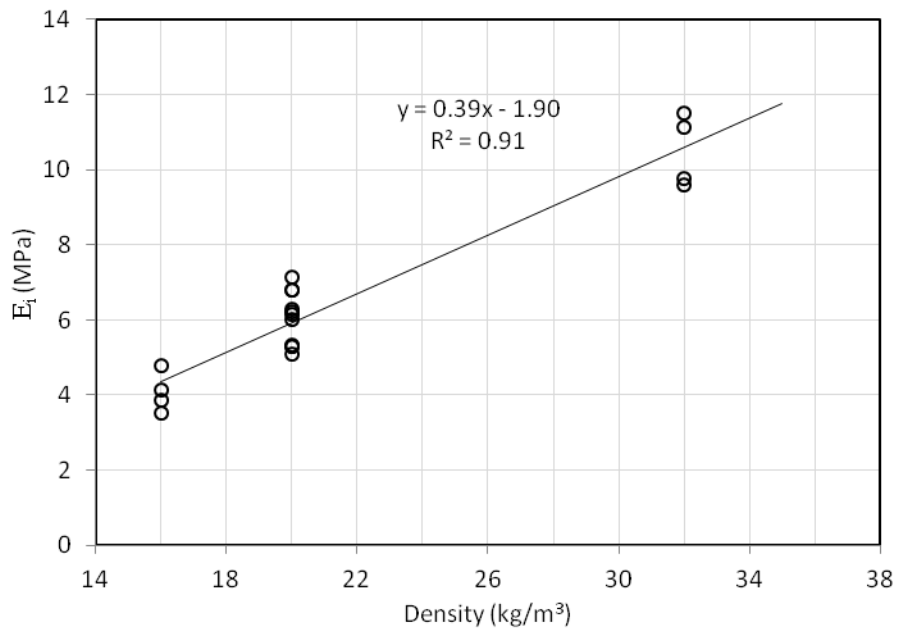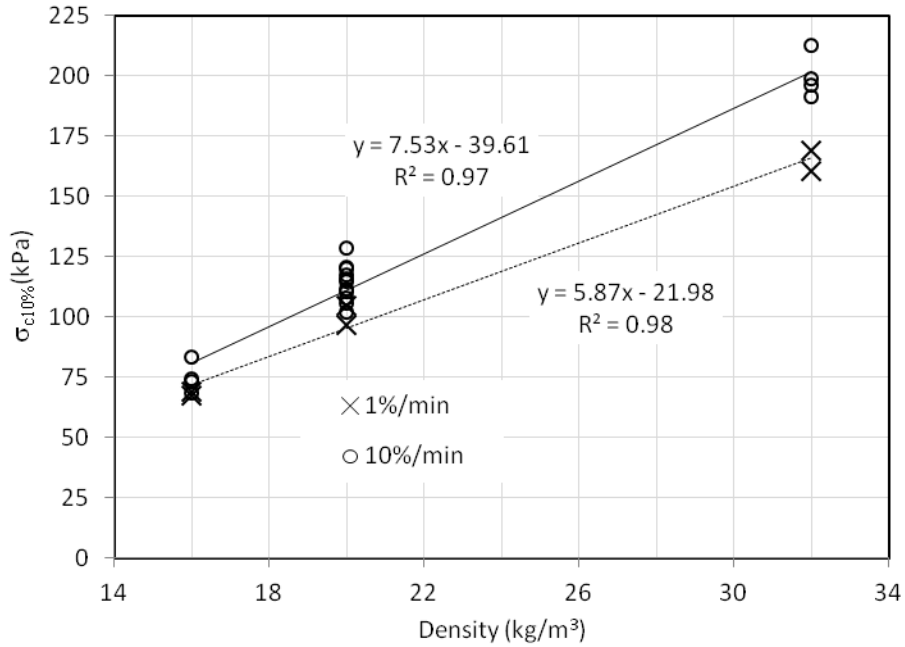
Figure 15. Variation of unconfined compression parameters with density

For sample sizes used in this study, sample size had little effect on the unconfined compressive strength. Parameters from unconfined compression tests will be compared and discussed with those obtained in confined tests later.

47

Initial moduli obtained in this study are shown in Figure 16 along with results from previous studies as a function EPS density. The initial moduli obtained here are seen to be in agreement with those on the upper bound.
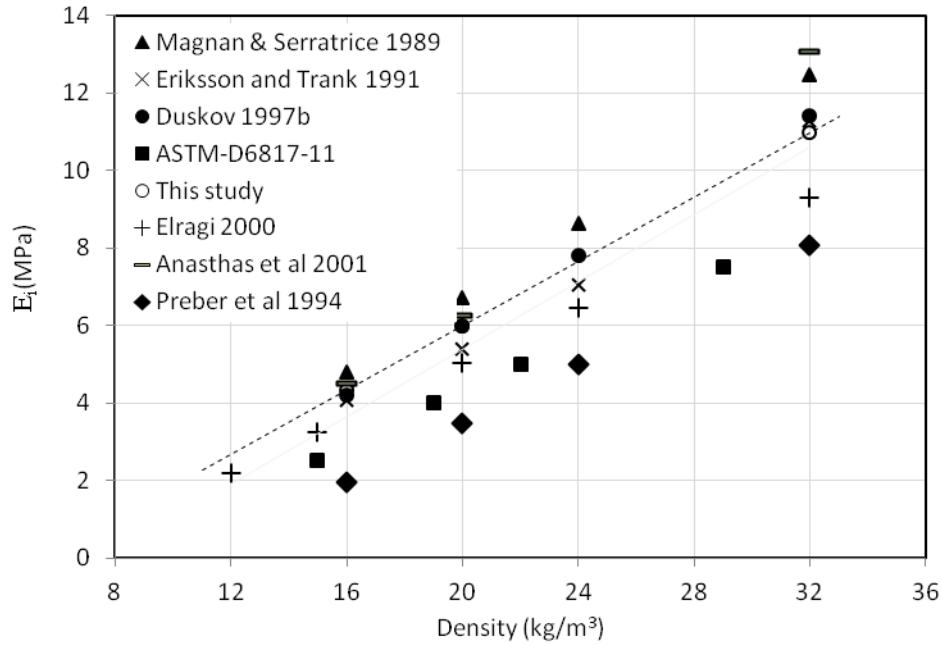
Figure 16. Initial modulus vs. density

The following expression is proposed for initial modulus as a function of density.

$$E_i = 0.4145\,\rho - 2.3039 \qquad (9)$$

where E_i is in MPa and ρ is in kg/m³.

Similarly compression strength at 10 % axial strain is compared with results from previous studies. Figure 17 shows the unconfined compression strength at 10 % axial strain linearly increases with density. There is a reasonably good agreement among the results shown.

48
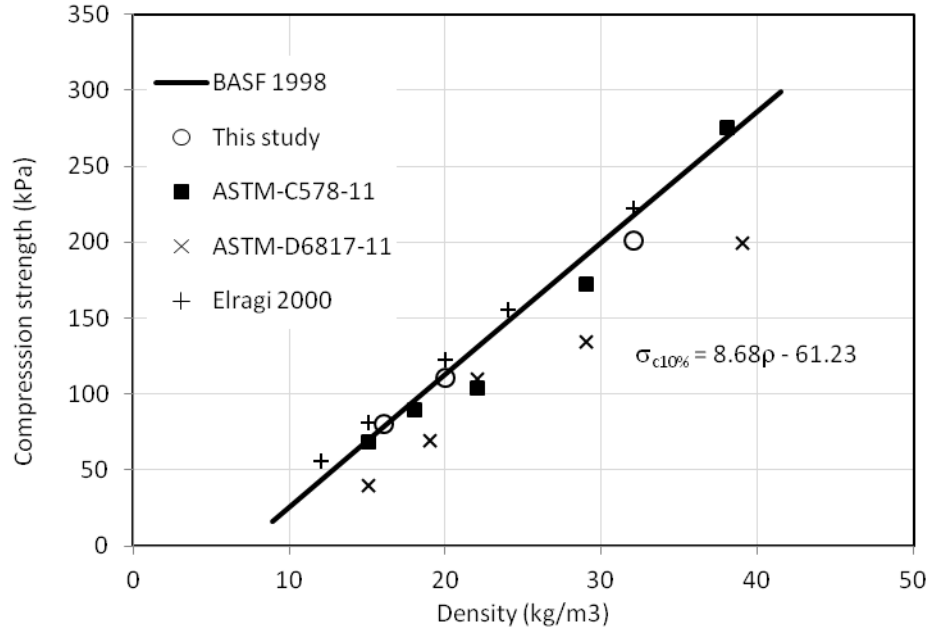
Figure 17. Compressive strength vs. density

The following expression is proposed for compression strength as a function of density.

$$\sigma_{10\%} = 8.6839\,\rho - 61.228 \tag{10}$$

where $\sigma_{10\%}$ is the compressive strength at 10 % axial strain in kPa and ρ is in kg/m^3.

Values of post yield moduli depend very little on density of geofoam, Figure 18. Results from this study and others show similar relation between the post yield modulus and density. The following relation with density is suggested in unconfined compression.

$$E_p = 0.0059\,\rho + 0.0607 \tag{11}$$

where E_p is in MPa and ρ is in kg/m^3.
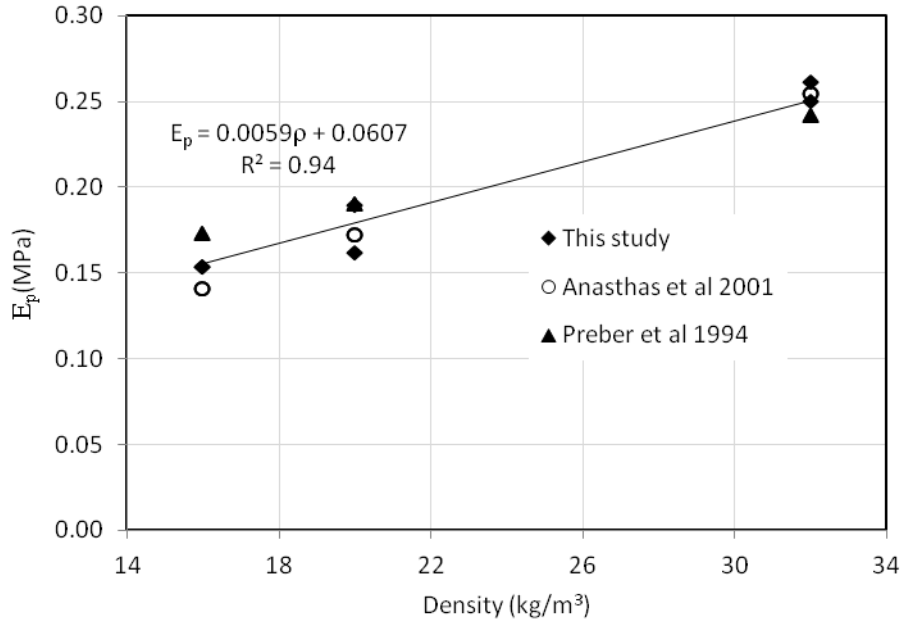
Figure 18. Post yield modulus vs. density in unconfined compression

Volumetric strains were calculated from changes in volume during uniaxial unconfined compression. Figure 19(a) shows a linear relation between volumetric and axial strains. Slope of this line is less than 1.0 suggesting that there is radial inward deformation. This was also evident during testing. However up to axial strain of 1 %, which is the elastic limit, this line has slope greater than 1.0, Figure 19(b). Hence the geofoam deformations were outward radially.
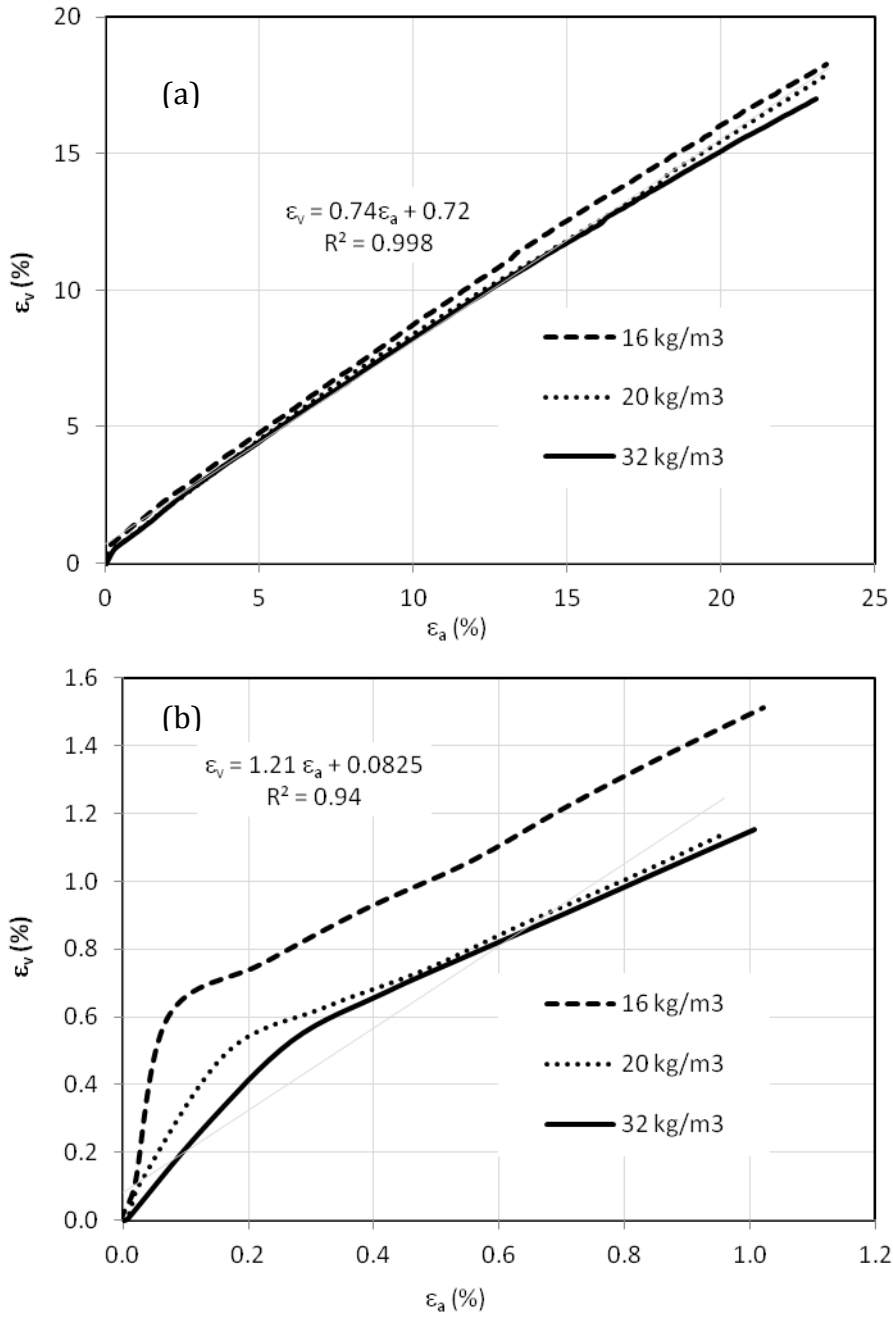
Figure 19. Volumetric strain vs. axial strain in unconfined compression

It should be noted that the relation between volumetric strain and axial strain is independent of density and sample size of the geofoam.

4.1.2 Confined Triaxial Tests

Most of the parameters used for characterization of EPS geofoam are obtained from unconfined compression tests. However, EPS geofoam is also employed in areas where confinement is unavoidable. Effect of confinement on general behavior of EPS geofoam has not been investigated adequately. Possibility of including confining stress effects on analysis and design of geofoams should be examined.

Effect of confinement on short term and long term compression characteristics of EPS geofoam was studied by conducting confined triaxial tests on samples of different densities and sizes. A wide range of confining pressures was employed so as to determine the critical confinement range where changes in the behavior of EPS geofoam can be captured. Bigger confinements were used for higher density geofoams. Confinement pressures of 0 to 207 kPa were used.

4.1.3 Effect of Confinement on the Short Term Compression

A preset constant confining pressure was applied on EPS sample jacketed in a rubber membrane at the same time as axial loading started. The cell pressure was measured by a pressure transducer; volumetric deformation of the sample was obtained from the volume of water pushed in to the triaxial cell using differential pressure transducer. The axial strain and stress were measured by use of LVDT and load cell, respectively. The stress-strain curves obtained in confined tests were similar in shape to those obtained during unconfined compression tests. The stress-strain response of EPS geofoam samples under uniaxial compression but with different confining pressures are shown in Figure 20 through Figure 22. These test results are for samples of nominal diameters 64 mm and 102

mm and aspect ratio 2:1. The stress vs. strain curves were corrected for seating errors and showed bilinear stress-strain relationship. For EPS geofoam of 16 kg/m^3 density Figure 21 shows consistent decrease in both the strength and initial tangent modulus as the confining stress increases. For confining pressure increase from 0 to 69 kPa, initial modulus decreased from 4.15 to 1.58 MPa and compression strength at 10 % axial strain reduced from 73 to 38 kPa. The modulus and strength decreased to about 40 and 50 % of unconfined compression values respectively. Such very big effect on these design parameters is not taken in to account in practice. Thus EPS fill designed with unconfined compression strength and modulus would experience about 50 % increase in deformation. Confining pressure of 69 kPa can result from pressure head of about 7 m. Further increase in the confinement pressure has an opposite effect on these parameters. The situation reversed at a certain confining pressure level. This confining pressure is between 69 and 103 kPa. The exact determination of its magnitude may not be easy but an attempt can be made by using smaller confinement pressure increases between tests having confinements of 69 to 103 kPa. The modulus and compressive strength started increasing from their smallest magnitude corresponding to the shift.

   Similar observations can be made from Figure 21 and Figure 22. For 20 kg/m^3 density, an increase in confining pressure from 0 to 103 kPa resulted in a decrease in the strength and modulus from 112 to 50 kPa and 6.80 to 1.92 MPa respectively. The reduction was about 45 and 30 % of strength and modulus of unconfined compression values respectively.

   When the confining pressure increased from 0 to 172 kPa, the initial modulus reduced from 9.78 to 5.81 MPa and the strength from 196 to 89 kPa for a density of 32 kg/m^3. Up to

60 % and 45 % of the unconfined compression values are obtained respectively for modulus and strength for confining pressure of 172 kPa.

The confining pressure level at which a shift from decrease in modulus and strength to increase was dependent on the density of the geofoam. This confining pressure was between 103 and 138 kPa for 20 kg/m³ and for 32 kg/m³ it was between 172 and 207 kPa. Denser geofoam required higher confining pressure to reach this shift in behavior. The exact confining pressure values at which this shift occur should be found by using a smaller pressure increase step between tests near the thresholds. These values are observed to be very close to the unconfined yield strength and are discussed later.
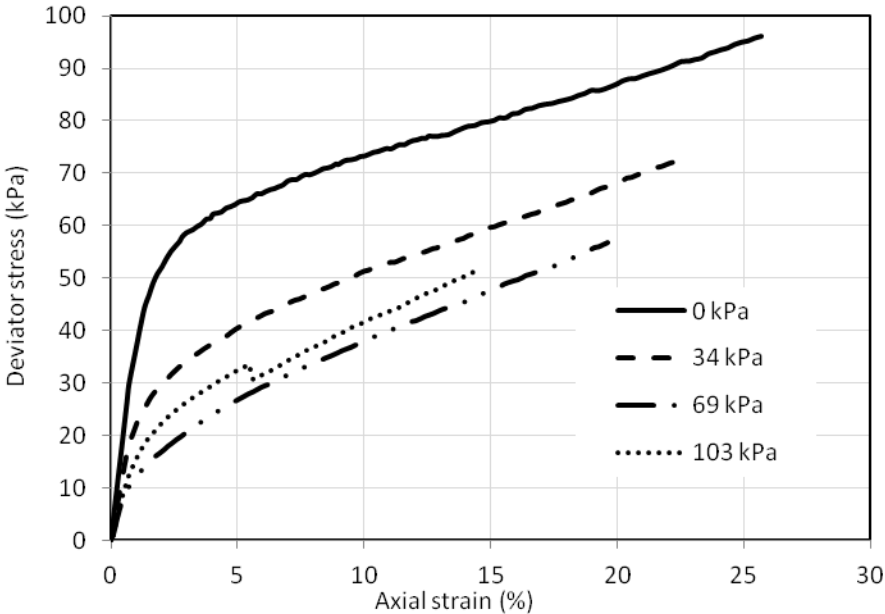
Figure 20. Deviator stress vs. strain plots (16 kg/m³ and 64 mm diameter)
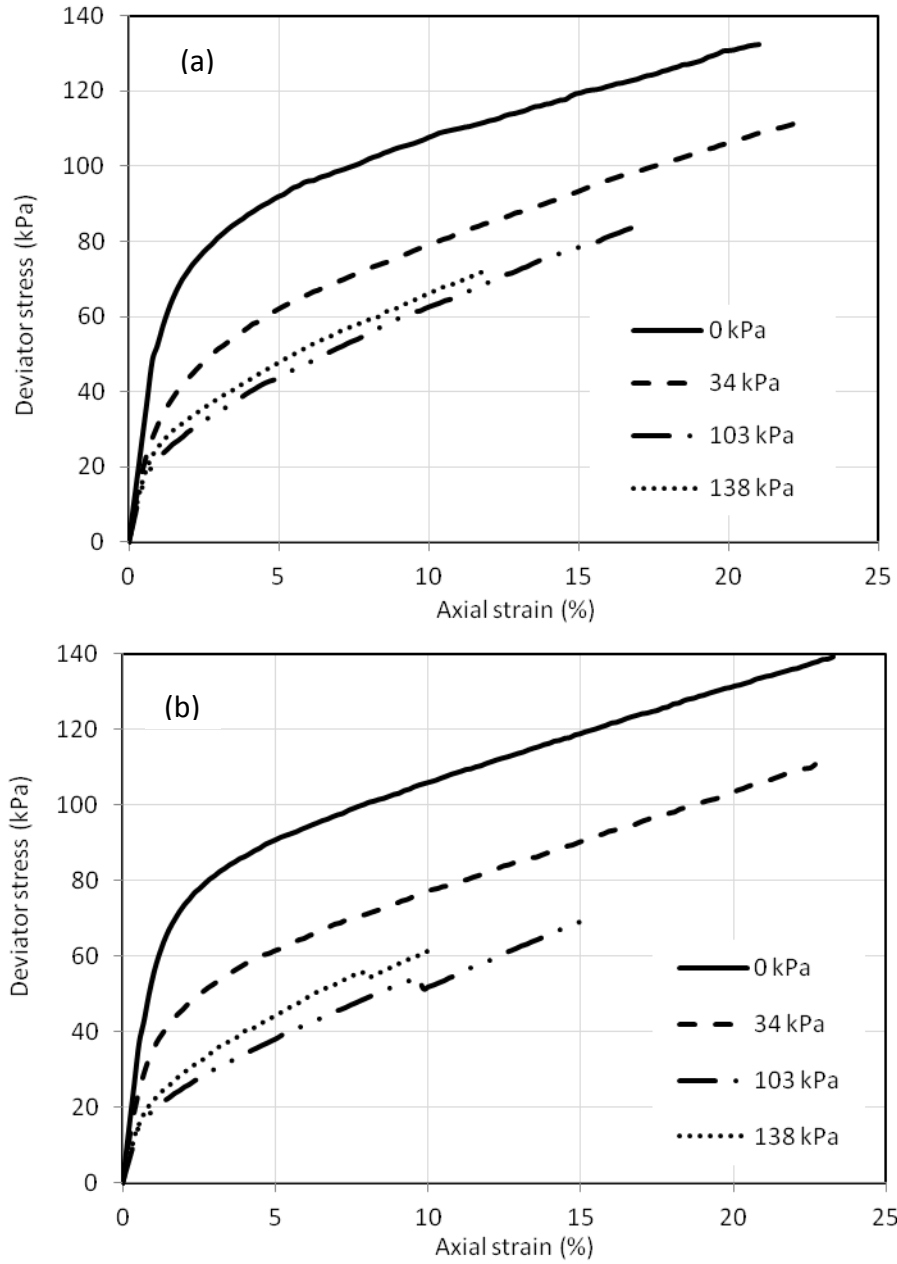
Figure 21. Deviator stress vs. strain for 20 kg/m³ (a)64 mm (b)127 mm diameter
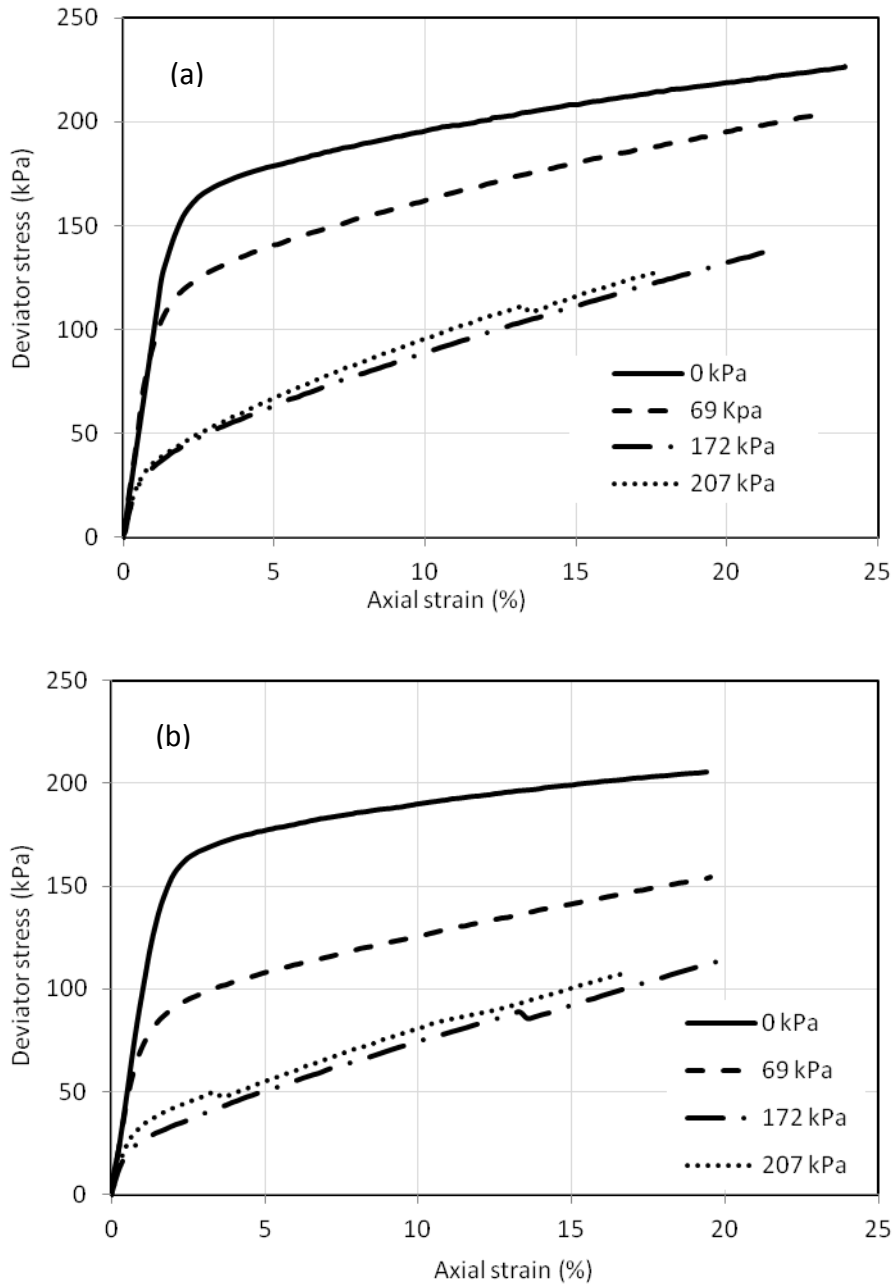
Figure 22. Deviator stress vs. strain for 32 kg/m³ (a)64 mm (b)127 mm diameter

Even though higher confining stresses are not common in practice, it is of academic

interest to investigate effect of such confinement on the behavior of EPS geofoam. Tests

were done for higher confining stresses and Figure 23 shows such test results. The

behavior observed is similar to that of soils; where the strength and initial modulus

increase with confining stresses. Thus there is confinement stress level at which the

geofoam will start behaving like soil towards application of confining pressure. This stress

level depends on the density of geofoam and gets higher as the density increases. It should

be pointed out here that the confinement level should be stated when referring to effects

on the behavior of EPS geofoam.
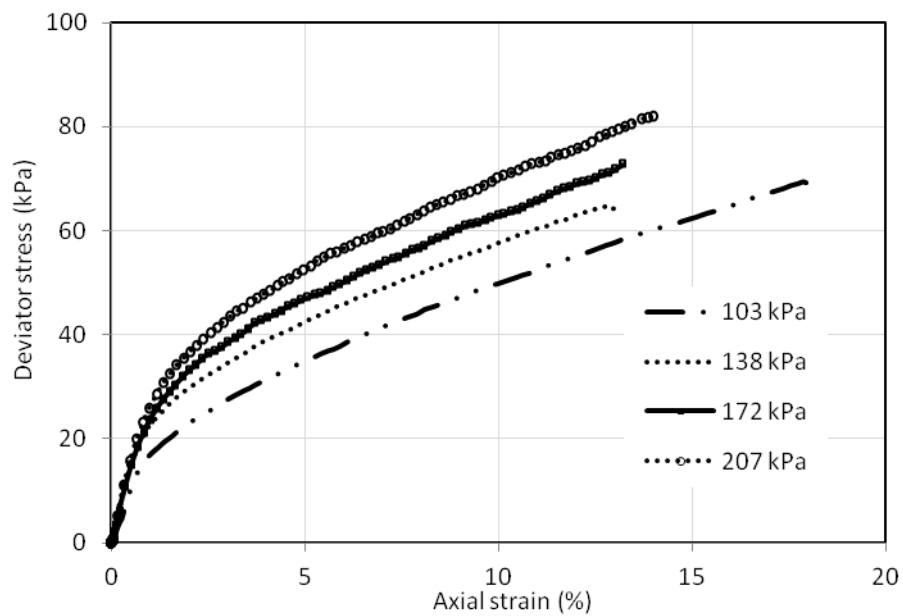
Figure 23. Deviator stress vs. strain plots for higher confining stresses (20 kg/m³)

Stress–strain curves for uniaxial compression stages as shown in Figure 24 are offset by

the axial strains that developed as confining pressures were applied. Strain contributions

from both the confining and uniaxial compression stages were considered to compare with

limit stress states at 1 or 10 percent axial strain. Depending on the confining pressure level,

limit stress states were reached with combination or separate application of confining and

deviator stresses. For example, the deviator stresses for 1 and 10 percent axial strain under

unconfined compression were about 55 and 101 kPa, respectively. For 69 kPa confinement; 1 percent axial strain occurred under the confining pressure only and the deviator stress at combined 10 percent strain was only 55 kPa. Whereas, both 1 and 10 percent limit strains developed only under 138 kPa or greater confining pressures.
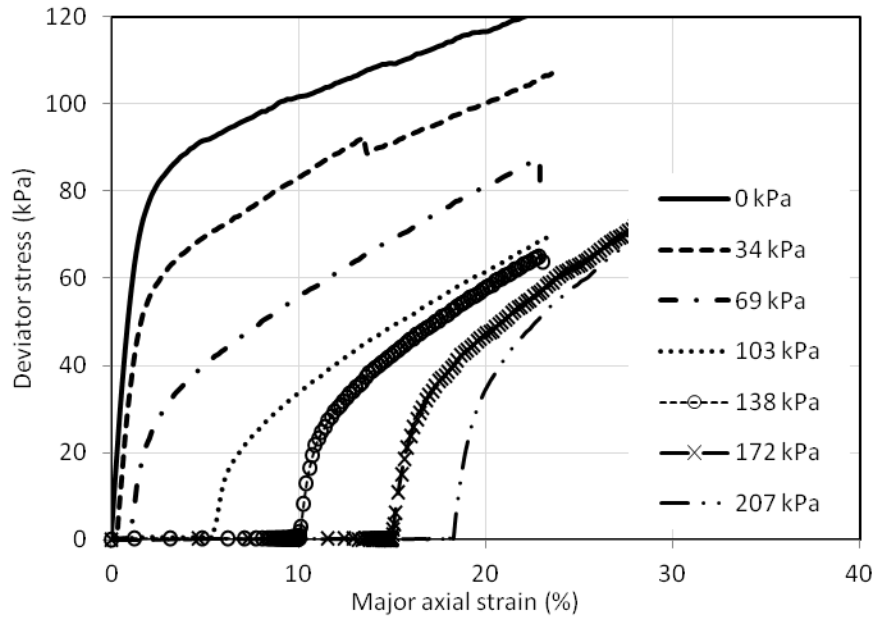
Figure 24. Deviator stress vs. major axial strain plots (20 kg/m³)

Volumetric strains that developed under different confining pressures and the respective uniaxial compression stages are shown in Figure 25. The uniaxial compression states began from close to the line of 1:3 slope. This line represents states for isotropic responses to neutral or hydrostatic pressures. Thus the EPS geofoam samples were inherently isotropic in responding to uniaxial loading at each confinement level.
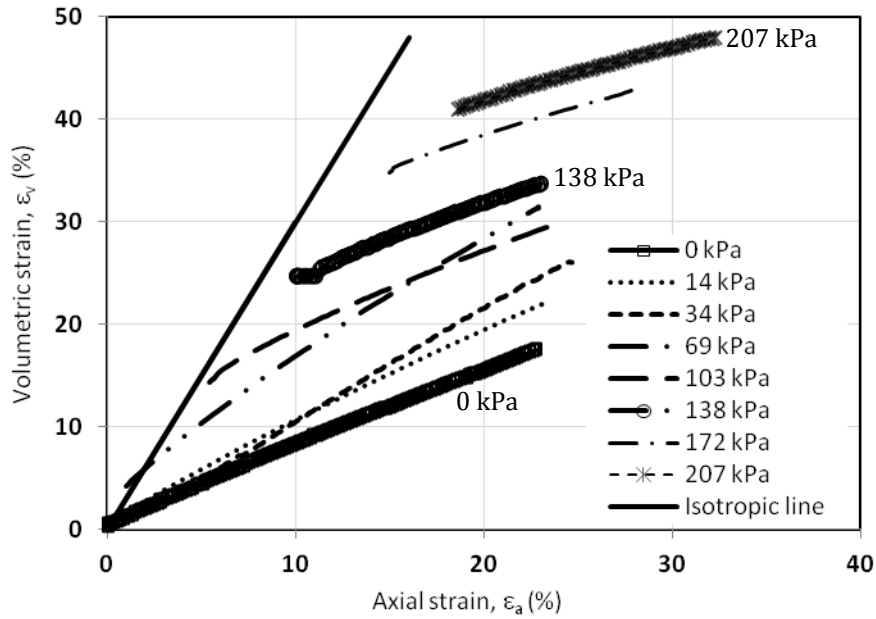
Figure 25. Volumetric and axial strains for uniaxial compression under different confining

pressures (20 kg/m³)

4.1.3.1 Effect of Duration of Confinement

It was stated that the confining pressure was applied at the same time as the initiation of

the axial loading. Tests were done to examine the effect of duration of confinement on the

response of EPS for the same state of test conditions. Figure 26 shows triaxial tests done

with a confining pressure of 34 kPa. In one case the confining and axial loading are applied

simultaneously. In the other case the axial loading was started after 15 days of application

of 34 kPa confining pressure. The initial elastic modulus and strength at 10 % axial strain

were not affected much. It looks like that margin of error is small like the one that could

have resulted when doing the same test using different samples.
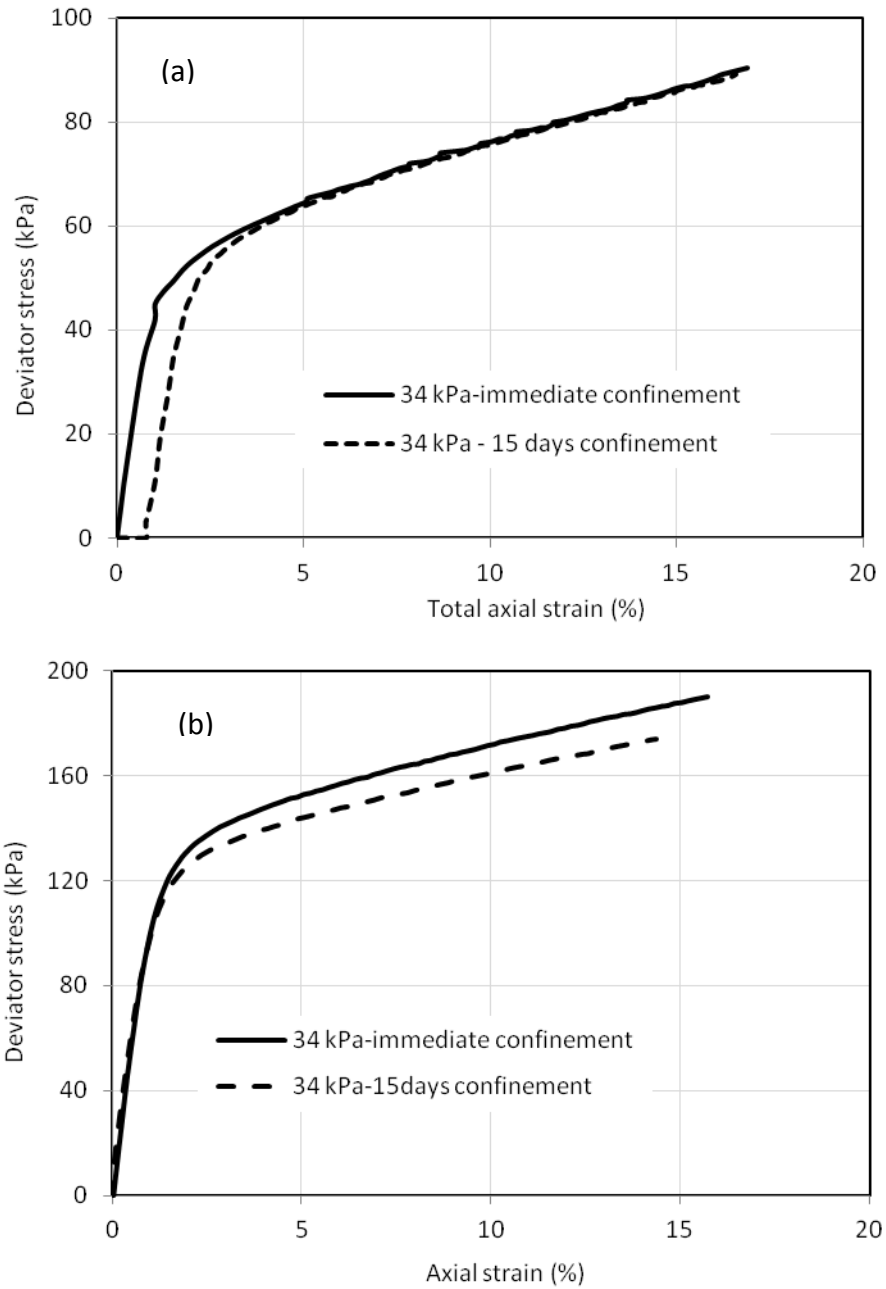
Figure 26. Effect of duration of confinement (a) 20 (b) 32 kg/m³

And hence effect of duration of confinement was neglected in this study and most of the tests were done by applying confining pressure and axial loading at the same time.

4.1.3.2   Effect of Density on Short Term Compression

The stress-strain curves for higher density samples in unconfined compression test were shown to plot above those with lower density. Elastic modulus and compressive strength values were higher for denser geofoams. Confining pressure effects for 64 mm diameter and 127 mm high samples but for two different densities are shown in Figure 27. The compression strength at 10 % strain decreased by about 20 % over confining pressures of 0 to 69 kPa for 32 kg/m³ density. It decreased by over 50 % for the same confining pressure range but 16 kg/m³ density. The moduli were relatively unchanged for the 32 kg/m³ density but successively decreased for the 16 kg/m³ density. The initial modulus decreased by about 60 % for confining pressure increase from 0 to 69 kPa. The lower density EPS geofoam was much more affected by the confining pressures of up to 69 kPa. This is because 69 kPa confining stress is close to the value at which the geofoam behaves much like soils, where increase in confinement favors strength. The confining pressure at which such shift in behavior towards confinement occurs is higher for denser geofoams as mentioned above. With much higher confining pressures, the dense EPS geofoam also experienced significant modulus and strength reduction.

For high confining pressures, the geofoam behaved like soils in that the stress-strain curves for higher confining pressures plotted above those with smaller confining pressure. Figure 28 shows results for samples of the same size but different density. However the increase in initial modulus and compression strength was relatively small.
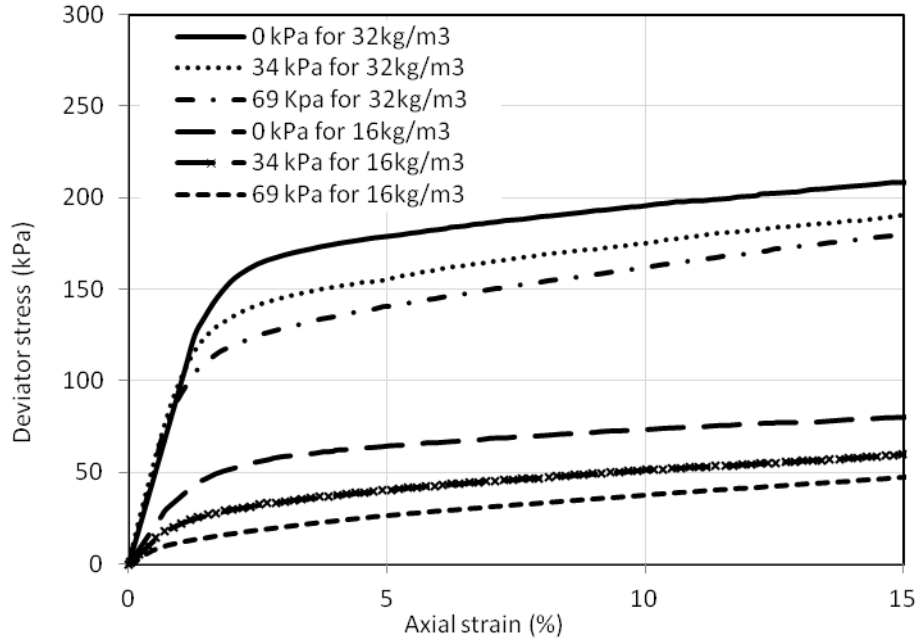
Figure 27. Effect of low confinement for different densities
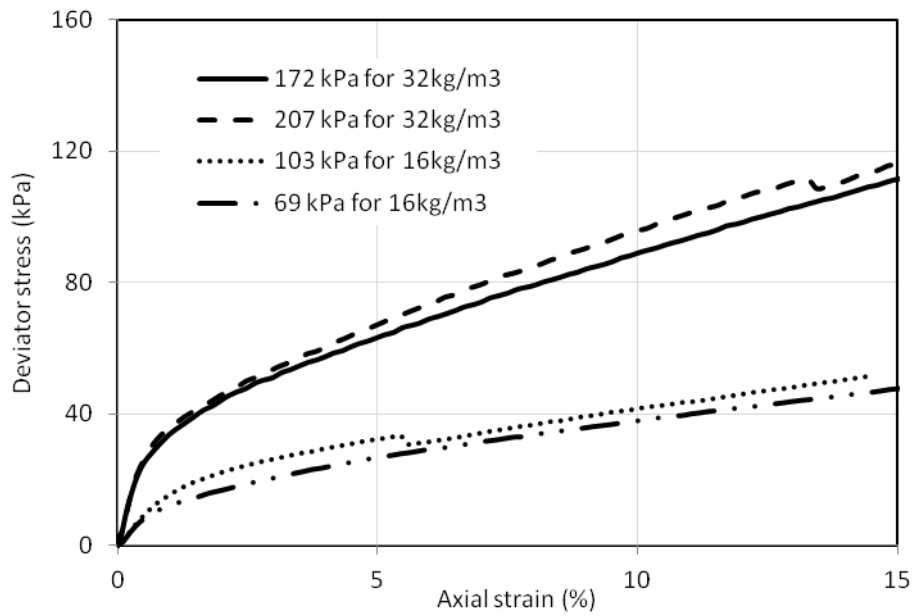
Figure 28. Effect of high confinement for different densities

4.2   Compressive Strength and Modulus of Elasticity

Compression strength and modulus are among the most important parameters for analysis and design of EPS geofoam. This section summarizes effect of confinement on the compressive strength and modulus of elasticity of EPS geofoam as obtained in this study. Practical relevance of effect of confinement in design and analysis of EPS geofoam will be discussed.

Triaxial tests were done for confining pressures ranging from 0 to 60 kPa to develop an elastoplastic hardening constitutive model for EPS geofoam(Leo et al. 2010; Wong and Leo 2007, 2006). The samples used were cylindrical of size 50 mm in diameter and 50 mm in height. All had the same density of 20 kg/m^3. Drained shearing was made with axial loading rate of 0.4 %/min after the volume change due to confining pressure stabilized. Results indicated increase in confining pressure caused in reduction in the strength (Figure 29). The initial Young's modulus for all cases was reported more or less constant (E=3.95 MPa). Triaxial compression tests were done by Atmatzidis and others (Atmatzidis et al. 2001) for a wide range of densities and limited confining pressures. Cylindrical samples 50 mm diameter with aspect ratio of 2 were used. Tests were conducted using three different cell pressures corresponding approximately to 20, 40 and 60 % of the yield stress. The axial load was applied at rate of 1 %/min. The experimental results indicated a reduction in initial modulus and strength as can be seen in Figure 29.

Chun et al. 2004, 2001 conducted triaxial tests for 15, 20, 25, and 30 kg/m^3 densities under confining stresses of 0, 20, 40 and 60 kPa. Cylindrical samples with 50 mm diameter and 100 mm height were used. The axial loading was applied at a strain rate of 1 %/min. Their results suggested higher compressive strengths and initial tangential moduli with

63

increasing either density or confining stresses. However the deviator stress was shown to decrease with increase in confining stress as in Figure 29.

Padade and Mandal 2012 conducted a series of unconsolidated undrained triaxial tests on cylindrical specimens (diameter=75 mm and height=150 mm) for four densities (15.3, 20.34, 22.43, and 30.59 kg/m^3) and presented the results as Mohr's circle plots. Shear strength parameters were inferred from such plots. Confining stresses of 50, 100 and 150 kPa were used for these tests. A constant strain rate of 0.8 %/min was used. Inferred strength results of this study are included in Figure 29. The authors suggested that the strength increased as the confining stress increased. However when the unconfined strength was plotted together with those from the confined tests, the strength decreased initially and then increased with further increase in the confining stress. Thus such outcomes call for stating the confinement range for a specific density when considering effect of confinement on strength.

(Leo et al. 2008) conducted true triaxial tests to investigate the behavior of EPS geofoam. Prismatic blocks of 70 x 70x 140 mm and 16 kg/m^3 density were tested by applying controlled stress at a rate of 75 kPa per minute. The strengths and moduli decreased under increasing confining pressures.

Preber et al. 1994 performed uniaxial compression and undrained triaxial tests on EPS geofoam for four densities (16, 20, 24, and 32 kg/m^3) and four confining stresses (0, 21, 41, and 62 kPa). Although use of cylindrical sample was implied, the size was not specified. The results indicated the strength and initial modulus decreased with increasing confining stresses. This confining stress effect on the strength is summarized in Figure 29.

64
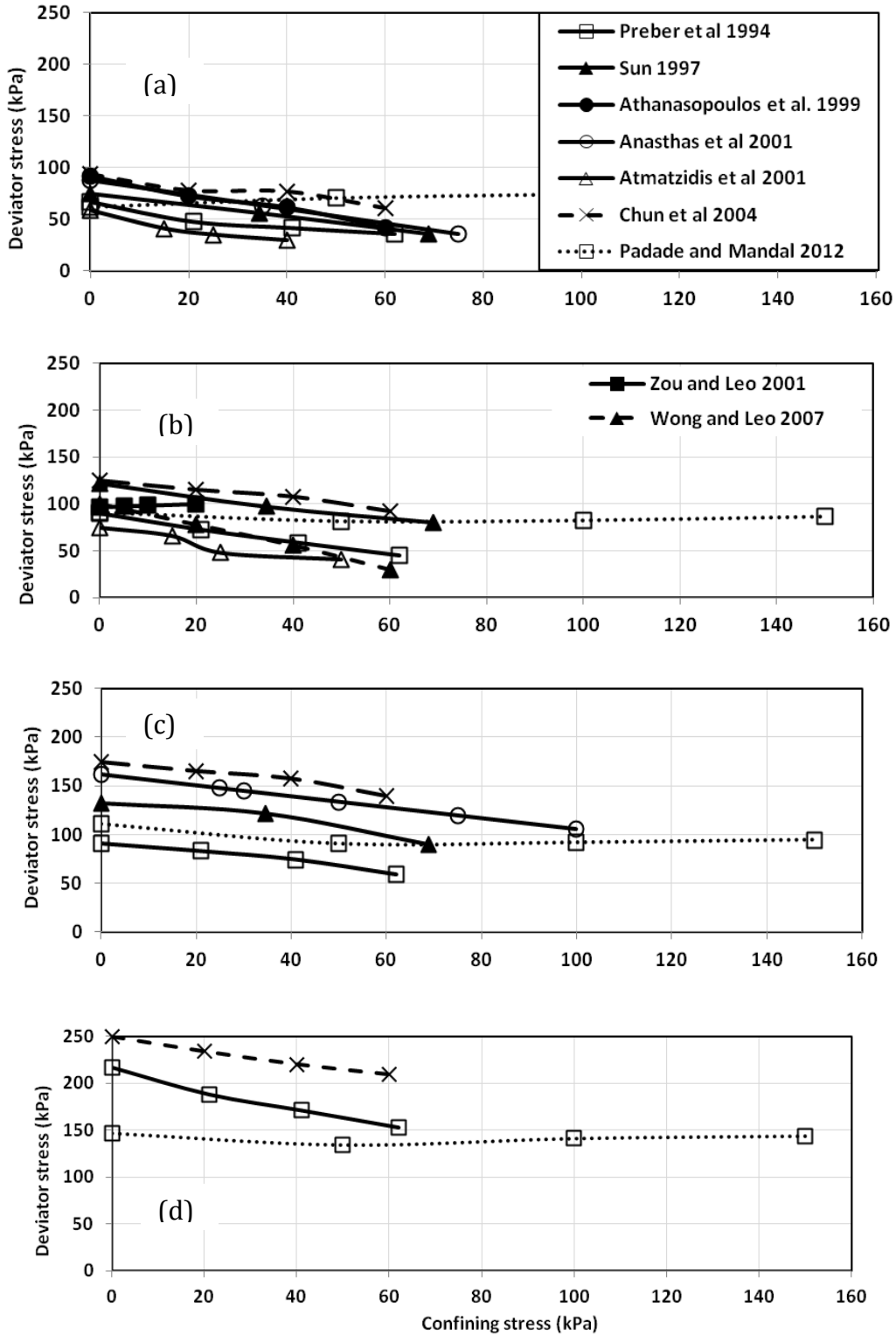
Figure 29. Plot of deviator stresses vs. confining stress from previous investigators

(a)16 kg/m³ (b) 20 kg/m³ (c) 24 kg/m³ (d) 32 kg/m³

Compressive strength results from undrained triaxial compression tests on 20kg/m^3 density cylindrical samples of 50 mm diameter and height reported by (Zou and Leo 2001) are shown in Figure 29. Gain in strength was observed with increasing confining stresses ranging from 5, 10, 15 and 20 kPa subjected to axial loading rate of 10%/min were employed during testing.

Athanasopoulos et al. 1999 reported that the compressive strengths and elastic moduli decreased with an increase in confining stress (see Figure 29). Triaxial tests were done on cylindrical samples of 71.5 mm in diameter and 150 mm in height at an axial loading rate of 3.3 %/minute. Confining stresses of 0, 20, 40, and 60 kPa were used. Only samples of 17.5kg/m^3 density were investigated.

Anasthas et al. 2001 performed triaxial tests on cylindrical samples of diameter and height 76 mm and 915 mm respectively. Nominal densities of 16 and 26 kg/m^3 were used with confining stresses of 0, 25, 35, 50, 75, and 100 kPa. A strain rate of 10 %/min was employed with the duration of confinements of 0, 3, and 24 hrs. The results from these tests showed that duration of confinement had little effect and the strength and modulus decreased with increase in confining stress. Expressions relating compressive strength with confinement were presented and results from these tests are included in Figure 29.

Sun 1997 reported a compressive strength reduction of up to 57 % when the confining stress increased from 0 to 68.9 kPa for 14.4 kg/m^3, density geofoam. For 50 mm cube samples of 14.4, 20.4 and 22.4 kg/m^3 density, confining stresses of 0, 34.5, and 68.9 kPa and constant strain rate of 10 %/min were used. Data obtained from these triaxial tests are also included in Figure 29.

Unconfined and triaxial tests done in this study considered wide range of confining stresses and three densities. Test results are discussed and compared with others. Figure 30 shows that modulus and compressive strength reduced with an increase in confining pressure up to a certain confining pressure value. These results are for 20 kg/m³ density and 64 mm nominal diameter samples. With further increase in confining pressure the modulus increased but the rate at which the modulus increased with confinement was gradual. The confining pressure value at which this shift happened was between 69 and 103 kPa but very close to 103 kPa.
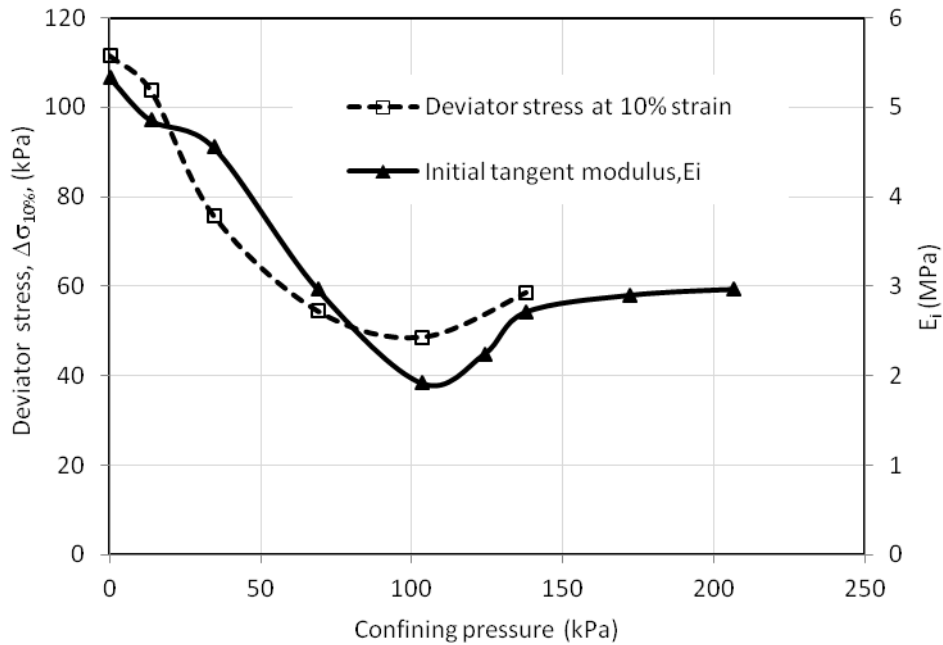
Figure 30. Effect of confining pressure on modulus and strength at 10 % strain, $\Delta\sigma_{10\%}$

Thus effect of confinement on EPS geofoam should be considered in two confining pressure ranges-low and high confining pressures. *Low confining pressure range* for a given density is the pressure range at which a decrease in both the initial modulus and strength

are observed with an increase in confining pressure. On the contrary, *high confining*

pressure range is the confining pressure range at which both strength and modulus

increase with an increase in confining pressure. EPS geofoam of 16 kg/m³ density showed

the low confining pressure range is from 0 to 69 kPa whereas the corresponding value for

32 kg/m³ density is about 0 to 172 kPa. But the high confining pressure ranges are

confinements greater than 69 kPa and 172 kPa for densities of 16 kg/m³ and 32 kg/m³

respectively.

Different densities of EPS geofoam samples were tested and Figure 31 and Figure 32

show effect of confining stresses on initial modulus and compression strength. It can be

noted that the higher the density, the higher are the initial tangent modulus and the

strength at 10 % axial strain.
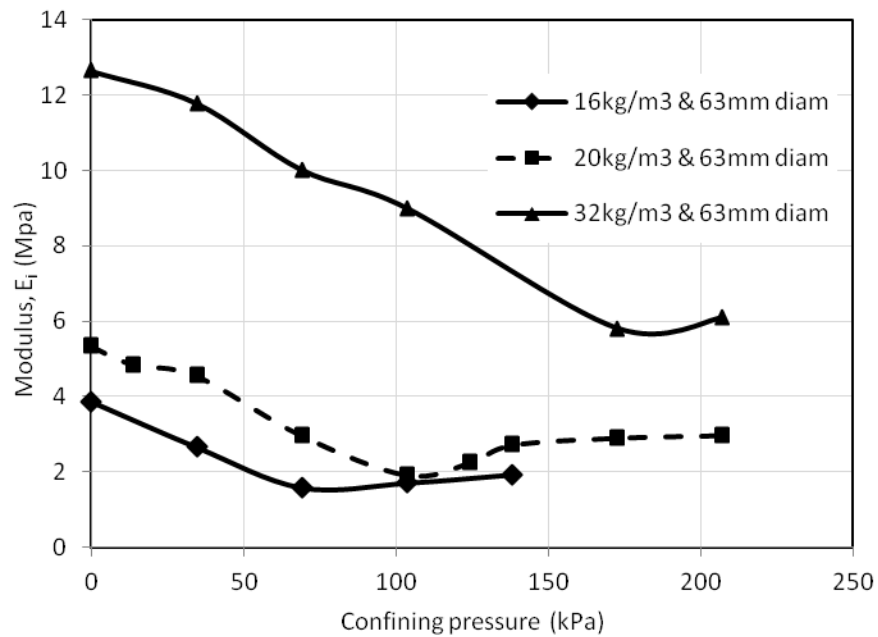
Figure 31. Effect of confining pressure on initial tangent modulus
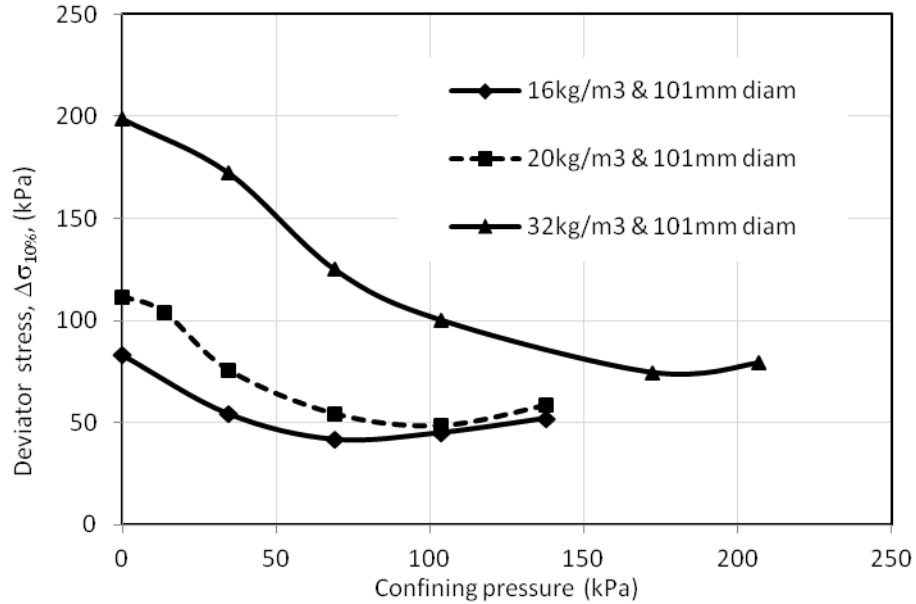
Figure 32. Effect of confining pressure on the strength, $\Delta\sigma_{10\%}$

Initial tangent modulus and compressive strength for low confining pressure ranges were used to fit curves that relate with density and confining pressures. Figure 33 shows relations between compression strength with confining pressure.

Sample size differences are shown to affect the expressions obtained. However variations in the results are minimal and thus are combined to get general expressions, Figure 33 (c). The expressions relating compression strength at 10 % axial strain and confinement are given below for different densities.

(16 kg/m³) $\qquad\qquad \Delta\sigma_{10\%} = -0.6\,\sigma_c + 77$ $\qquad\qquad\qquad$ (12)

(20 kg/m³) $\qquad\qquad \Delta\sigma_{10\%} = -0.6\,\sigma_c + 105$ $\qquad\qquad\quad$ (13)

(32 kg/m³) $\qquad\qquad \Delta\sigma_{10\%} = -0.7\,\sigma_c + 199$ $\qquad\qquad\quad$ (14)

σ_c and $\Delta\sigma_{10\%}$ are in kPa.

69
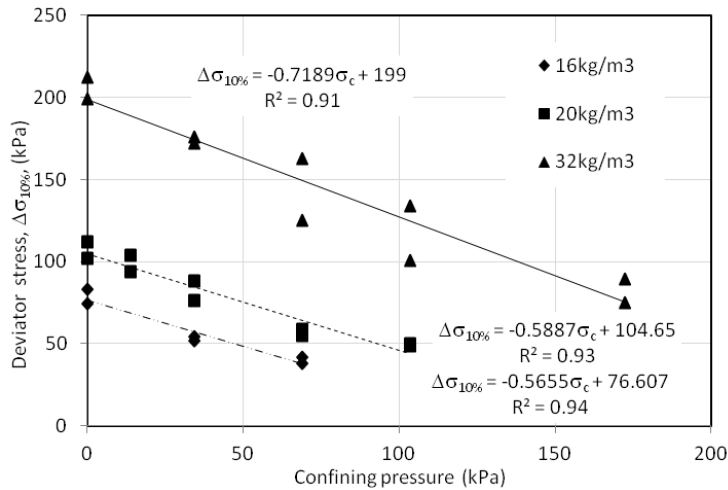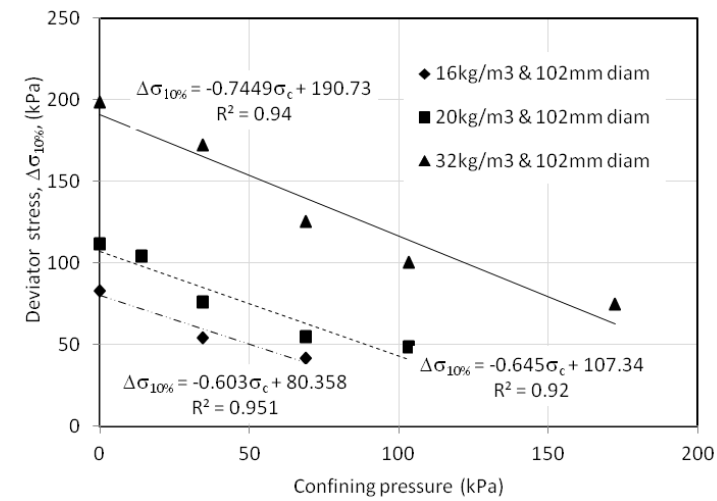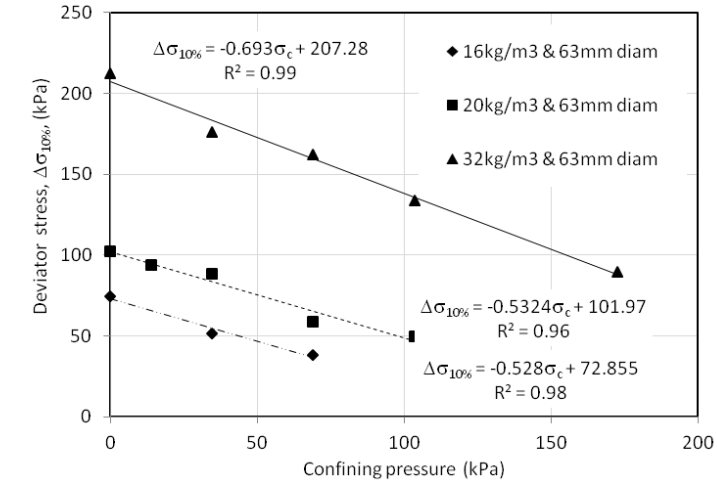
Figure 33. Deviator stress vs. confinement for different densities (a) 64 mm (b)102mm (c) 64 & 102 mm diam. combined

The compression strength at 10 % axial strain was plotted with results of other previous investigators. The trend followed was same among most of the results. All results from different investigators are lumped to one for same density as shown in Figure 34. Even though the trends followed were similar in most studies, smaller R^2 values suggest that combined plots fit poorly for each density. Such scattered results may be due to differences in sample densities, sizes and shapes.
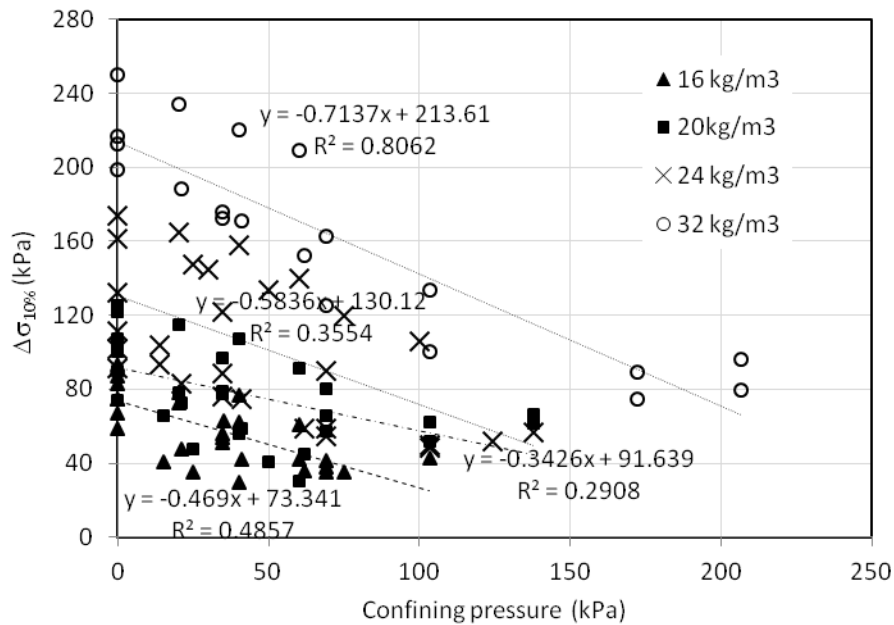
Figure 34. Deviator stress vs. confinement for different densities (Lumped results)

Initial tangent modulus decreased linearly with confinement for low confining pressure ranges. This is explained by the R^2 values which are about 1.0 in Figure 35. Figure 35 (a) and (b) show that if only one sample size was considered for a given density, the linear fit was excellent. Results from mixed sample sizes showed the same linear variation but the fit has less R^2 values but still acceptable, Figure 35 (c). However, use of such expressions obtained from mixed sample sizes may not result in big variations in the results.

71
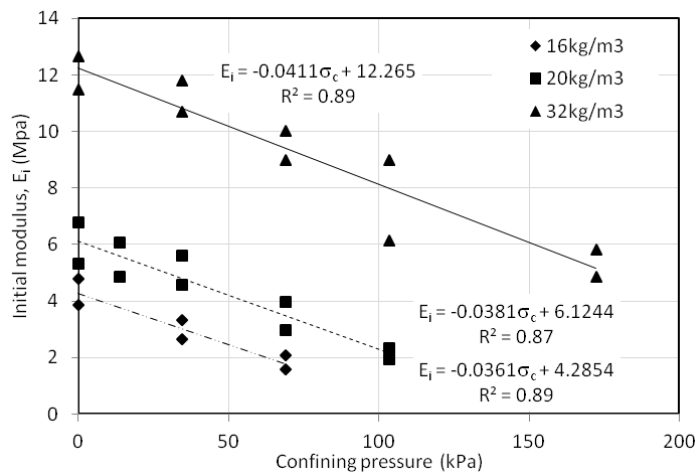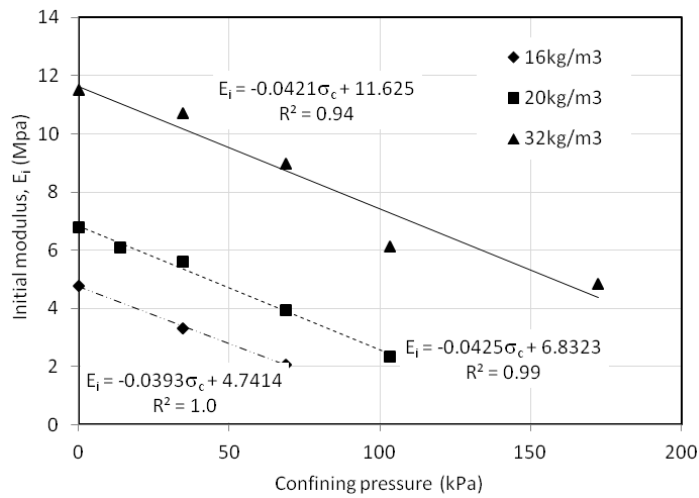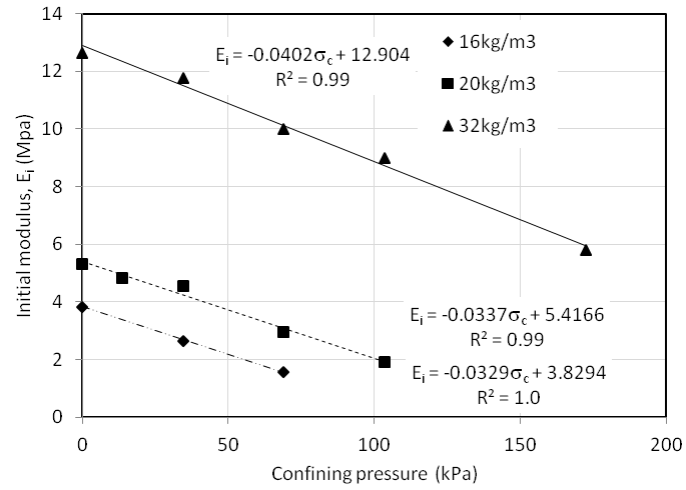
Figure 35. Modulus vs. confining pressure for different densities (a) 64 mm

(b)102mm (c) 64 & 102 mm diam. combined

Anasthas et al. 2001 provided general expressions relating the initial and post yield modulus as follows.

$$E_i(\text{MPa}) = 0.0001\,\rho\,\sigma_c + 0.008\,\rho^2 + 0.152\,\rho + 0.015 - 0.041\,\sigma_c + 0.00006\sigma_c^2 \quad (15)$$

$$E_p(\text{kPa}) = -0.01\,\rho\,\sigma_c - 0.051\,\rho^2 + 9.566\,\rho + 0.966 + 1.812\,\sigma_c - 0.005\sigma_c^2 \quad (16)$$

where ρ is density in kg/m^3 and σ_c is the confining pressure in kPa

Preber et al. 1994 conducted confined triaxial tests with samples of density 16, 20, 24 and 32 kg/m^3. Confining pressures of 0, 21, 41 and 62 kPa were used. The initial modulus, yield strength and post yield modulus were related with both density and confining pressure using generalized equations given below.

$$E_i = (-4180 + 39000\,\gamma) + (-6.2 - 53\,\gamma\,)\sigma_c \quad (17)$$

$$E_p = (104 + 440\,\gamma) + (-3.6 + 150\,\gamma\,)\sigma_c \quad (18)$$

$$Y_o = (1.4 + 905\,\gamma) + (-1.1 + 4.50\,\gamma\,)\sigma_c \quad (19)$$

$$I = (-107 + 910\,\gamma) + (0.63 - 6.32\,\gamma\,)\sigma_c \quad (20)$$

$$Y_o = (1.4 + 905\,\gamma) + (-1.1 + 4.50\,\gamma\,)\sigma_c \quad (21)$$

$$X_o = {}^I\!/\!{}_{(E_i - E_p)} \quad (22)$$

where σ_c = confining pressure in kPa

γ = unit weight of EPS geofoam in kN/m^3

E_i and E_p is the initial and post yield modulus respectively in kPa

X_o is the strain value at the intersection of the initial tangent line and the plastic tangent line.

Y_o is the axial stress value corresponding to strain X_o

I = intersection of the axial stress axis and the plastic tangent line

The following expression was proposed for axial stress-strain relationship of EPS block.

$$\sigma = \left(I + E_p \, \varepsilon\right) \left[1 - \exp\left(-C \, \varepsilon^2 - \frac{E_i \, \varepsilon}{I}\right)\right] \qquad (23)$$

where $\qquad C = -\dfrac{E_i}{I \, X_o} - \dfrac{1}{X_o{}^2} \, \ln\left[1 - \dfrac{Y_o}{(I + E_p X_o)}\right]$ $\qquad$ and all other terms are given above

Figure 36 shows plots of initial tangent modulus vs. confining pressure from this study with others. The initial moduli from Preber (Preber et al. 1994) seem to be underestimated. It can be seen that the rate of decrease of modulus with confinement is similar irrespective of density. This is suggested based on slope of the lines. Thus the moduli in the presence of confining pressure can be obtained if the initial moduli for zero confinement are obtained from unconfined compression tests.
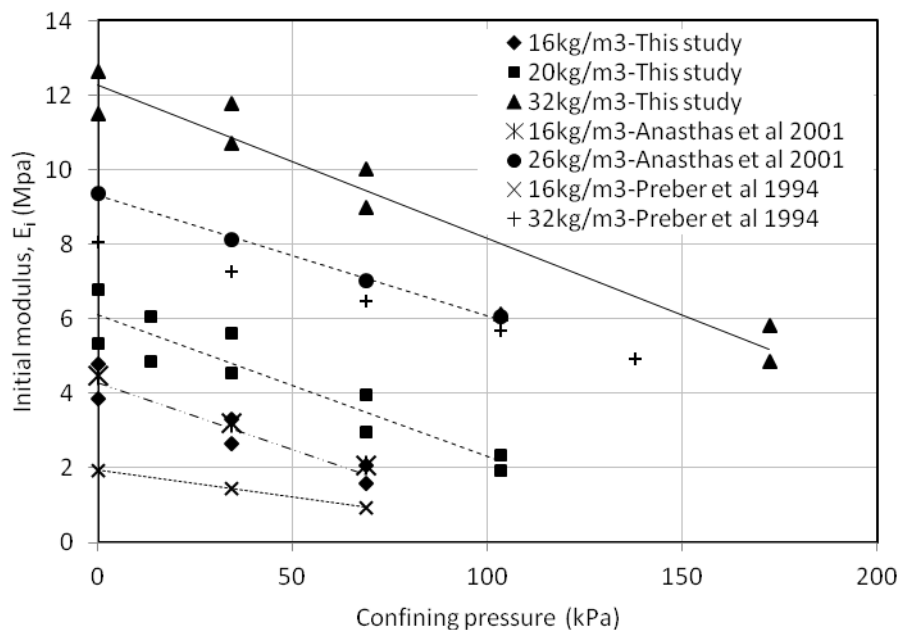
Figure 36. Modulus vs. confining pressure for different densities

The following expression provides the initial modulus for low confining pressures which are in the practical ranges of confinement.

$$E_{i,\sigma_c} = E_{io} - 0.034\,\sigma_c \tag{24}$$

Where E_{i,σ_c} = initial modulus in MPa at a confining pressure of σ_c

                 E_{io} = initial modulus in MPa for unconfined compression

                 σ_c = confining pressure in kPa

Figure 37 shows plot of post yield modulus with confining pressure. Results from this study and others are shown. Linear increasing trend is observed for the post yield modulus as the confining pressure increases. It has some dependence on the density of geofoam. The following general expression is provided for post yield modulus as a function of confining pressure and unconfined post yield modulus.

$$E_{p,\sigma_c} = E_{Po} + 0.0012\,\sigma_c \tag{25}$$

Where E_{p,σ_c} = Post yield modulus in MPa at a confining pressure of σ_c

                 E_{Po} = Post yield modulus in MPa for unconfined compression

                 σ_c = confining pressure in kPa
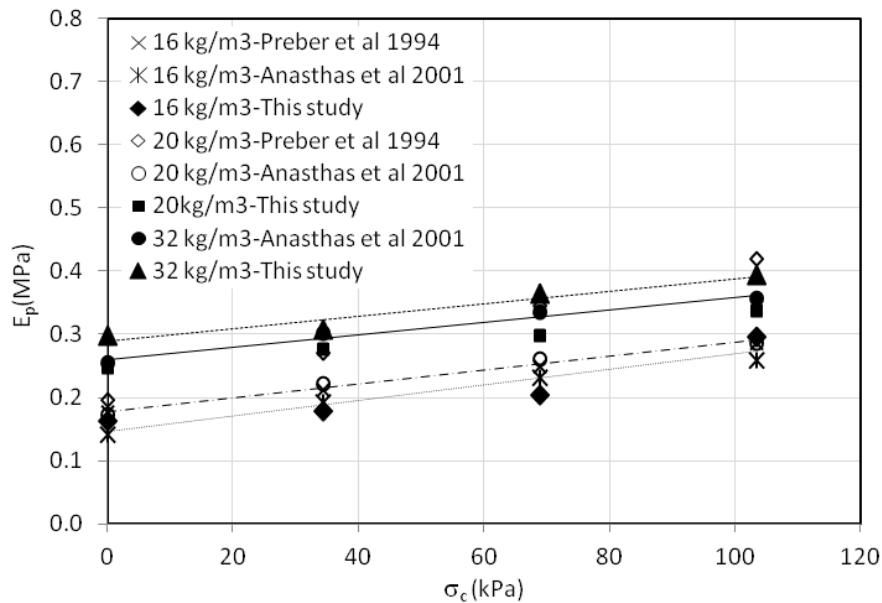
Figure 37. Post yield modulus vs. confining pressure for different densities

4.3   Yield Stress of EPS Geofoam

Yield stress is not used as a basic parameter in analysis and design of EPS geofoam. However, during investigation of effect of confinement on the property of geofoam, it is observed to be the main parameter. In this section an attempt is made to relate yield stress to density and modulus of resin beads.

Yield stress was defined as stress corresponding to intersection of the initial tangent line and the post yield tangent line, see Figure 13. Yield stresses in unconfined compression tests are shown as a function of density in Figure 38. The yield stress increased with density and was dependent on axial strain rate during testing. Yield stresses from tests with axial strain rate of 10 % per min were greater than those obtained with 1 % per minute strain rate.
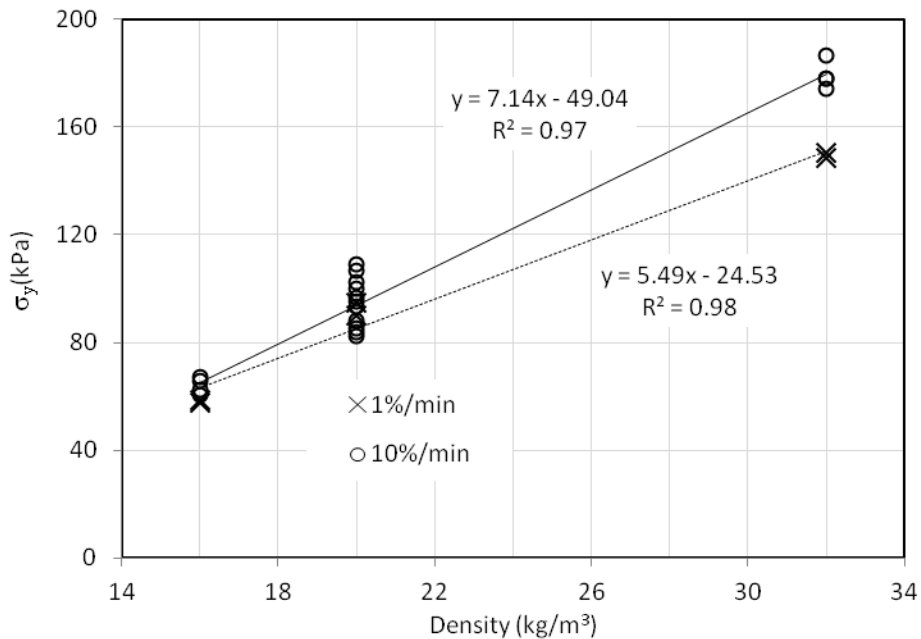
Figure 38. Yield stress vs. density from unconfined compression tests

Compression strength at 10 % axial strain is plotted against yield stress in Figure 39. The plot is linear and the following expression is provided between the strength and yield stress.

$$\sigma_{c10\%} = \sigma_{yo} + 13.05 \tag{26}$$

where both the compressive strength $\sigma_{c10\%}$ and the yield stress σ_{yo} are in kPa.
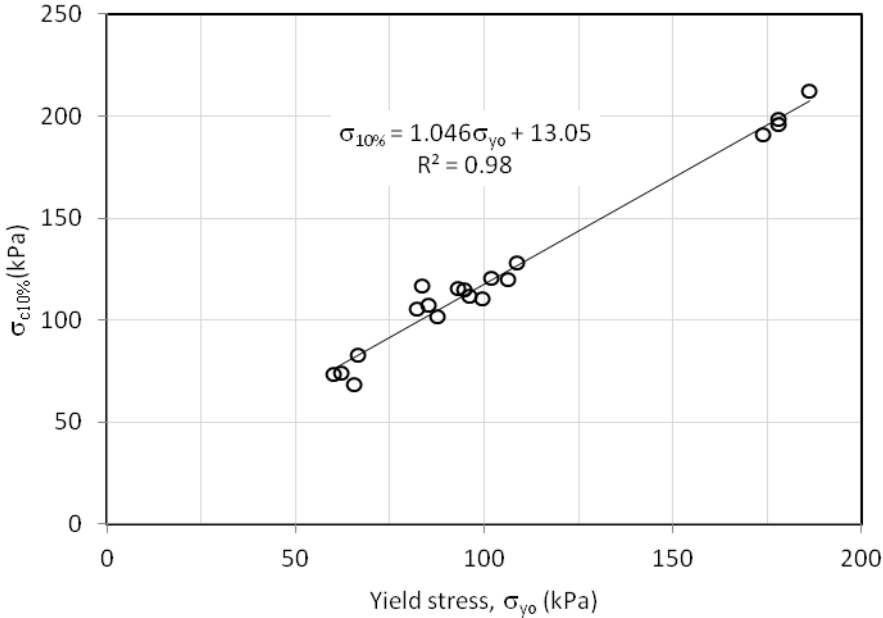
Figure 39. Compression stress vs. yield stress in unconfined compression tests

Different densities of EPS geofoam samples were tested under a range of confining pressures and yield stress is shown in Figure 40. Yield stress is shown to decrease with confining pressure up to a confining pressure close to the yield stress in unconfined compression for the same density.

77
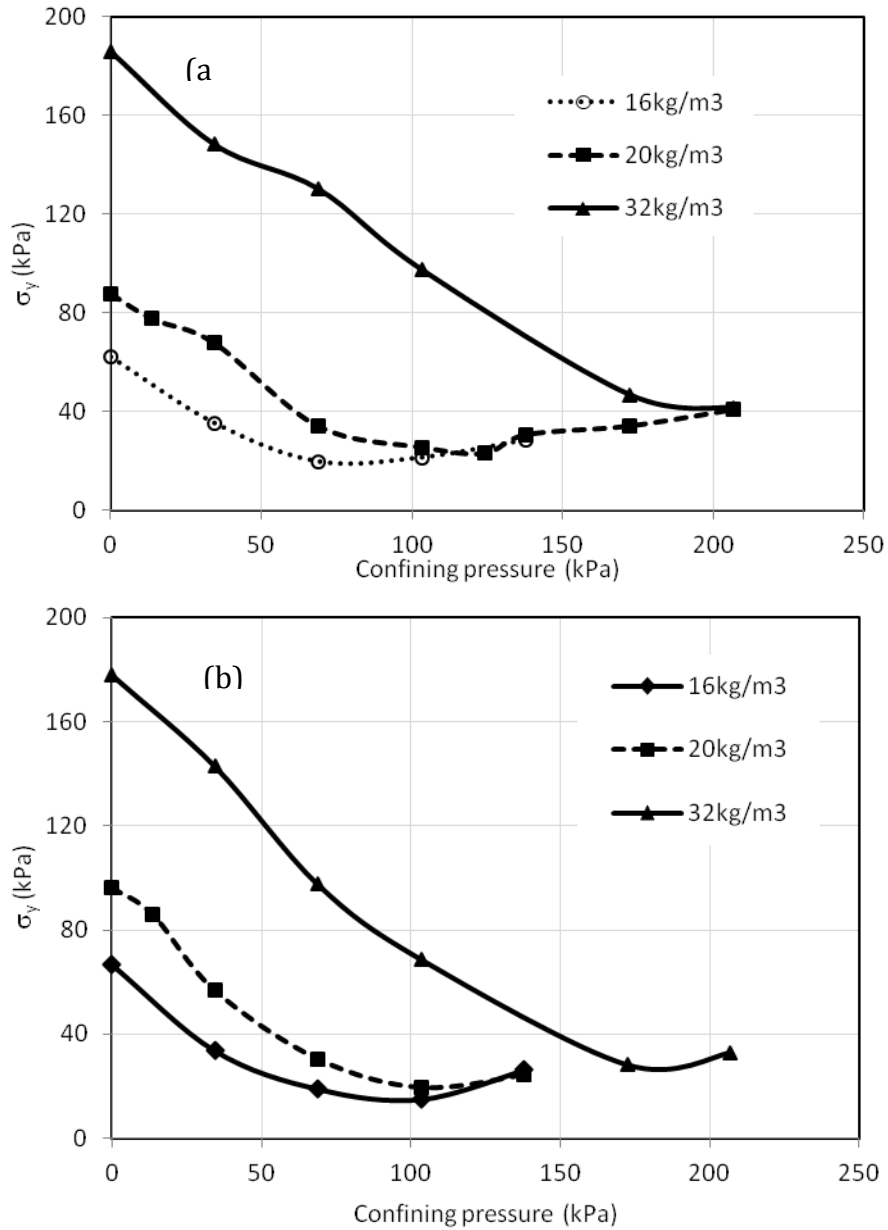
Figure 40. Yield stress vs. confining pressure (a) 64mm (b) 102 mm diameter sample

The yield stresses decreased by about 35 % over confining pressures of 0 to 69 kPa for 32 kg/m³ density. The yield stresses decreased by about 75 % for the same confining pressure range but 16 kg/m³ density. The 69 kPa confining pressure was lower than the yield stress of the 32 kg/m³ density and higher than the yield stress for the 16 kg/m³ density. The

lower density EPS geofoam was much more affected by the confining pressures of up to 69 kPa. Confining limit pressures for each density over which yield stresses decreased were in the range of the respective yield stresses for unconfined compression. With much higher confining pressures, the dense EPS geofoam also experienced significant modulus and yield stress reduction. Further decreases of modulus and yield stresses with increasing confining pressures were small for 16 kg/m^3 density geofoam, Figure 40.

Yield stress and confining pressure were normalized with the unconfined compression yield stress, σ_{yo}, of same density, Figure 41. It can be seen that decline in yield stress with an increase in confinement was up to the point where the ratio of the confining pressure to the unconfined yield stress is about 1.0. Thus, the upper bound of low confining pressure range for a given density can be taken as a confining pressure value equal to the unconfined compression yield stress, σ_{yo}.
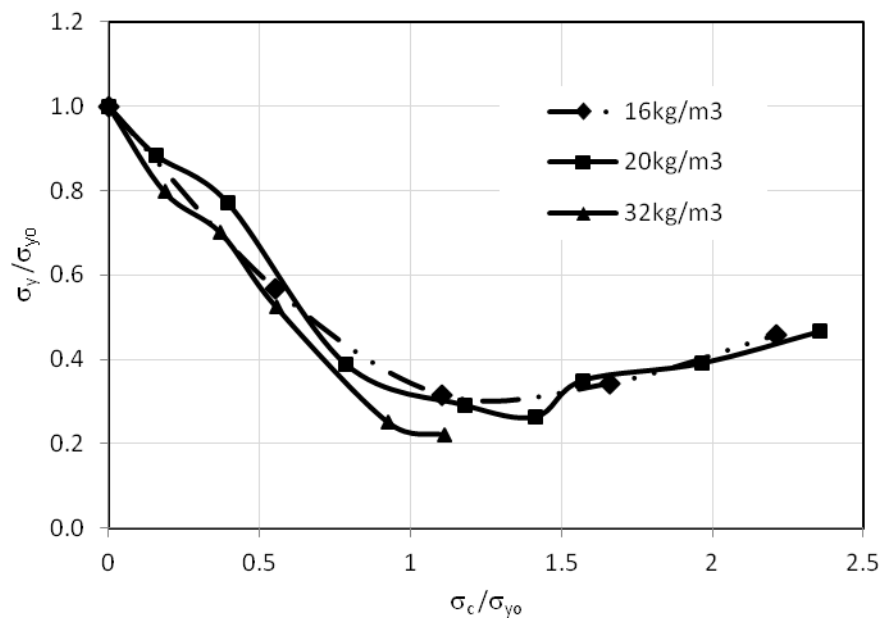
Figure 41. Normalized stresses with respect to the unconfined yield stress

The rate at which the yield stress decreases with confinement was the same irrespective of density, Figure 41. This trend was also shown in Figure 42. Hence yield stress for any confining pressure can be obtained from the unconfined compression yield stress and is discussed below. At low confining pressures, for confining pressure ratios less than 1.0, yield stresses decrease with confining pressures. At higher confining pressures, for confining pressure ratios greater than 1.0, yield stresses increase. A confining pressure ratio of 1.0 means the confining pressure is equal to the unconfined compression yield stress of the same density. Hence for EPS geofoam of 16 kg/m³ density, the unconfined compression yield stress is 69 kPa and the low confining pressure range is from 0 to 69 kPa. Whereas for 32 kg/m³ density, the yield stress for unconfined compression is 172 kPa and the low confining pressure range is 0 to 172 kPa. Confining pressures greater than 69 and 172 kPa are high confining pressures for 16 and 32 kg/m³ densities, respectively. Note that the decreasing yield stresses were in the elastic range for each confining stress level.
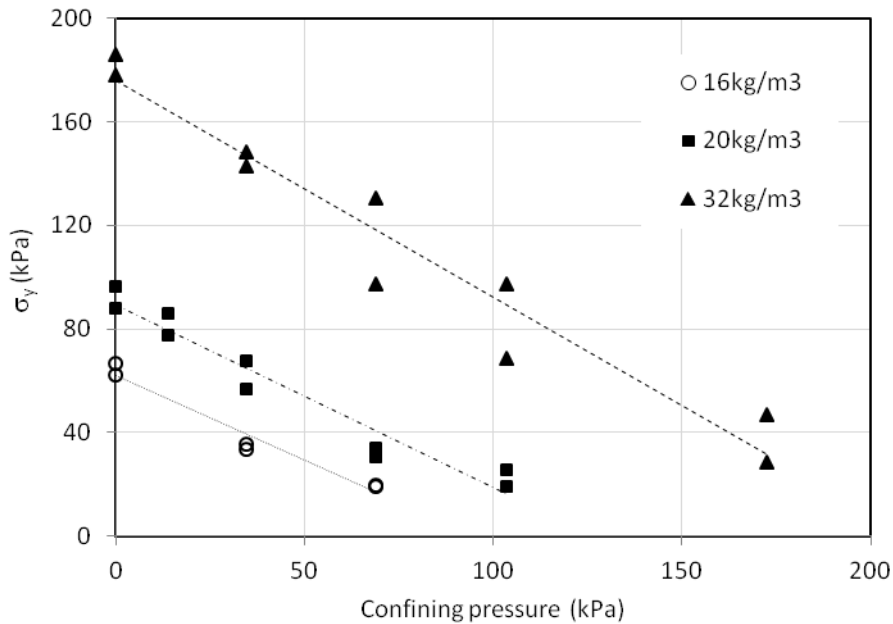
Figure 42. Yield stress vs. confining pressure for low confinement

An expression is provided for the yield stress corresponding to any confining pressure.

$$\sigma_{y,\sigma_c} = \sigma_{yo} - 0.73\, \sigma_c \qquad (27)$$

where σ_{y,σ_c} = yield strength in MPa for a confining pressure of σ_c

σ_{yo} = yield strength in MPa for unconfined compression

σ_c = confining pressure in kPa

Major yield stress, i.e. yield stress with confining stress, and confining stress were normalized with the unconfined yield stress, σ_{yo}, of the respective density as shown in Figure 43. It can be seen that the ratio is close to one and hence the major yield stress remained constant especially for low confining stresses. In other words the major principal stresses remained relatively constant over the lower or elastic range of confining pressures. At higher confining stress ratios, yield stress ratios increased gradually.
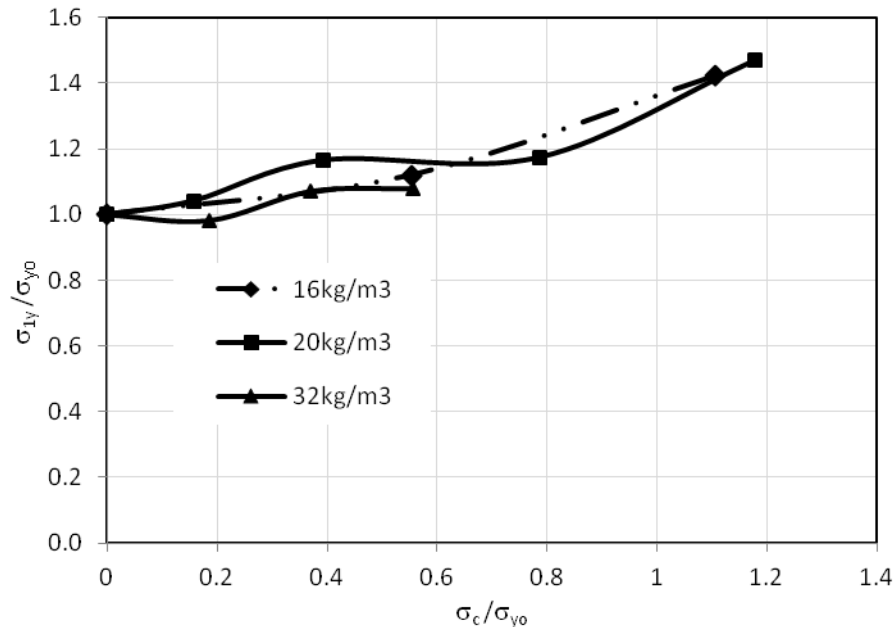
Figure 43. Major yield stress vs. confining pressure normalized by unconfined yield stress

81

Overall, for each density and confining stress level, yield states can be approximated as major principal stress states, and thus equal to the yield stress for unconfined compression, Figure 44. This was also evident in results reported by Wong and Leo 2006.
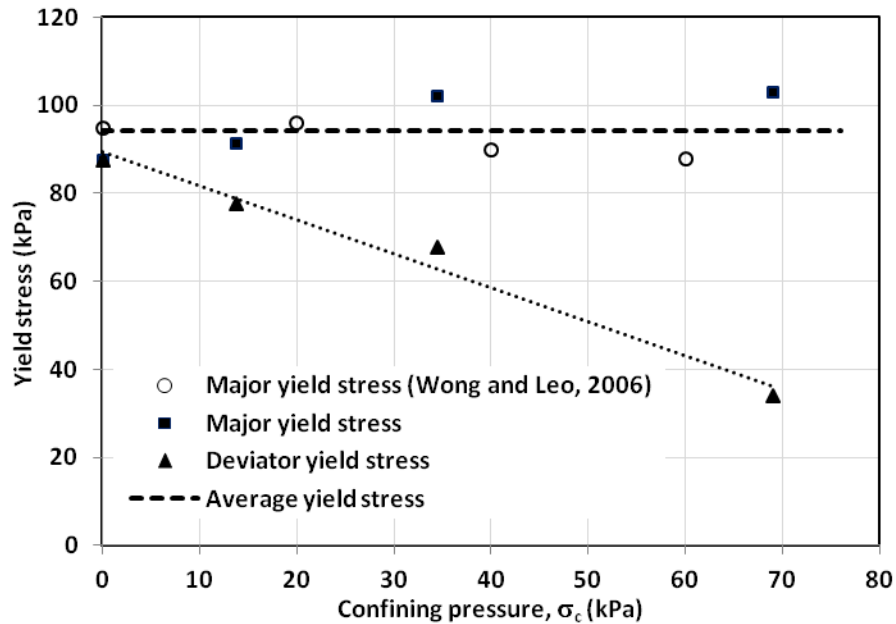
Figure 44. Confining stress effect on yield and major stresses

Yield stresses, for unconfined compression can be estimated for the EPS density, ρ, in terms of the density, ρ_s, and modulus, E_s, of polystyrene; the solid constituent as:

$$\sigma_{yo} = 0.05 \left(\frac{\rho}{\rho_s}\right)^2 E_s \tag{28}$$

Equation (28) is a variation of the theoretical expression suggested by Gibson and Ashby (Gibson and Ashby 1999) to represent deviator stress states. The unconfined yield stress calculated from (28) agrees very well with the test results as shown in Figure 45. The calculated yield stress of 101 kPa for unconfined compression is significantly greater than

the allowable working stress of 50 kPa at 1 percent limit strain reported in ASTM D 6817 for EPS22.
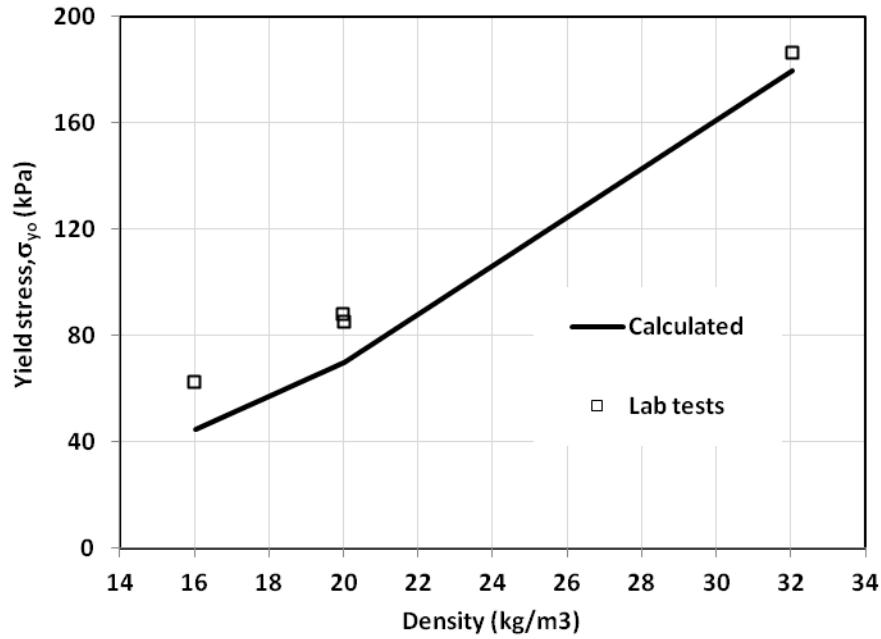
Figure 45. Unconfined compression yield stresses

Major principal stresses for low confining pressures, σ_c, remained reasonably constant as:

$$\sigma_{1y} = \sigma_y + \sigma_c \tag{29}$$

For unconfined compression, the yield and the major principal stresses are the same. Hence, the yield stress at a confining pressure, σ_c, would be;

$$\sigma_y = \sigma_{yo} - \sigma_c \tag{30}$$

Thus, yield stresses at different confining pressures can be estimated by:

$$\sigma_y = 0.05 \left(\frac{\rho}{\rho_s}\right)^2 E_s - \sigma_c \tag{31}$$

Yield stresses calculated from (31) were normalized by atmospheric pressure to compare

with results for 16 and 32 kg/m³ nominal densities, Figure 46. The low confining pressures

range for the 16 kg/m³ density is much lower than for the 32kg/m³ density. Thus Equation

(31) follows the results for the higher density geofoam over a wider range of confining

pressures. This is due to the fact that the higher the density the more is the polystyrene.
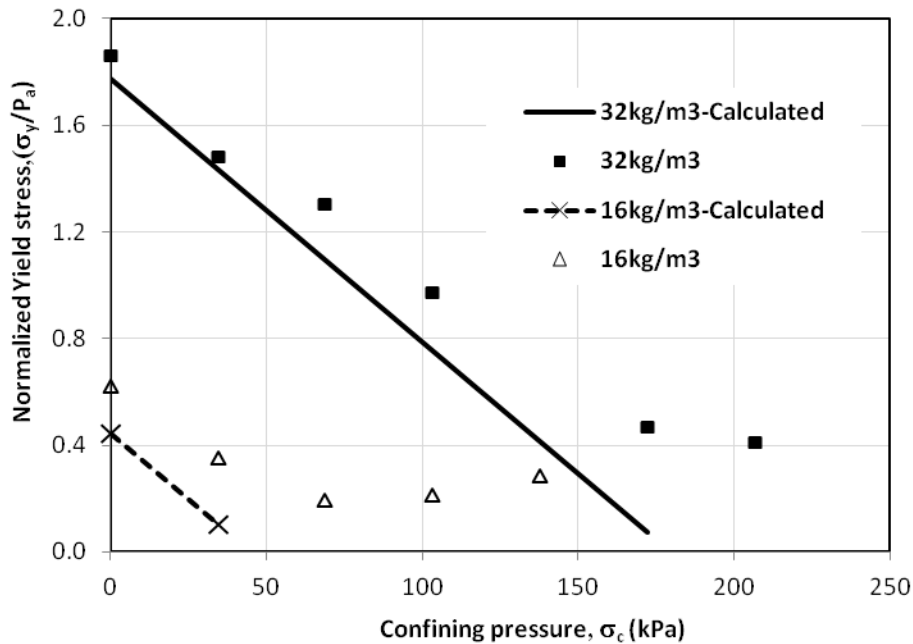
Figure 46. Normalized yield stresses with respect to atmospheric pressure

1. Unconfined compression stress-strain curve from density and yield stress

The yield stress was given as a function of density of EPS block (Eq. 28). The initial and

post yield moduli can also be obtained as a function of density of geofoam from (Eq. 9) and

(Eq. 11) respectively. Expression in (Eq.23) was employed for generating the stress-strain
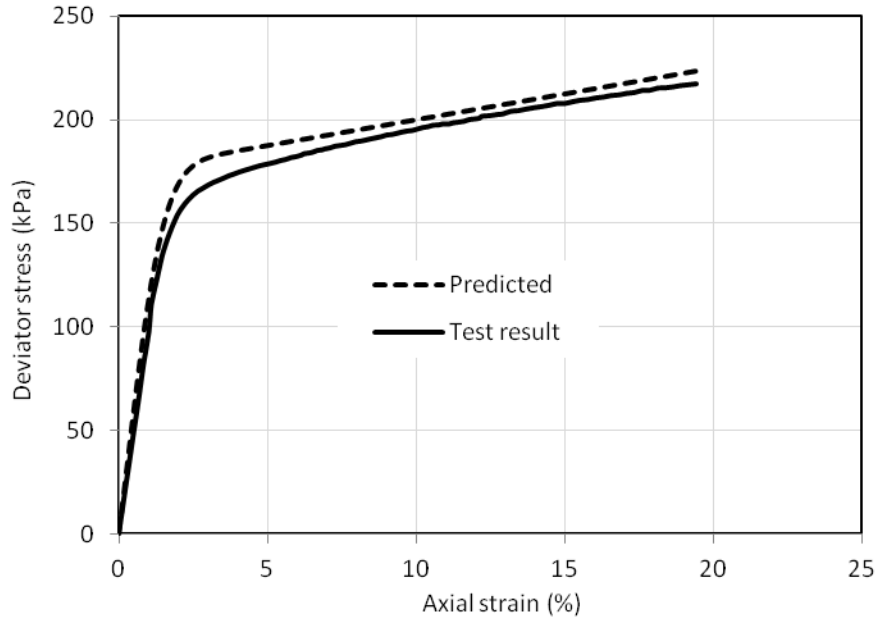
curve.

Figure 47 Prediction of stress-strain curve from density of geofoam (32 kg/m³)

In Figure 47, the stress-strain curve labeled as "this study" was generated from density of geofoam block and known properties of the polystyrene beads. Very good agreement was obtained with lab test data. However, prediction accuracy is shown to reduce as the density of the geofoam decreases because the yield stress obtained from density and modulus of polystyrene (Eq. 28) is smaller than the actual yield stress. Density decreases as polystyrene amount per unit volume of geofoam decreases. In addition the gas contained within cells starts to take part in carrying stresses as the cell walls collapse. This could be part of the reason for getting less yield stress values in case of low density geofoams.
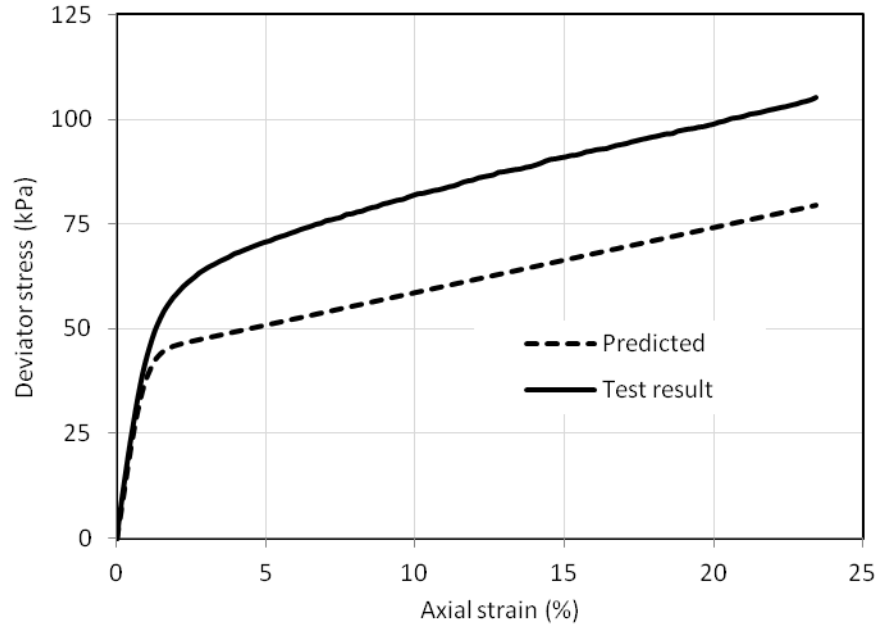
Figure 48. Prediction of stress-strain curve from density of geofoam (16 kg/m³)

The deformation resistance of closed cell geofoam is the sum of the following three contributions: contribution of cell-edges, compression of the cell fluid and the membrane action of the cell faces(Gibson and Ashby 1999). At small stress, the resistance for loading is contributed from cell edges and membrane action of the cell faces. But as the stresses increase, the cell walls collapse and transfer the stresses to the cell fluid which is commonly air in geofoam and hence the increase in pressure will be greatly resisted by the fluid or the air within the cells. When the sample is compressed its volume decreases from V_o to V. And assuming the temperature remains constant, the pressure in cell increases from P_o to P and Boyle's law yields

$$P_o V_o = P V \tag{32}$$

The pressure increase in the cell fluid will give the geofoam some additional carrying capacity. The total stress resistance expected during testing geofoam would be

$$\sigma_{yo} = 0.05 \left(\frac{\rho}{\rho_s}\right)^2 E_s + \frac{P_o V_o}{V} \tag{33}$$

Figure 48 showed that the strain stress curve obtained using (Eq. 28) plots below the test result due to the fact that the resistance contribution from the cell fluid is not taken into account.
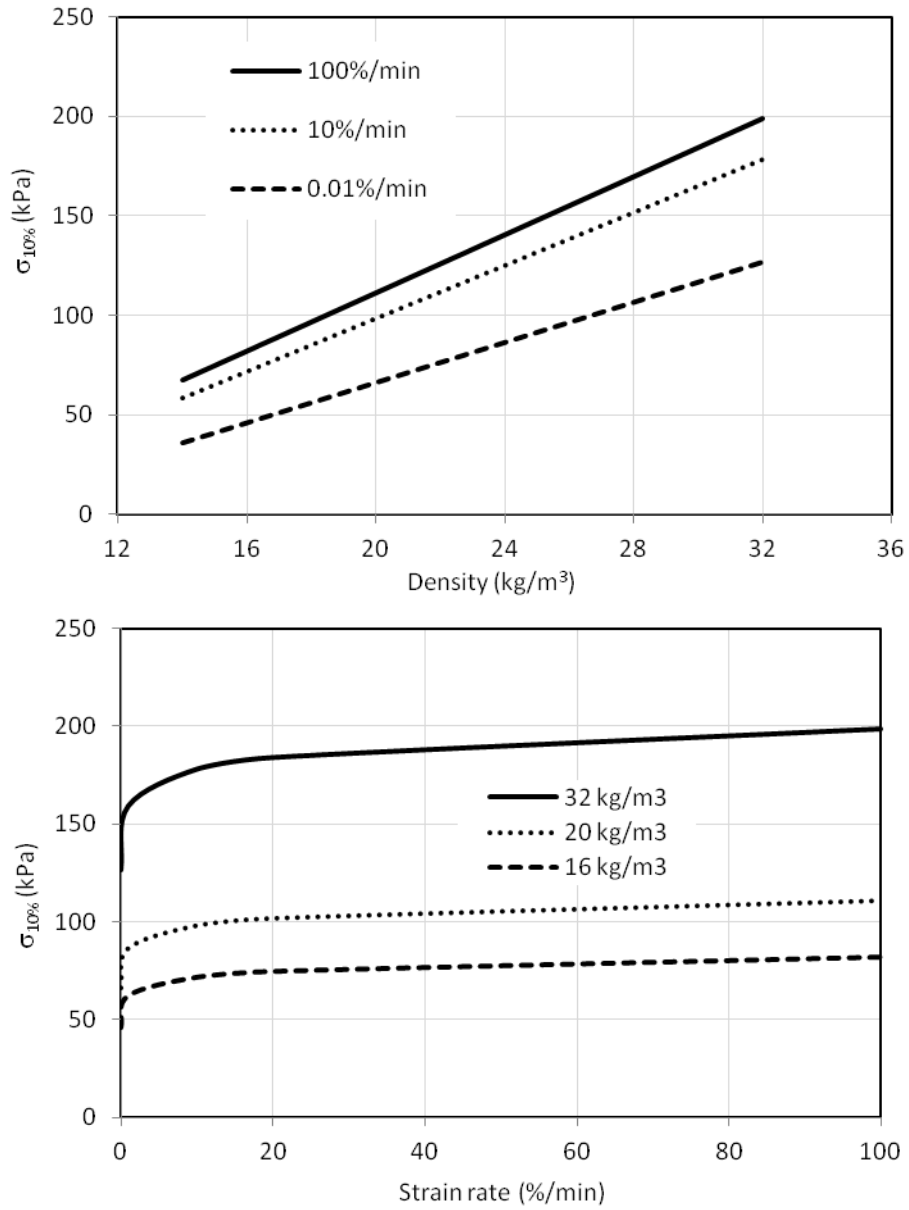
Figure 49. Strain rate effect on the unconfined compression strength

Strain rate effects on the stress-strain relations were studied (Elragi 2000). The stress-strain curves for slower loading rates plot below those of fast loading rates and the following expression was given for unconfined compressive strength.

$$\sigma_{10\%} = 7.3 \, R^{0.04} \, \rho - 35 \tag{34}$$

Where $\quad \sigma_{10\%}$ = compressive strength in kPa at 10 % strain

R = strain rate in % / min

ρ = density in kg/m^3

Figure 49 shows plots obtained from (Eq.34). The right plot shows that strain rate effect is higher when rate is below about 10 % and relatively constant when the rate is greater than 10 % per min. The left plot shows that as the density increases the rate effect also increases.
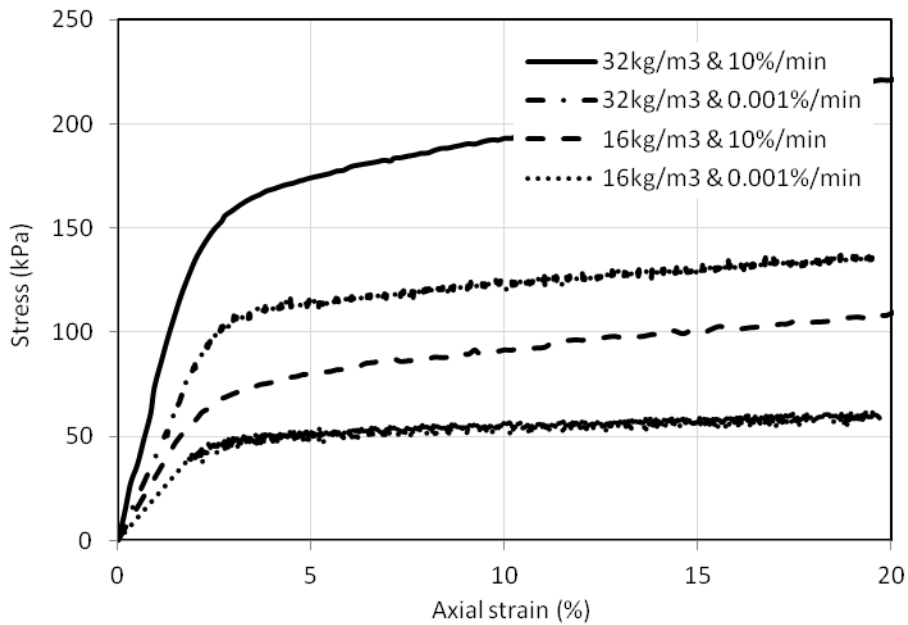
Figure 50. Effect of loading rate on the stress-strain behavior

Loading rate dependency of stress-strain relation is thus related to load carrying contribution of air in the cells. Load resistance of air within the cell is shown to be higher in tests which are done at faster loading rates. Figure 50 shows tests done at different loading rates for different densities.

Table 8. Values of different parameters for different strain rates

Parameter	16 kg/m^3		32 kg/m^3	
	10 %/min	0.001 %/min	10 %/min	0.001 %/min
E_i (MPa)	3.16	2.13	7.55	4.14
E_p (MPa)	0.17	0.06	0.28	0.15
σ_y (kPa)	78.8	50.0	172.0	111.7
$\sigma_{10\%}$ (kPa)	91.7	54.4	193.5	122.5

Expressions for initial and post yield modulus as a function of strain rate (R) and density(ρ) were provided (Elragi 2000).

$$E_i = 0.35 \ R^{0.01} \ \rho - 2.2 \tag{35}$$

$$E_P = 0.007 \ R^{0.04} \ \rho \tag{36}$$

where E_i and E_p are in MPa ; R in %/min and ρ in kg/m^3.

It can be noted from Figure 49 and (Eq.34) through (Eq.36) that initial modulus, post yield modulus, yield stress and compressive stress at 10 % decrease as the strain rate decreases.

Taking the strain rate effect in to account, the prediction from (Eq. 28) has improved a lot for lower density as shown in Figure 51.
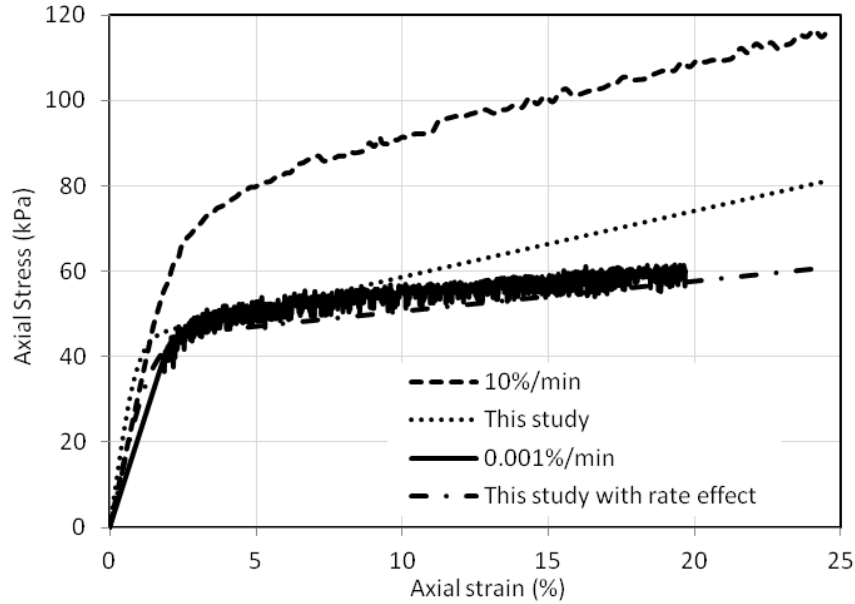
Figure 51. Prediction of stress-strain curve from density of geofoam (16 kg/m³)

The yield stress in unconfined compression test is shown to be linearly related with density of EPS block geofoam, see Figure 38. They are related by the expression:

$$\sigma_{y0} = 7.1433 \, \rho - 49.043 \tag{37}$$

Where σ_{y0} = yield stress in kPa in unconfined compression

ρ = density in kg/m³

For geofoams with lower densities, (Eq.37) was used for σ_{yo} instead of (Eq. 28) and the prediction of the stress-strain relationship is improved a lot as shown in Figure 52.

2. Confined compression stress-strain curve from density and yield stress

In this section a similar approach is followed to develop the stress-strain curves for confined triaxial tests. The yield stress expression of geofoam tested at a confining pressure of σ_c was given in (Eq.27). Note that in the equation the only variables are density of geofoam and confining stress as the unconfined yield stress σ_{yo} is a function of density of

geofoam block and bead density and modulus as explained above. The initial and post yield

moduli of a confined test can also be obtained as a function of density of geofoam and

confining stress from (Eq. 24) with (Eq. 9) and (Eq. 25) with (Eq. 11) respectively.

Expression in (Eq.23) was employed for generating the stress-strain curve.
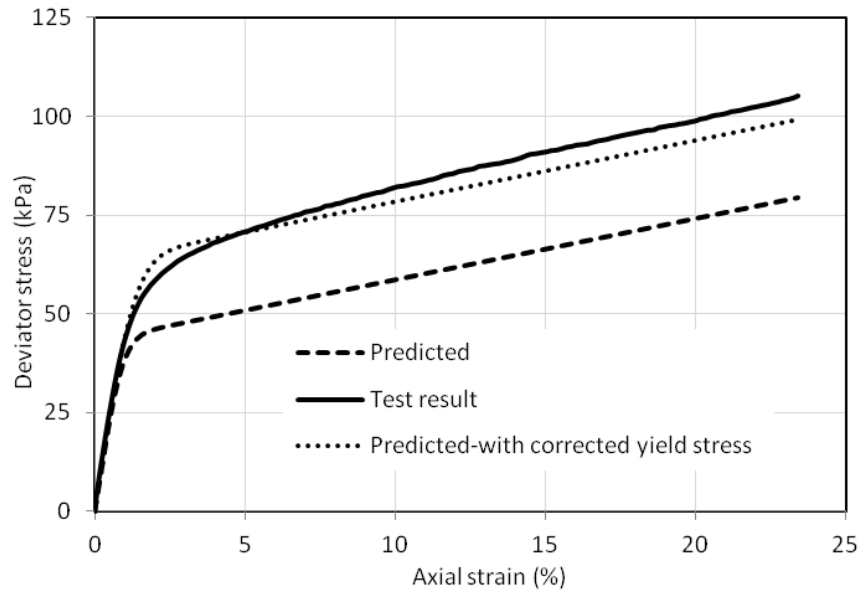
Figure 52. Prediction of stress-strain curve from density of geofoam (16 kg/m³)
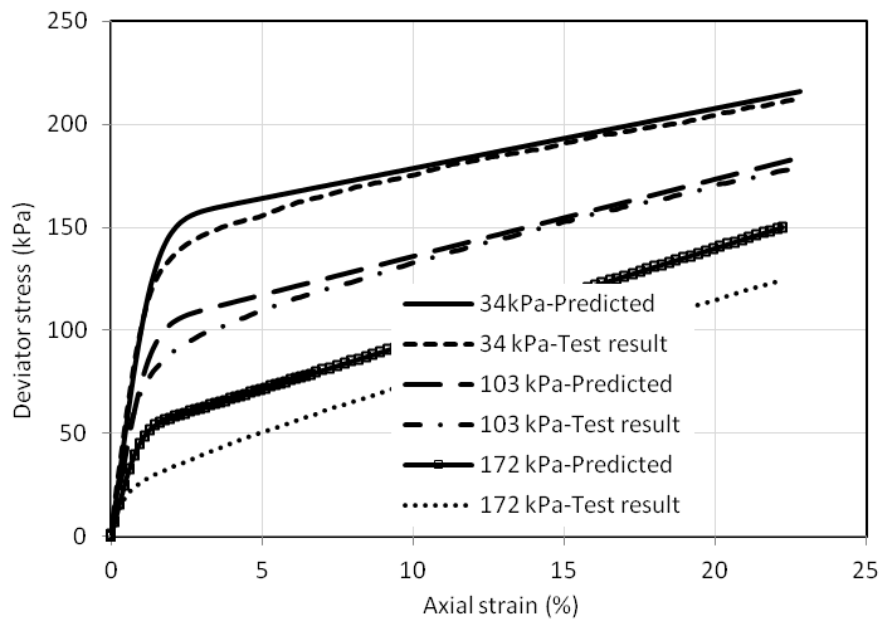
Figure 53. Prediction of stress-strain curve from density of geofoam (32 kg/m³)

The stress-strain curves obtained in this study are shown in Figure 53 along with the corresponding lab test results. Very good agreement between lab results and the proposed method is evident especially for low range of confining stresses. The stress-strain curve for lower density geofoam is shown Figure 54. As discussed above there is some effect of resistance by the air in the cells of the geofoam and hence lab test results show higher stresses than predicted results.
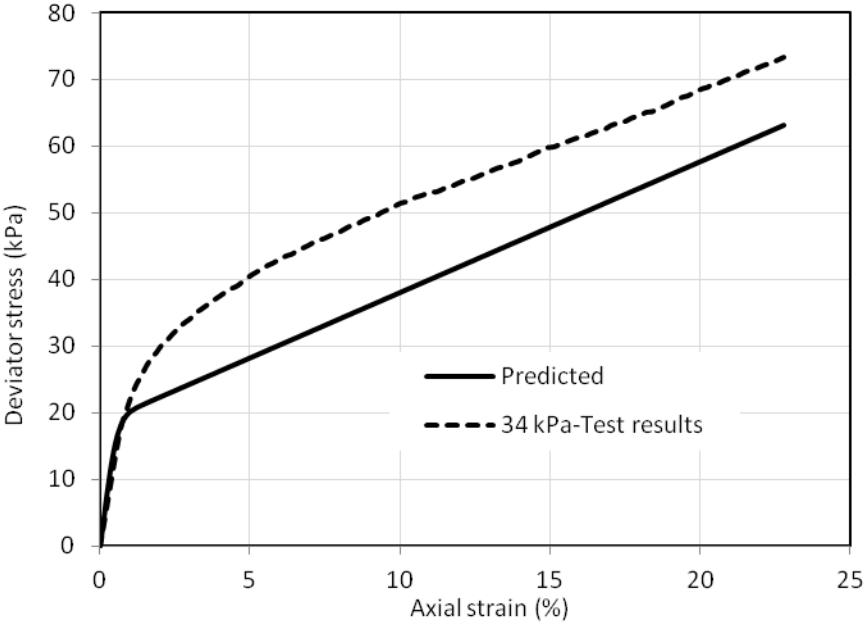
Figure 54. Stress-strain curve from density of geofoam (16 kg/m³)

4.4   Use of Hyperbolic Relationship to Characterize Stress-Strain Behavior

EPS geofoam blocks underlying compacted soil interact with the surrounding materials and are subjected to multi-axial loading. Moreover prediction of EPS-soil-structure interaction requires a reasonable representation of stress-strain relationships for numerical modeling. Existing constitutive representations of stress-strain relations for EPS geofoam are limited. Some require many parameters which should be obtained from long procedures and predictions from some are very poor when compared with lab test data. In this work, an attempt is made to employ the hyperbolic stress-strain relationships with some modifications for EPS geofoam in such a way that effect of confining stresses on stress-strain relationship can be properly represented in analysis. This modified hyperbolic stress-strain model requires only three parameters which can be obtained from triaxial tests conducted with different confining stresses. The prediction accuracy of this model was compared with data obtained from triaxial tests which were not part of data sets used to obtain model parameters. Comparison was made with other models and the stress-strain relationships predicted using the proposed model agreed very well with test data.

Introduction

Instability and settlement problems in compressible and weak soils have been resolved through use of EPS geofoam as light weight fill material (Duškov 1997a; Elragi et al. 2001; Frydenlund and Aabøe 1996; Murphy 1997; Negussey and Srirajan 2001; Negussey and Stuedlein 2003). EPS geofoam in service can experience pressures from biaxial or triaxial directions. In addition to overburden pressure, confining pressures on EPS geofoam may develop from active soil or hydrostatic pressures. In most prior applications, EPS geofoam placements were near surface and above groundwater levels. EPS geofoam installations at

93

larger burial depths and below groundwater or extreme flood levels experience confining pressures. Analysis of substructures involving EPS geofoam requires constitutive relations to properly model soil-EPS-structure interactions. Stress-strain behavior of geofoam in compression can be considered reasonably linear elastic up to about 1 % strain and apparent yield. Beyond yield, behavior of EPS geofoam is non linear, inelastic and depend on the strain level and hence, the assumption of elastic analysis may not suffice. The stress and strain behavior was approximated as linear elastic perfectly plastic (Takahara and Miura 1998) and as nonlinear elastoplastic (Hazarika 2006). Two classes of models are reported in the literature for EPS geofoam: those which do not consider time dependent stress-strain behavior or creep (Chun et al. 2004; Hazarika 2006; Preber et al. 1994); and those which consider creep (Findley and Khosla 1956; Findley 1960) The modified hyperbolic relationship proposed here is for a rapid loading test where the axial stress was applied at a strain rate of 10 %/min. Triaxial tests were done for different confining pressures and densities. Three parameters -K, n and m were determined from tests to calibrate the modified hyperbolic stress-strain relations. The modified hyperbolic model representations from this study are compared with previous models

Triaxial Compression Tests and Results

Triaxial tests with cell pressures of 0, 34, 69, 103 and 172 kPa; and three nominal densities of 16, 20 and 32 kg/m^3 were conducted in this study. Two cylindrical sample groups were tested. The first group was 64 mm in diameter and 127 mm in height. The second group has 102 and 203 mm as diameters and height, respectively. Samples were precision cut to required dimensions in a factory. Tests were conducted at constant room temperature and axial strain rate of 10 %/minute. Both volumetric and axial deformations were recorded.

94

The stress-strain response of EPS geofoam samples under uniaxial compression but with different confining pressures are shown in Figure 55 These test results are for samples of nominal 64 mm diameter and 127 mm height. For each test, the pre-set confining pressure was applied immediately before axial compression at 10 %/ min displacement was initiated. Load, displacement and volume changes were recorded with time. The stress vs. strain curves were corrected for seating errors and show reasonably bilinear stress-strain relationships. Figure 55 also shows consistent decreases in both strength and initial tangent modulus with increasing confining pressures. At higher confining pressures which are greater than unconfined yield stress, decreasing trends in strength and modulus reversed(Birhan and Negussey 2014). Such high confining pressure states are not considered in this modified hyperbolic modeling of EPS geofoam behavior.

The Hyperbolic Relationship

Hyperbolic stress-strain models has been used to characterize soil stress-strain behavior for a long time(Duncan and Chang 1970; Duncan 1980; Kondner and Zelasko 1963). The hyperbolic equation proposed by Konder and his coworkers is of the form

$$(\sigma_1 - \sigma_3) = \frac{\epsilon}{\frac{1}{E_i} + \frac{\epsilon}{(\sigma_1 - \sigma_3)_{ult}}} \tag{38}$$

in which σ_1 and σ_3 are the major and the minor principal stresses; ε = the axial strain, E_i=the initial tangent modulus and $(\sigma_1 - \sigma_3)_{ult}$ = the asymptotic value of the stress differences or limit of stress-strain curve at large strain. In order to obtain values of E_i and $(\sigma_1 - \sigma_3)_{ult}$ Equation (38) is rewritten as

$$\frac{\epsilon}{(\sigma_1 - \sigma_3)} = \frac{1}{E_i} + \frac{\epsilon}{(\sigma_1 - \sigma_3)_{ult}} \tag{39}$$
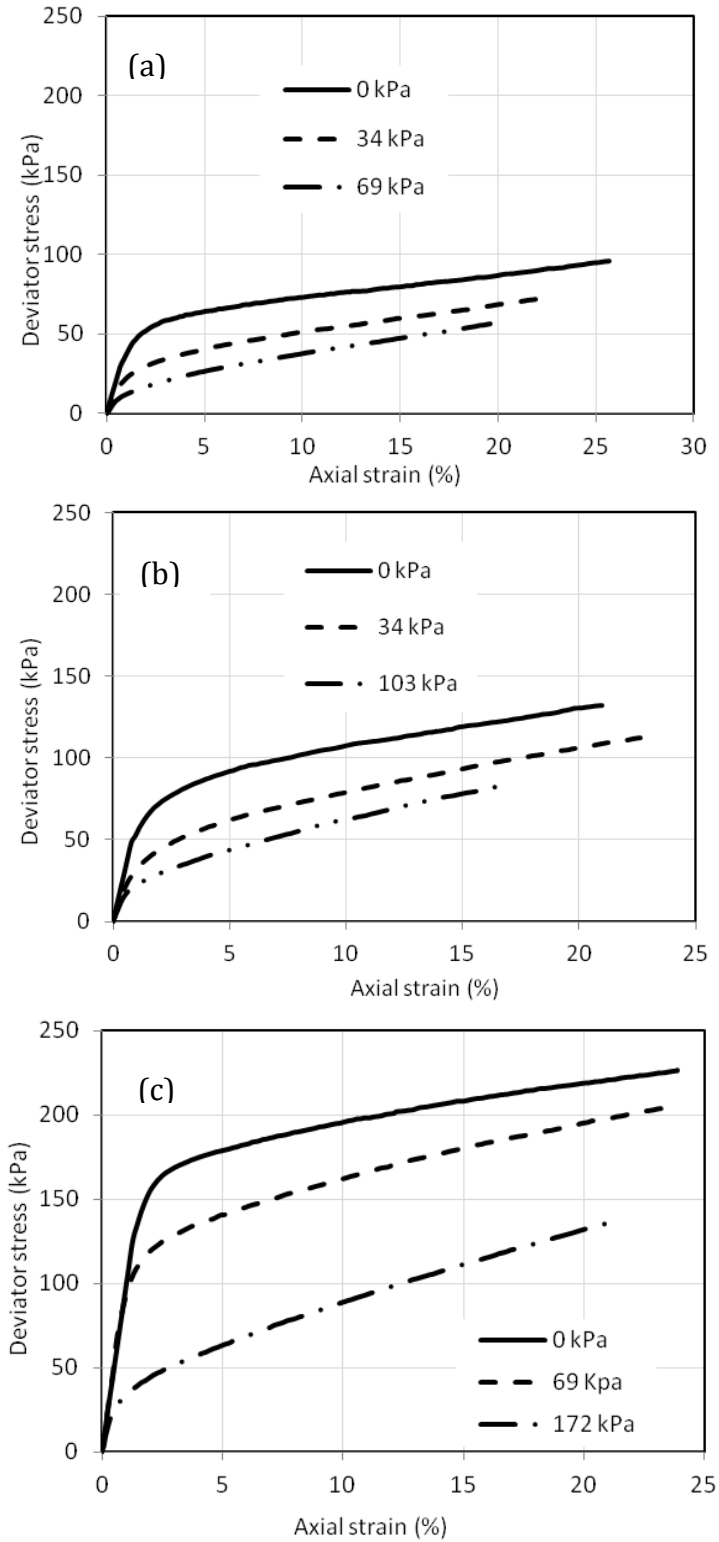
Figure 55. Deviator stress vs. strain for EPS geofoam (a) 16 (b) 20 (c) 32 kg/m³

density

and plots as a transformed straight line on ϵ and $\frac{\epsilon}{(\sigma_1-\sigma_3)}$ axes. Test data are plotted on the

transformed axes and E_i is obtained from the $\frac{\epsilon}{(\sigma_1-\sigma_3)}$ intercept of the best fit line and the

slope corresponds to $\frac{1}{(\sigma_1-\sigma_3)_{ult}}$.

Effect of confining stresses on the stress-strain relationship is represented by empirical

equation of the form

$$E_i = K\,P_a\,e^{n\left(\frac{\sigma_3}{P_a}\right)} \tag{40}$$

The parameter K and n are modulus number and modulus exponent respectively and P_a is

atmospheric pressure with same unit as σ_3. Eq. (40) is a modification on the empirical

relation given by Duncan and Chang 1970. K and n are determined from two steps (see

Figure 56): (*i*) for each test obtain E_i from transformed plots (*ii*) plot $\frac{E_i}{P_a}$ vs. $\frac{\sigma_3}{P_a}$ where $\frac{E_i}{P_a}$ is in

logarithmic and $\frac{\sigma_3}{P_a}$ in arithmetic scale. And hence slope of an exponential trend line fit is K

and the exponent is n. The value of K is obtained when confining pressure is zero, and it is

very close to the initial modulus in unconfined compression multiplied by atmospheric

pressure.
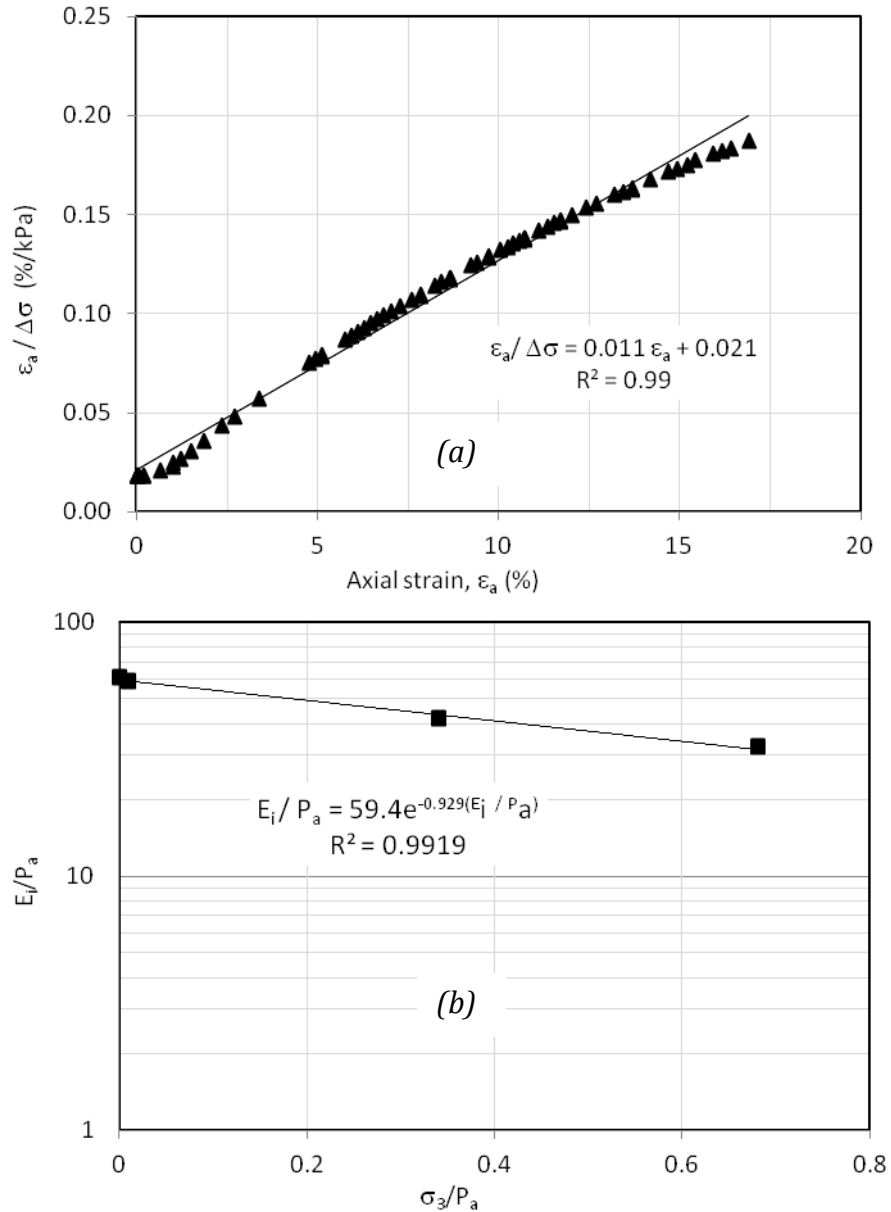
Figure 56. Parameters for modified hyperbolic stress-strain relation *(a)*

Transformed plot *(b)* Plot for obtaining K and n

Triaxial test data were analyzed and are summarized in Table 9 for three densities. Values

of n for EPS geofoam are negative contrary to that of soils. This suggests that there will be

reduction in initial modulus as confining pressure increases. The exponential fits have R^2

values essentially close to 1.0.

Table 9. Summary of modulus number (K) and modulus exponent (n)

Density (kg/m^3)	Sample diameter (mm)	K	n	R^2
16	64	38.11	-1.18	1.00
16	102	47.53	-1.22	1.00
20	64	59.4	-0.93	0.97
20	102	70.37	-1.02	0.96
32	64	127.89	-0.41	0.97
32	102	117.21	-0.54	0.96

It can be seen in Table 9 that sample size and density gave little variations on values of n, but higher variations on values of K. K was related to the initial modulus in unconfined compression. Effects of specimen size and density on properties of EPS geofoam were also reported previously (Elragi et al. 2001; Hazarika 2006). However, sensitivity of the current proposed method to the variation of such small values was observed to be negligible. Use of these parameters was made to determine E_i, Eq. (40), and to characterize stress-strain curves. When $\frac{1}{(\sigma_1 - \sigma_3)_{ult}}$.was plotted against confining pressure, linear relationship was observed for a given density, Figure 57.
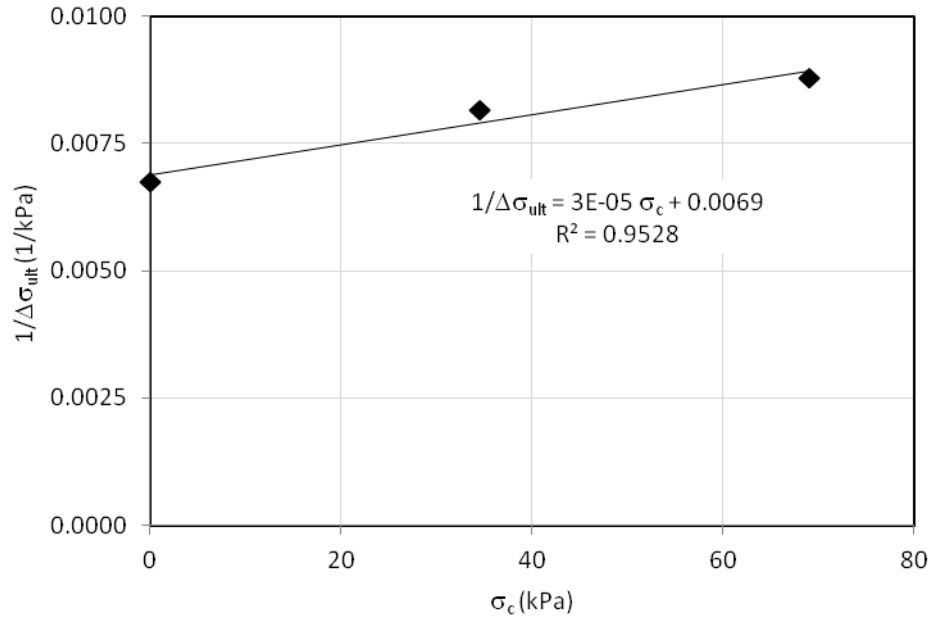
Figure 57. Variation of $1/(\sigma_1 - \sigma_3)_{ult}$ with confining stresses for 20 kg/m³ EPS geofoam

It should be noted that the stress-strain curve for EPS geofoam will not have an asymptotic value of $(\sigma_1 - \sigma_3)_{ult}$ like that of soils. EPS geofoam gets stronger at very high strains and thus the hyperbolic stress-strain relation will not appropriately represent the behavior for very high strains which are beyond relevance for modeling. However it is found to be appropriately representing the stress-strain relationship for strain levels in practical strain ranges, say about up to 10 % to 15 %.

Modified hyperbolic parameters obtained above were employed to plot stress-strain curves. Figure 58 shows such plots and data obtained from triaxial tests. It can be seen that the curves obtained from the modified hyperbolic relation agreed reasonably with the test data. The model was able to capture the effect of confinement on the stress-strain behavior.
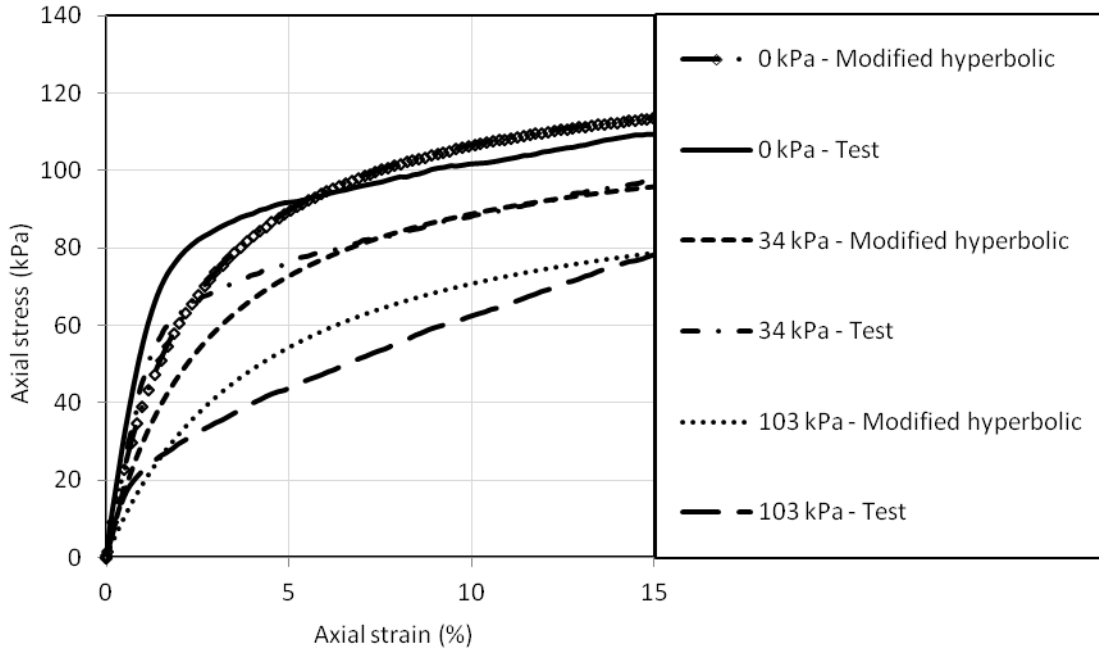
Figure 58. Modified hyperbolic stress-strain relation and test data

Modeling of Triaxial Tests in FLAC

Triaxial loading of EPS geofoam was modeled in FLAC (FLAC V.6 2008), a finite difference program. A programming language called FISH- which is embedded within FLAC was used for modeling non-linear stress or strain dependent behavior. Non linear elastic moduli of soils were evaluated as a function of confining stress and mobilized strength using hyperbolic model (Duncan and Chang 1970). Here, the hyperbolic model was used to model EPS geofoam in FLAC.

The triaxial test was modeled as axisymetric and fixed in the horizontal direction on the left boundary. Platens used for applying the load were very stiff as compared to the EPS sample and the boundary was treated as rigid. To simulate this rigid boundary, a constant velocity was applied at the top of the sample keeping the bottom fixed. Even though the

real boundary condition applied at the top was free, the top boundary was shown fixed in Figure 59 only due to the application of constant velocity to displace the sample downward.
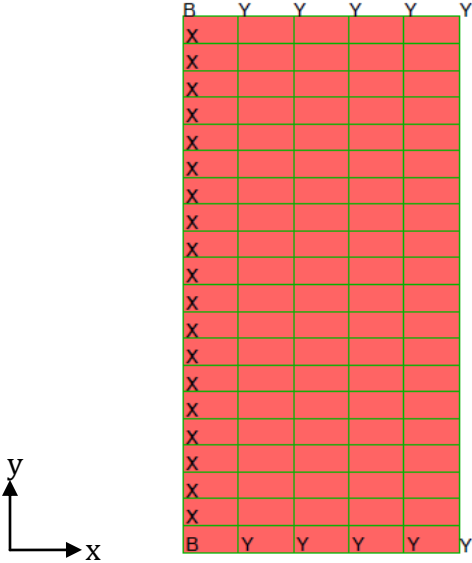
Figure 59. Typical axisymetric geometric model

Unlike soils, EPS geofoam gains strength at very large strains and failure cannot be defined for the model. However, deviatoric stress at 10 % axial strain ($\Delta\sigma_{10\%}$) was taken as the deviator stress at failure, $(\sigma_1-\sigma_3)_f$. The deviator stress reduced with confining pressure increase, Figure 60. The deviator stress at any confinement was observed to vary as

$$\Delta\sigma_{10\%} = \Delta\sigma_{10\%,o} - m\ \sigma_c \tag{41}$$

The reduction rate, m, was about 0.60 kPa per 1 kPa confining pressure increase and $\Delta\sigma_{10\%,o}$ is unconfined compression stress at 10 % strain.
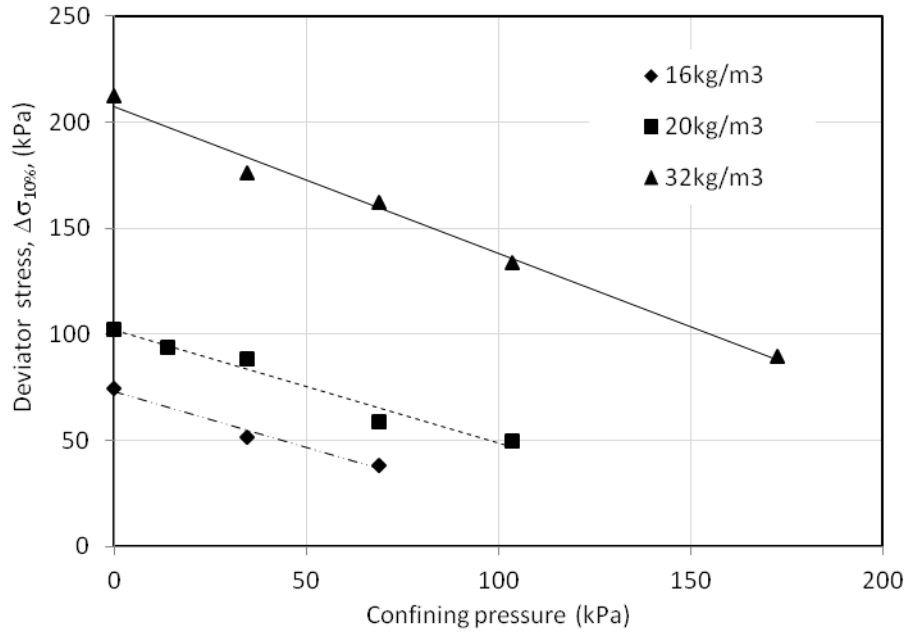
Figure 60. Deviator stress at 10 % strain vs. confining pressure

Three major parameters: K, n and m were used for the proposed model. Unconfined compression stress and initial modulus are readily available. With these parameters, FLAC was used to model triaxial test response for EPS geofoam. The stress stain relationship obtained from such analysis is presented in Figure 61 with the accompanying lab data. Within working strain levels, the results from the FLAC output agree reasonably with the test data.

Comparison with Results from Other Constitutive Models

In order to compare the prediction capability of the proposed model, comparison has been made with models from Chun et al. 2004; Preber et al. 1994; Wong and Leo 2006. Chun et al. 2004 proposed a constitutive model for EPS geofoam where the major principal stress was related with the major principal strain. This mathematical model takes into account the density and confining pressure effects on the stress-strain behavior. Preber et

al. 1994 provided generalized equations for model parameters as a function of density and confining pressure. An elastoplastic hardening constitutive model proposed by Wong and Leo 2006 has six independent parameters which can be obtained from triaxial test data.
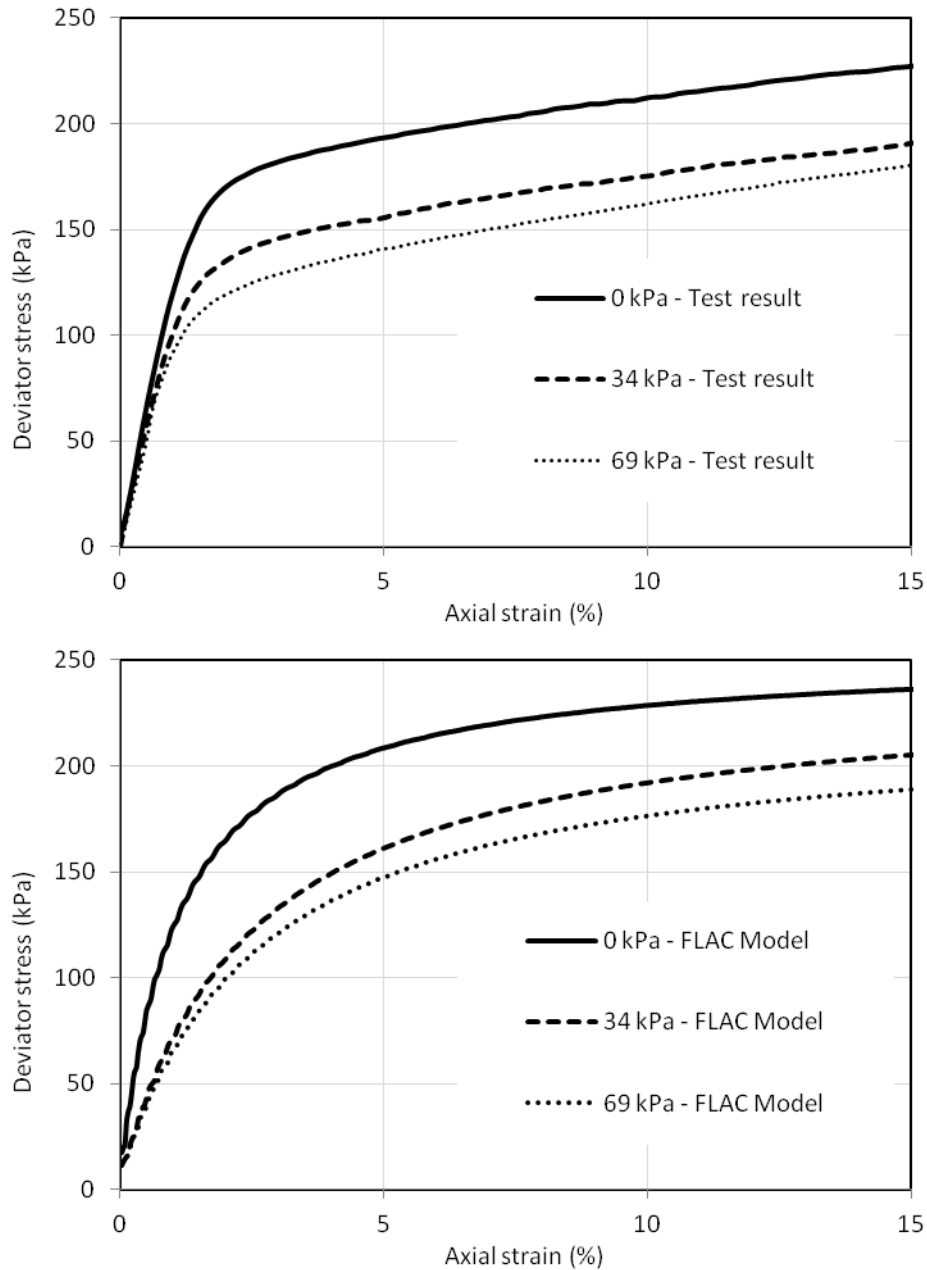
Figure 61. Deviator stress variation with confining stresses-FLAC and test data
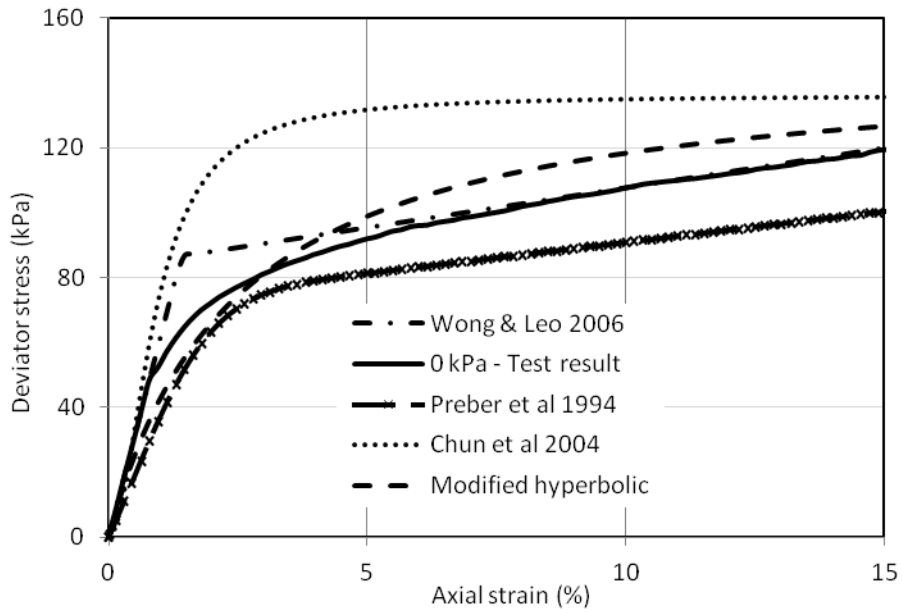
Figure 62. Comparison with other models (σ_c=0 kPa and 20 kg/m^3 density)
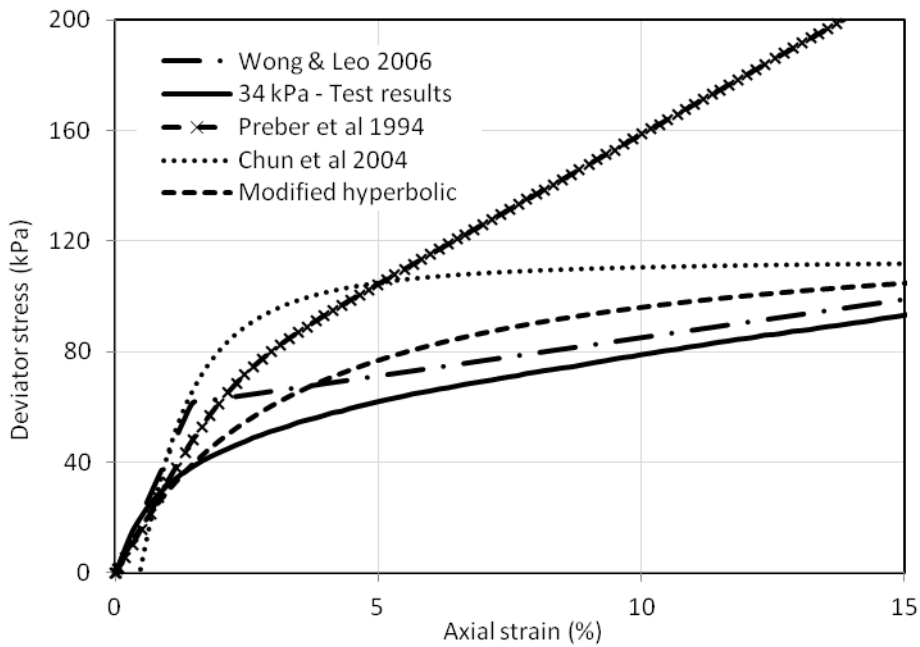
Figure 63. Comparison with other models (σ_c=34 kPa and 20 kg/m^3 density)

Figure 62 and Figure 63 show the stress-strain relation predictions by Chun et al. 2004, Preber et al. 1994, Wong and Leo 2006 and the proposed model. The model presented in this study is reasonably in agreement with the test results. The hyperbolic model can be incorporated for numerical analysis.

Conclusion

Modified hyperbolic model proposed in this study can take in to account the effect of confinement on the stress-strain behavior of EPS geofoam. The model can account for reduction in strength and modulus as a result of confinement increase. The three parameters for the model-K, n and m were determined from triaxial tests performed at different confining pressures. Results from the modified hyperbolic model agree with test results and can easily be integrated in numerical modeling.

4.5   Effect of Induced Anisotropy on the Behavior of EPS Geofoam

EPS geofoam is commonly installed under pavement structures in very soft and compressible soils to minimize settlements. Loading and unloading occur due to live loads either during construction or operation of the pavement structure. Stresses beyond the elastic limit induce plastic strains and hence induce anisotropy. Thus, effect of such introduction of stress or strain anisotropy on EPS geofoam performance should be investigated to appropriately design geofoam fills. Design of EPS geofoam fill is based on the premises that strain induced in the fill remains within the 1 to 2 % strain. In addition EPS geofoam is assumed isotropic irrespective of the stresses acting on it. However, unanticipated strains may exist either due to machinery operation during construction or confining stress effects. Effect of induced anisotropy on EPS characteristics was investigated by triaxial tests conducted on pre-stressed geofoam. Practical significance of induced anisotropy was discussed.

Design parameters for EPS geofoam are commonly derived from unconfined compression tests on 50 mm EPS cube samples(ASTM D1621 2010). A typical corrected stress-strain curve for a 20 kg/m3 EPS geofoam is shown in Figure 64. The initial modulus of elasticity, E_i (slope of the initial linear segment of the stress-strain curve), the compressive strength, σ_{c10} (usually defined as the axial stress at 10 % axial strain) and the yield stress, σ_y (point of intersection of the initial linear segment and a post yield linear segment of the stress-strain curve) are used to characterize the stress stain curves obtained from the unconfined compression tests(Preber et al. 1994). Results from conventional 50 mm cube samples significantly underestimate Young's modulus values for EPS geofoam(Duškov 1997a; Elragi 2000). Modulus values that are obtained from small size (50 mm cubes) laboratory

107

samples are about half of the values that were estimated from field observations and

should be increased for design applications (Negussey 2007).
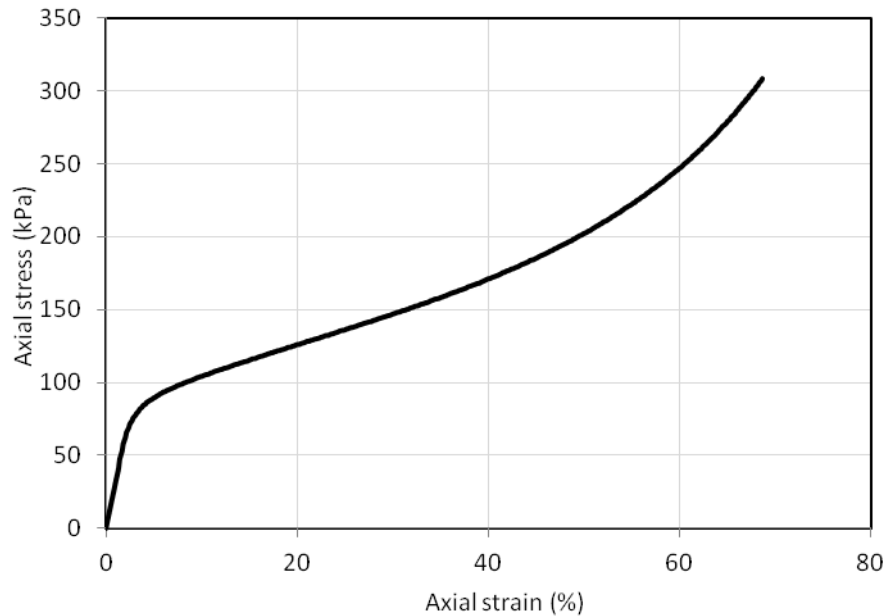
Figure 64. Load-deformation behavior of 20 kg/m³ EPS under short-term unconfined

axial compression loading

Compressive strength of EPS geofoam increase with increasing sample size; but this

increase was small (Atmatzidis et al. 2001). Results from unconfined compression tests

adequately represent the mechanical behavior of EPS geofoams in applications where

applied normal stresses remain well below yield stress or conceptual elastic strain limit.

Shape, size and aspect ratio of EPS geofoam samples tested in unconfined compression

have relatively insignificant effects on measured compressive strength at 10 %

strain(Atmatzidis et al. 2001; Eriksson and Tränk 1991).

Density of the EPS geofoam has a significant effect on the values of the compressive

strength. The strength increases as the density of the geofoam increases (Negussey 2007).

Kutara et al. 1989 reported anisotropic behavior of EPS geofoam may affect the deformation characteristics of the material. Loading perpendicular to the direction of fabrication showed higher deviatoric stresses at failure. The compressibility of EPS geofoam is highly affected by the shape of the cells. Cells close to the mold wall are usually flattened due to the moulding processes. If the compressive loads are applied perpendicular to the direction of stretching, the flattened cells will be flattened more and smaller values of compressive strength are obtained (BASF 1998).

Compression tests were performed on EPS geofoam samples of different densities, sizes and shapes. Nominal density of 20 kg/m^3 EPS geofoam was tested. Cubic samples of size 50, 75, 127 mm and cylindrical samples of 64 and 102 mm nominal diameters with aspect ratio of 2:1 were tested. The cylindrical samples were precision cut to required dimensions in the factory. Unconfined compression tests were done. In triaxial tests, samples were encapsulated in rubber membrane prior to assembling in a triaxial cell. The cell was filled with water and confining pressures were applied through an attached accumulator. Tests were conducted at constant room temperature. Load, volume change and axial deformation were recorded.

Isotropic Compression Test

Isotropic compression tests were conducted on cylindrical EPS geofoam samples of 64 mm diameter and 127 mm height. Cell pressure was applied at a specified rate. For constant pressure infusion setting, average pressure rates detected by the cell pressure transducer were 234 and 15 kPa/minute during the initial and post yield stages, respectively. The axial strain rates were 2.4 and 0.8 %/minute during the initial and post yield stages. The corresponding volumetric strain rates were 6.9 and 1.9 %/min. Axial and

volumetric deformations were recorded. Figure 65 shows the deformation response from

isotropic compression test. The slope of volumetric vs. axial strain plot is 3.0, which

suggests EPS geofoam is isotropic. Repeat tests for three different densities from same

manufacturer resulted consistent isotropic responses irrespective of the density tested.
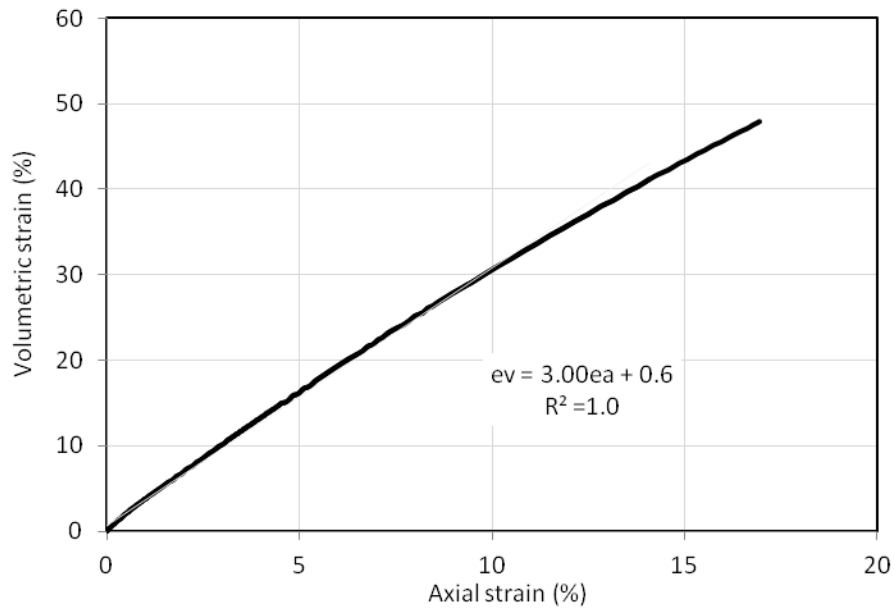
Figure 65. Deformation response due to isotropic compression

Uniaxial Loading and Unloading Tests

   Figure 66 is the stress-strain plot for 20 cycles of loading and unloading to an axial strain

of 2 % and final loading to 25 % axial strain after the 20 cycles at strain rate of 10

%/minute. The cyclic loading and unloading did not change the initial modulus of elasticity.

This suggests the EPS geofoam behaved elastically when the axial strain limit remained

below 2 %. Flaate 1987 reported cyclic load tests on EPS geofoam withstood unlimited

number of cyclic loads as long as the loads were below 80 % of the compressive strength.

van Dorp 1988 also reported that there was no change in the initial tangent modulus when

a 20 kg/m^3 EPS was subjected to 2 million cycles of straining between 0 and 1 % at cyclic

strain rate of 10 Hz.
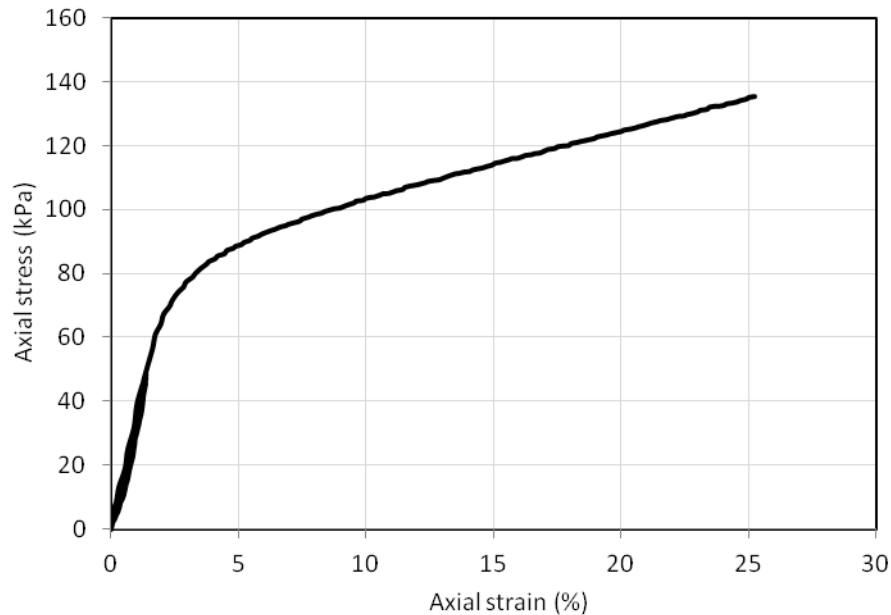
Figure 66. Loading and unloading in the elastic range

   When loading and unloading occurred at a strain level outside of the elastic range, there

was plastic strain accumulation and reloading modulus degraded relative to the initial

elastic moduls. Figure 67 shows 20 cycles of loading and unloading at a strain level of about

5 %. The initial elastic modulus is 3.69 MPa whereas the rebound and the reload moduli are

2.85 and 2.64 MPa, respectively. Decrease in modulus got pronounced as the strain level for

loading and unloading increased. Eriksson and Tränk 1991 reported that the initial moduli

in the second and third cycles were much less than the first cycle when EPS geofoam was

loaded to 10 % strain level in three loading and unloading cycles.
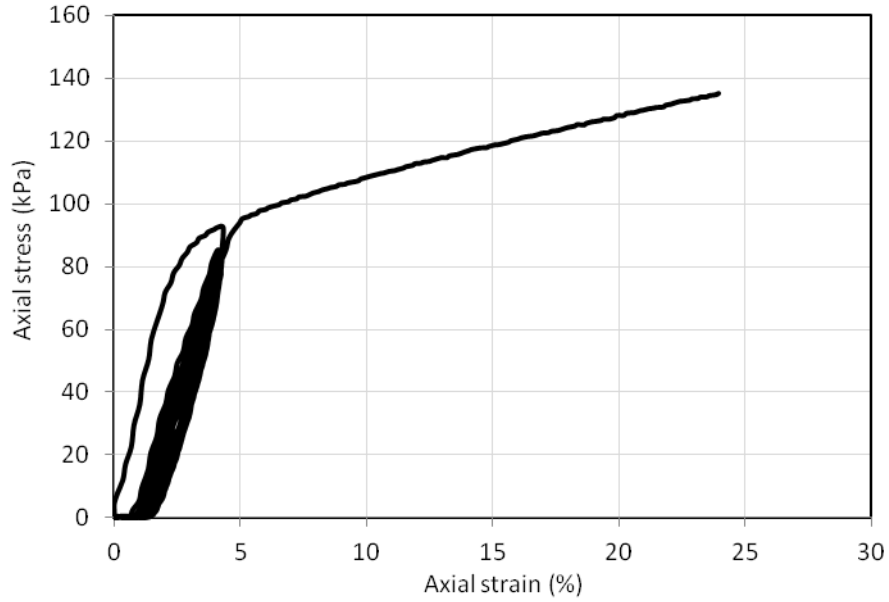
Figure 67. Loading and unloading out of the elastic range

Figure 68 is a plot showing effect of axial strain level at the time of loading and unloading cycles. It is evident that the reloading modulus gets smaller and smaller as the pre-strain level increases.
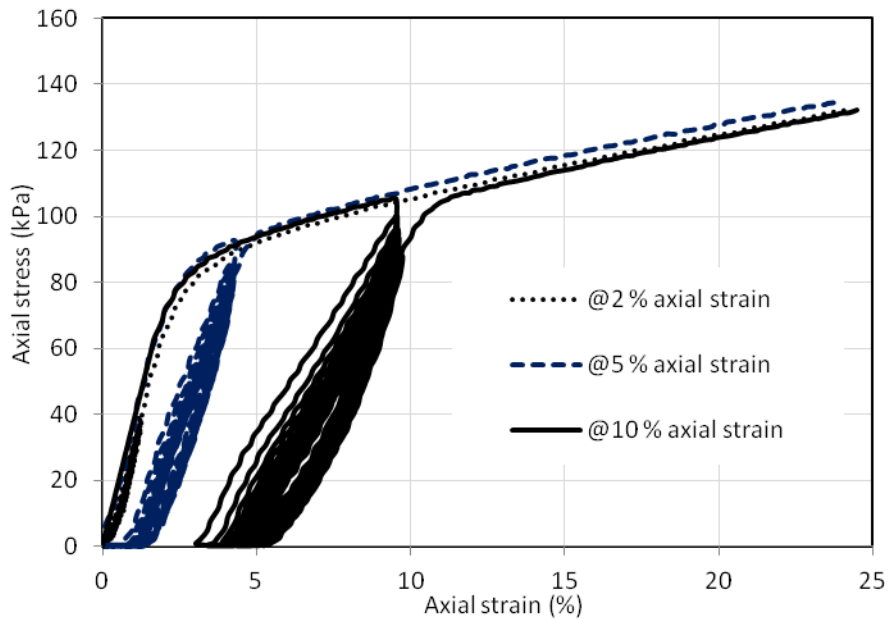
Figure 68. Loading and unloading at different axial strains

Magnitude of plastic strain as a result of loading and unloading depends on the amount of pre-stressing or pre straining. For example when a stress value corresponding to 10 % axial strain is used as the pre-stress, there was 4 % plastic strain accumulation at the end of 20 cycles of loading and unloading. But at the end of the 20 cycles, the plastic strain was 2% for a pre-stress value corresponding to 5 % axial strain, Figure 68.

Effect of Induced Anisotropy on Stress-Strain Relations

When EPS geofoam is used as a fill there can be pre-straining during construction due to operation of heavy trucks and machineries. In addition, improper working loads may produce strains outside of the elastic range. Effects of such induced strains on the stress-strain characteristics were studied by doing tests on samples of pre-strained EPS geofoam. Big cubes (76 and 127 mm) of EPS geofoam were loaded to different strain levels at a strain rate of 10 percent per minute. From these strained big cubes, 50 mm cube samples are cut from the middle by noting the orientation of loading. Unconfined compression tests were done on 50 mm cube samples as per ASTM - D1621 2010. Tests were done both in the same and orthogonal directions to the pre loading.

Figure 69 shows the effect of pre-stressing on the stress-strain relation when the sample is reloaded in the same direction as the pre-loading. The initial elastic modulus degraded as the percentage of pre straining increased. When similar tests were conducted in the orthogonal direction to the pre straining, the stress-strain curves remained relatively unaffected, Figure 70.
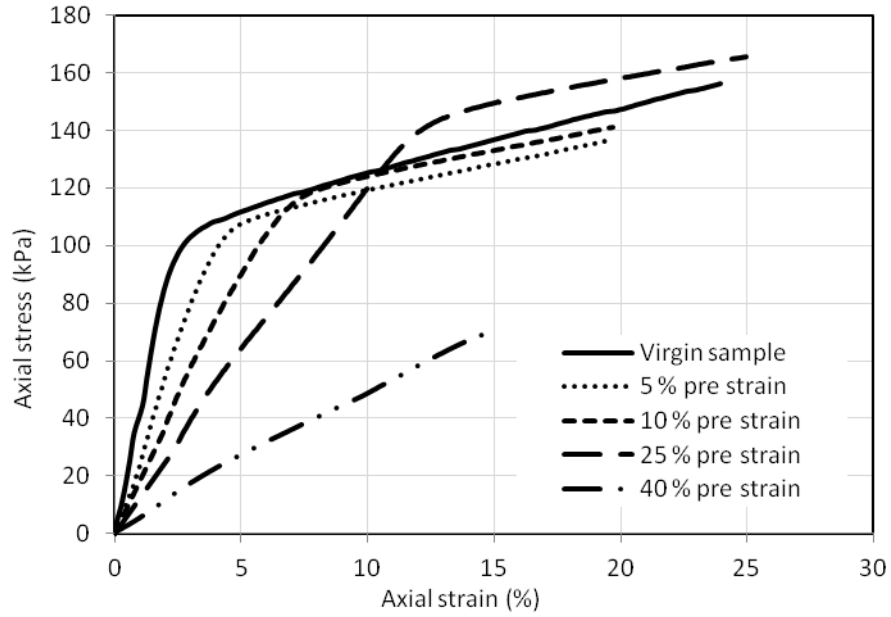
Figure 69. Stress vs. strain plots for same direction of reloading
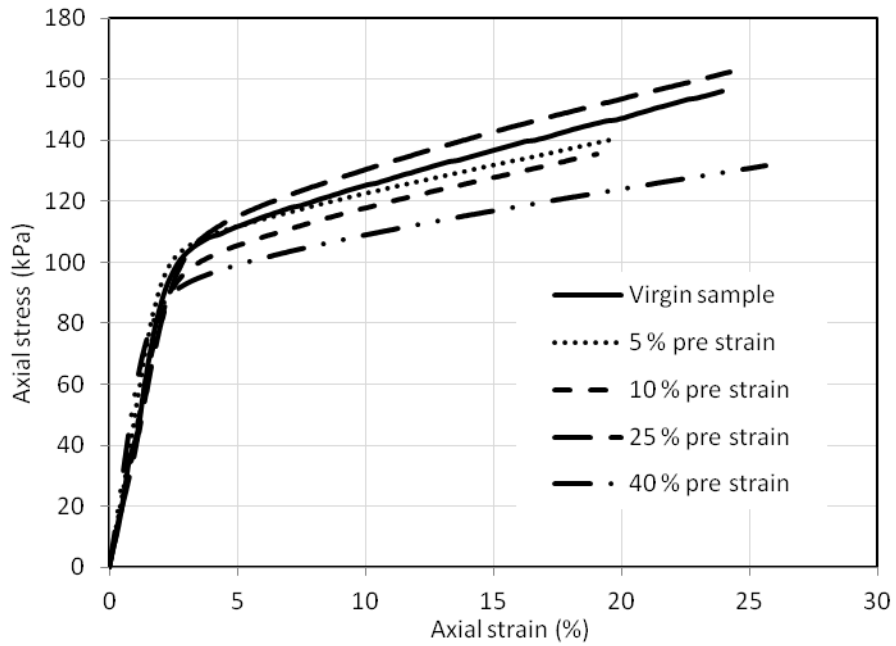
Figure 70. Stress vs. strain plots for orthogonal direction of reloading
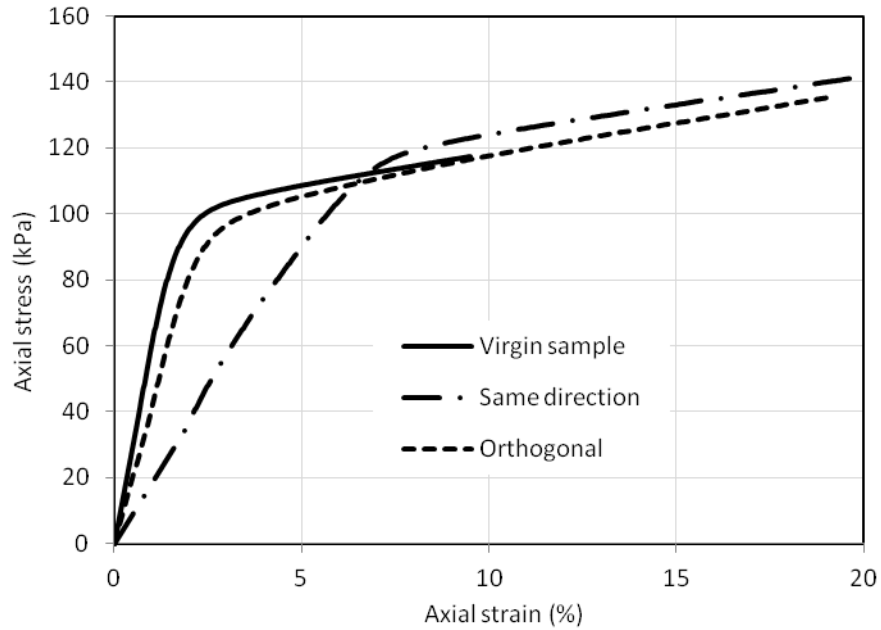
Figure 71. Combined stress vs. strain plots for 10 % pre straining

The practical implications of such tests can be seen as in Figure 71. If analysis of EPS fill is based on elastic parameters obtained from virgin samples, the deformations computed would be small due to higher values of initial modulus. However such computed deformations would be greater if some percentage of pre straining of EPS geofoam during construction or operation had occurred. Figure 72 shows the degradation of initial modulus with increasing level of pre-straining in the same direction. About 50 % reduction in the initial elastic modulus is observed when the percentage of pre straining increases from 0 to 10 %.

The chart shows a curve with the equation:

$$y = -4\text{E-}06x^4 - 0.0001x^3 + 0.0149x^2 - 0.3783x + 4.9068$$
$$R^2 = 0.9995$$

The y-axis is labeled "E (MPa)" ranging from 0 to 6, and the x-axis is labeled "% of pre-straining" ranging from 0 to 30.
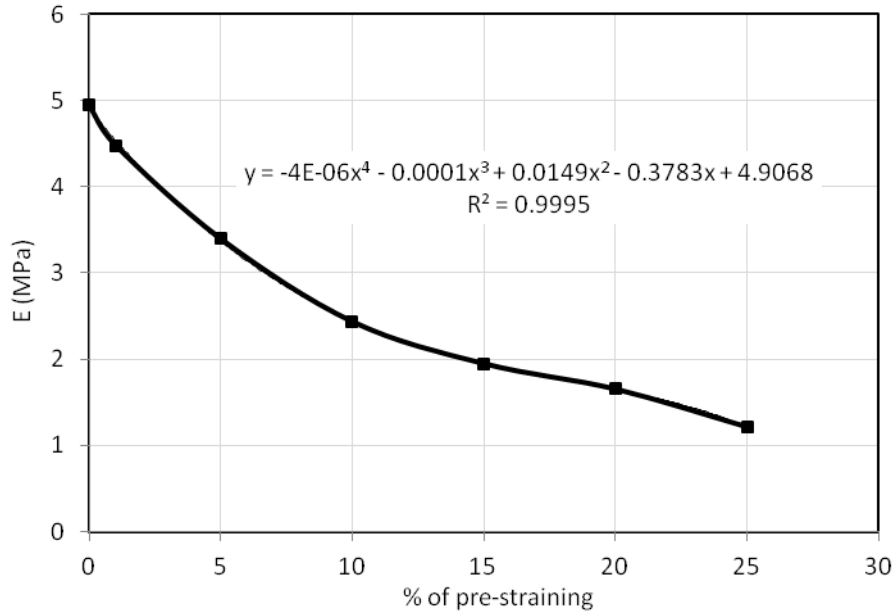
Figure 72. Initial modulus vs. percent of pre straining

Effects of isotropic pre-straining were also investigated. Cylindrical samples of 102 mm diameter and 203 mm height were confined isotropicaly with a cell pressure of 69 kPa until there was no further reduction in volume. It was observed during isotropic compression that the samples were compressed about 30 % in volume and 10 % in height. Small 50 mm cube samples were cut from these pre compressed big cylindrical samples and tested as per (ASTM D1621 2010). Results showed that effect of isotropic pre-straining on the elastic modulus was very small, Figure 73. Test results from very slow axial strain rate loading and staged loading test are also shown. Axial strain rate of 0.005 %/min was used for the very slow test. In the staged loading test, each load was made to stay for 2 hrs so that most of the strains, both elastic and inelastic, would be recorded. Staged and slow tests gave relatively same results and showed very small difference with value of elastic modulus which was obtained from fast loadings with axial strain rate of 10 %/min. However it should be noted

that yield stress and compressive stress at 10 % strain are less than from fast loading results.
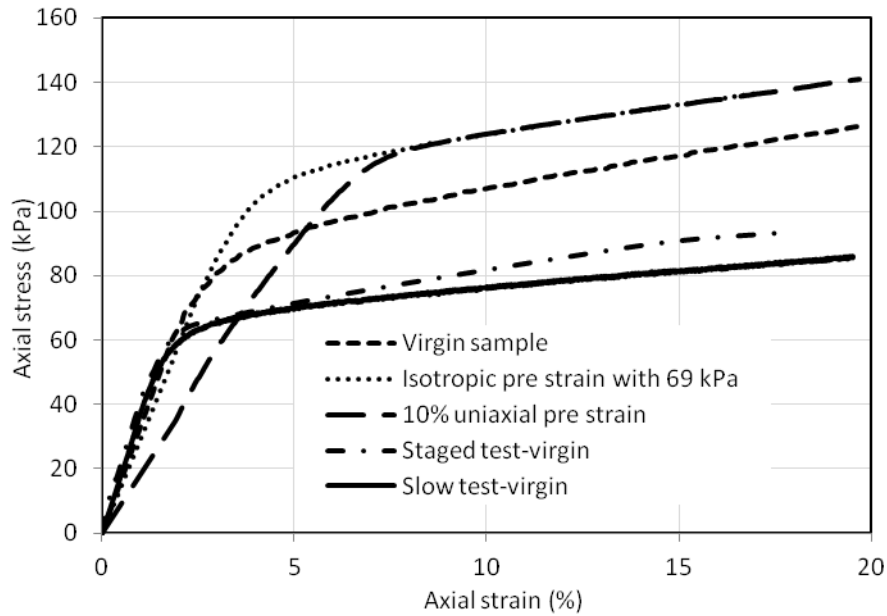
Figure 73. Varieties of unconfined compression tests (20 kg/m³)

Yield stresses from fast and slow tests were about 91 and 68 kPa respectively. There was about 25 % increase in the yield stress when fast strain rate of 10 %/min was used. Similarly compressive stresses at 10 % strain were 107 and 76 kPa for fast and slow tests respectively. About 30 % increase in strength was observed in the fast test. Axial stress at 10 % strain for both pre-strained tests (isotropic and uniaxial) was about 124 kPa as presented in Figure 73. This was comparable with axial stress at 20 % strain on the virgin sample as the pre-strained samples had already 10 % axial strain. The yield stress in the virgin and pre-strained samples done at the same strain rate was reasonably the same. Hence yield stress was not dependent on pre-straining but depended on strain rate.

Results of Exhumed Blocks from I88 over Carrs Creek

 A culvert that carried Carrs Creek under Interstate 88 was washed away by a heavy storm in June 2006 in the town of Sydney, Delaware County, NY. In the reconstruction of the culvert, EPS geofoam fill was selected for light weight and rapid placement. The reconstructed pavement on the culvert settled excessively and the EPS geofoam fill was exhumed. EPS geofoam of 20 kg/m^3 density was used at a depth of about 3.4 m under a 0.6 m pavement structure and 2.8 m soil fill. Unconfined compression tests were conducted on exhumed and fresh geofoam samples and results are shown in Figure 74. Plots designated as highly strained and least strained are for samples cut from highly and least deformed exhumed geofoam blocks respectively. Results of virgin samples were found to be similar to those of least strained samples.
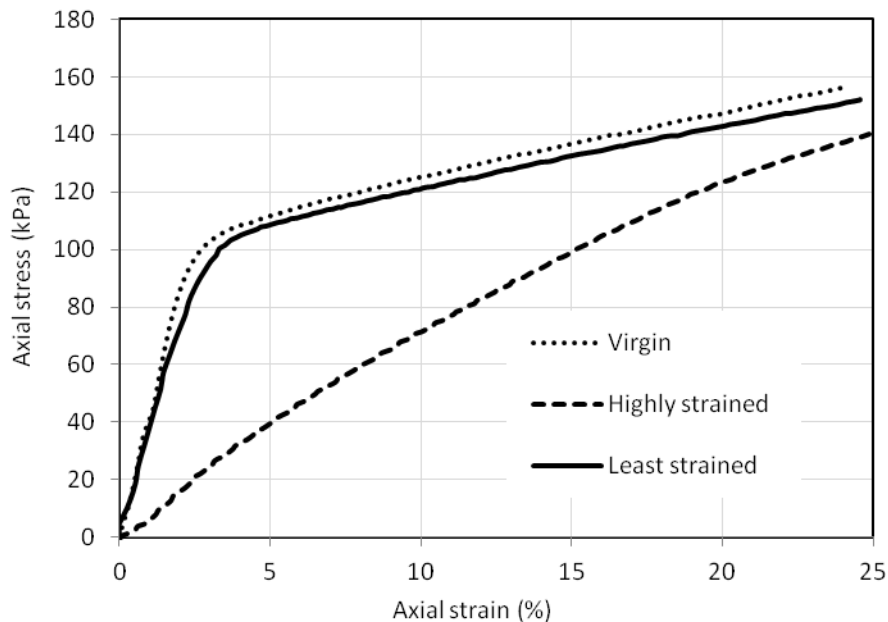
Figure 74. Results from exhumed geofoam blocks (20 kg/m^3)

Modulus of highly strained samples is about 0.82 MPa and that of fresh geofoam is about 3.78 MPa. Up to about 80 % modulus reduction was observed. Similarly, compression strength at 10 % axial strain reduced from 120 to 71 kPa due to pre-strain, which is 40 % reduction. These reduced modulus and compression strength could be contributors to settlement of the pavement. It should also be noted that the overburden pressure on the EPS geofoam fill in the project was about 70 kPa. This was excessive as compared to the recommended 30 % of the strength at 10 % axial strain, which is about 40 kPa for EPS geofoam of 20 kg/m^3 density.

Effect of induced anisotropy on the stress-strain characteristics of EPS geofoam is not considered in the design of fills. Pre-straining of EPS fills may result from operation of heavy machineries or trucks during construction. Such pre-straining is shown to result in degradation of the initial elastic modulus and hence higher magnitudes of deformation in service.

4.6   Creep Tests

Time dependent deformation under sustained loading or creep is an important consideration in the long term performance of EPS geofoam. Design of EPS geofoam fills is mainly based on limiting working stresses to produce tolerable deformations. Results from unconfined uniaxial creep tests have provided justification for such design criteria. With different types of applications involving submergence and higher surcharge loads, creep deformations under confining pressures have been occurring. A series of creep tests were performed on different densities of EPS geofoam with and without confining pressures. The results showed confining pressures can significantly affect the creep responses of EPS geofoam. Effects of confining pressures on creep deformations were more pronounced for lower densities.

EPS geofoams under service loads can develop significant creep deformations. Live loads due to traffic can introduce changes in confining pressure states. However, magnitudes and durations of transient stresses increments in EPS geofoams due to live loads remain small with benefit of concrete load distribution slabs or deeper cover. For large heights of EPS geofoam installations and potential submergence, larger surcharge depths may be required to resist potential uplift due to buoyancy. The combination of large hydrostatic pressures and saturated surcharge depths can produce significant sustained confining pressure increases on buried EPS geofoam installations. Post construction creep deformations of geofoam mainly depend on the level and duration of dead loading. Both creep and transient deformations can be of main concern in design of geofoams. Working stress values are usually selected so as to limit creep deformations to acceptable levels over the service life of the facility. The design approach developed in Norway is most commonly used and is

based on limiting allowable dead loads on geofoam to 30 % of the compressive strength at

5 % strain. In addition, another 10 % of the compressive strength is allowed for transient

live loads. Design values are based on unconfined compression loading of 50 mm cube

samples at a strain rate of 10 % per minute (Frydenlund and Aabøe 1996). Creep tests

were conducted on 50 mm geofoam cubes using nominal stress levels of 30, 50, and 70 %

of the compressive strength (Anasthas 2001; Sheeley and Negussey 2001; Srirajan et al.

2001; Sun 1997). Results showed that creep deformations can be considered negligible for

stress levels less than 30 % of compressive strengths at 5 % strain. Creep behavior of EPS

geofoam is affected by sample size and density (Srirajan et al. 2001). Larger samples

experienced less creep deformation over a given time period and equivalent loading. Small

samples tend to overestimate creep deformations of EPS geofoam due to end effects and

more pronounced seating error (Elragi et al. 2001; Negussey 2007). Denser samples

developed less creep strains for the same duration and magnitude of loading (BASF 1998,

Srirajan et al. 2001). Full scale laboratory creep tests for axial stress of 50 % of the

unconfined compressive strength showed that total observed axial strains were 1.2 % after

1270 days, out of which 64 % was in the first two days (Aabøe 1993). For the same sample

size, density and duration of loading, (Srirajan et al. 2001) and (Duškov 1997b) reported

reasonably linear elastic range of response to stress levels of up to 50 % of the unconfined

compressive strength at 5 % strain. Duškov 1997, van Dorp 1988, Sheeley and Negussey

2001 also reported that with sustained loadings greater than 50 % of the compressive

strength at 5 % strain, creep deformations develop. (Srirajan et al. 2001) suggested

working stress levels of up to 50 % of the unconfined compressive strength at 5 % strain

may be reasonable. With deeper burial of EPS geofoam blocks and possible submergence

and flooding, in post construction, conditions that can produce significant lateral pressures can develop. The experimental investigation and findings in this work are aimed to provide a better understanding of the significance and effects of confining pressures on EPS geofoam engineering behavior.

A series of uniaxial (unconfined), isotropic and conventional triaxial monotonic loading or confined creep compression tests were performed EPS geofoam samples. Three grades, nominal densities of 16, 20, and 32 kg/m^3, of EPS geofoam were tested. Cylindrical samples were pre-cut to required dimensions at the factory. Most of the 64 and 102 mm nominal diameter samples were of 2:1 (H:D) aspect ratio. Calibration curves were developed to provide compliance corrections for triaxial cell volume expansion. Test samples were encapsulated in rubber membrane prior to assembling in a triaxial cell for confined creep tests. Triaxial cell was filled with water and confining pressures of 0, 34 and 69 kPa were rapidly applied through an attached accumulator. Constant axial loads corresponding to 0, 30 or 50 % of unconfined compression strength at 10 % axial strain were applied immediately following application of confining pressure. The feedback loop controlled testing system was programmed to follow desired stress paths or maintain set loading rates. Actual dimensions and weights for each test specimen were determined as selected for testing. All tests were performed at constant room temperature. Axial loads and deformations, cell pressures and volume changes were monitored and recorded through the data acquisitions system.

Results of unconfined and isotropic compression tests on 64 mm diameter EPS geofoam samples of 20 kg/m^3 density are shown in Figure 75. Axial strain rate of 10 % per minute was maintained for the unconfined compression and volumetric strain rate of about 7 %

122

per minute was observed. In isotropic compression, for a constant pressure infusion setting, average pressure rates detected by the cell pressure transducer were 234 and 15 kPa/minute during the initial and post yield stages, respectively. The axial strain rates were 2.4 and 0.8 %/minute during the initial and post yield stages. The corresponding volumetric strain rates were 6.9 and 1.9 %/min. The stress-strain plot for unconfined compression is in terms of axial stress and strain; whereas the isotropic compression result is in terms of cell pressure and volumetric strain. As yielding and crushing of cell walls occurred in both unconfined and isotropic compression, response curves of similar shape developed [Figure 75 (a)]. Both unconfined and isotropic compression responses develop apparent yielding at approximately 93 and 63 kPa, respectively. The corresponding estimates of E_i and B_i suggest a Poisson's ratio of about 0.25. At 10 % axial and volumetric strains, the respective unconfined and isotropic compression strengths were 116 and 82 kPa. The yield stresses are at about 80 % of the corresponding compressive strengths for both the unconfined and isotropic compression. Throughout the isotropic compression, the proportion of axial to volumetric strains remained about 1:3,Figure 75 (b). Thus the inherent isotropy of the material was preserved in both the elastic and plastic range of deformations.
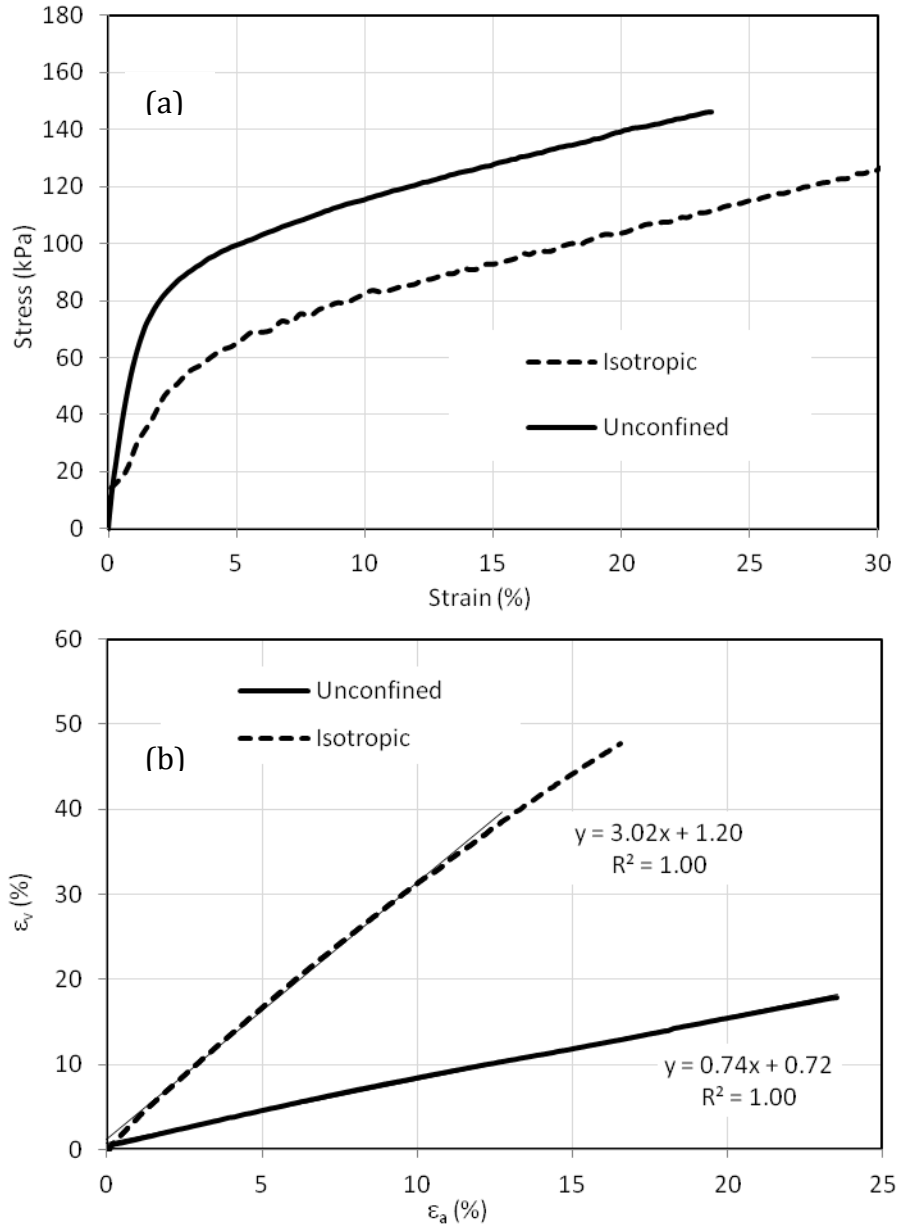
Figure 75. Isotropic and unconfined compression tests (20 kg/m³)

4.6.1 Isotropic Creep

Figure 76 presents axial and volumetric strains that occurred over 14 days under isotropic pressures of 34 and 69 kPa. The 20 kg/m³ and 64 mm diameter samples produced about 2 and 17 % axial strain and about 6 and 33 % volumetric strain,

respectively. The 34 kPa pressure was at about 50 % of the yield stress and produced relatively lower strains.
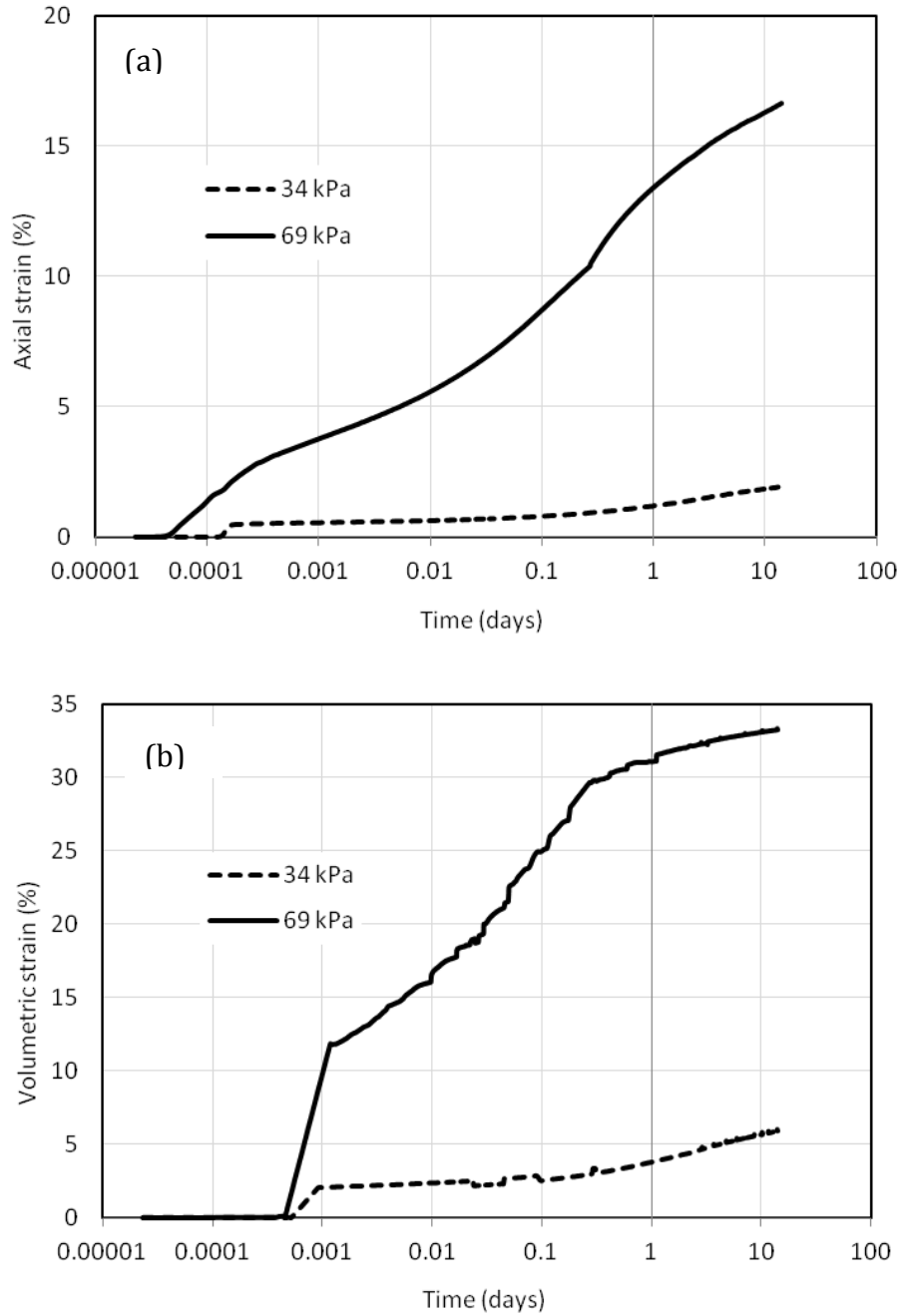
Figure 76. Isotropic creep test results (20 kg/m³)

Whereas the 69 kPa isotropic pressure was just higher than the yield stress in isotropic compression and produced significantly higher strains. Most of the deformations at both pressure levels occurred early. About 62 and 76 % of the total observed axial strains for 34 and 69 kPa compression over 14 days developed after 1 day of loading.
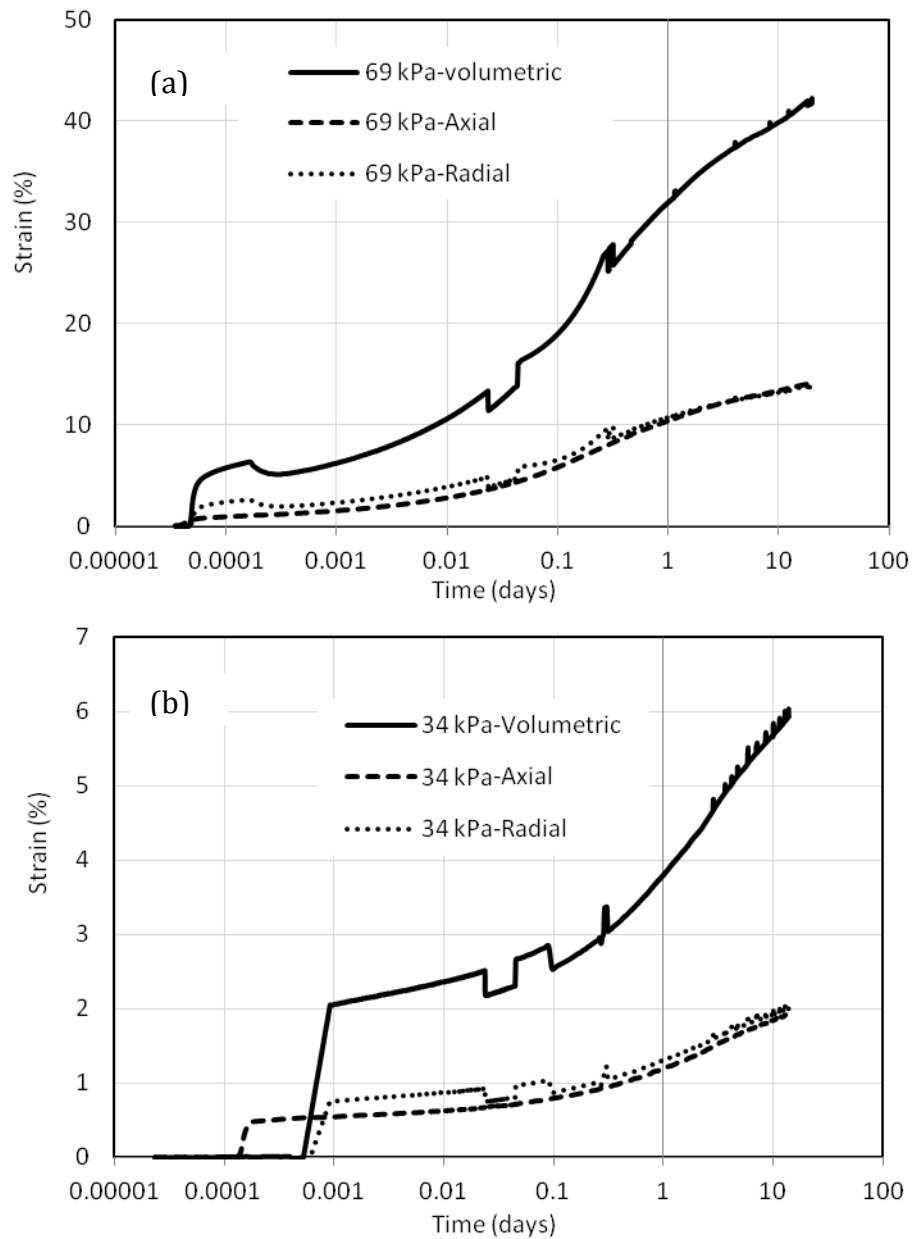
Figure 77. Axial, radial and volumetric strains with time (20 kg/m³)

Inferred radial deformations from observed axial and volumetric deformations indicate the samples deformed isotropicaly in response to the sustained 34 and 69 kPa cell pressures, Figure 77. The initial axial and volumetric strain rates were high and included the respective elastic deformations on immediate application of the confining pressures.
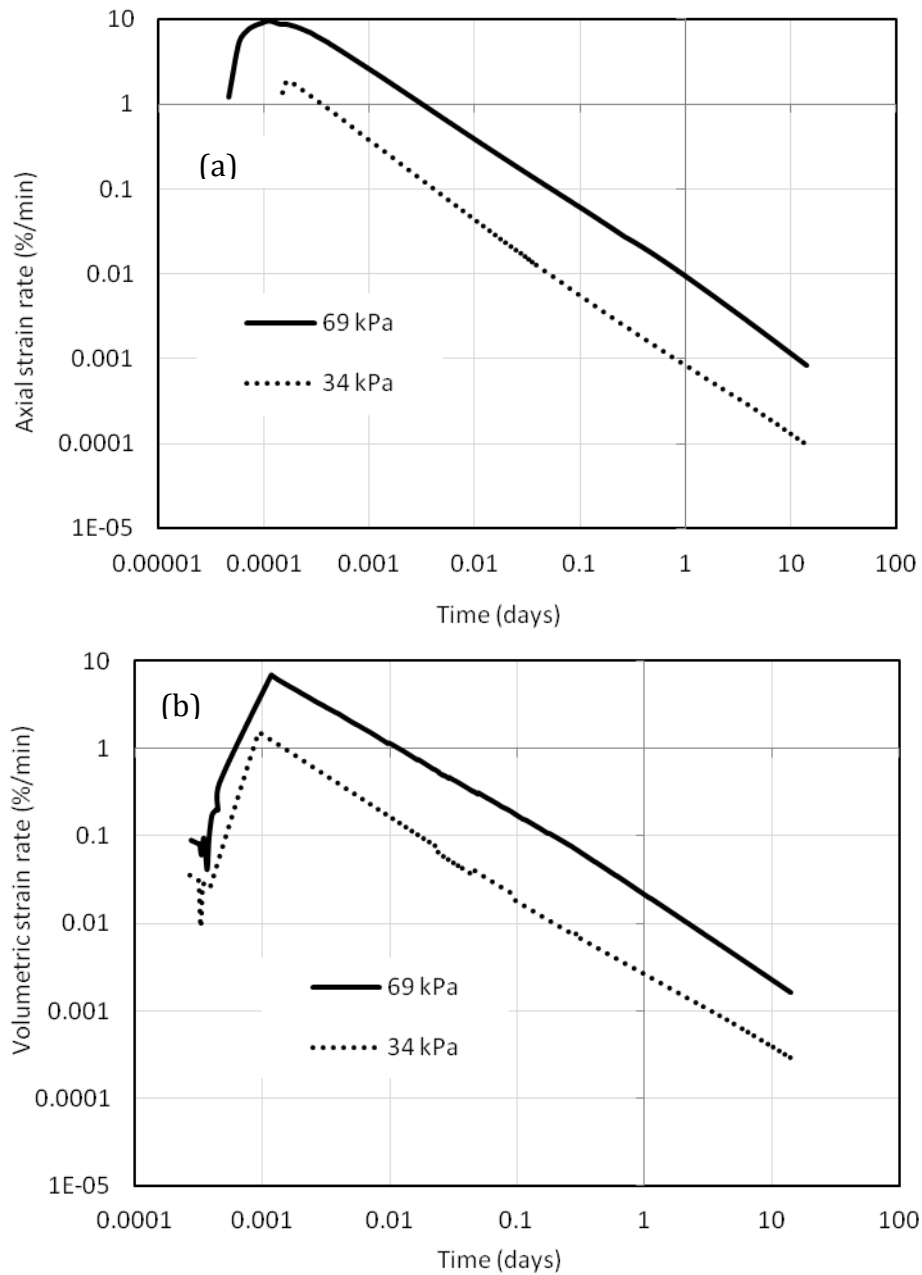
Figure 78. Axial and volumetric strain rates with time (20 kg/m³)

Strain rates continued to decrease and remained in apparent primary stages throughout the creep loading of 14 days, Figure 78.

Figure 79 shows isotropic creep results for 16 and 32 kg/m³ EPS geofoam densities. Total axial strains of 12 and 32 % were observed in 14 days for EPS geofoam of 16 kg/m³ density under 34 and 69 kPa confining pressures. The axial strains for 32 kg/m³ density were negligible for both 34 and 69 kPa confining pressures, also over 14 days. Strain rates continued to decrease for both densities, Figure 80, and remained in apparent primary stages. Effects of confinement were much more pronounced for the lower density EPS geofoams.
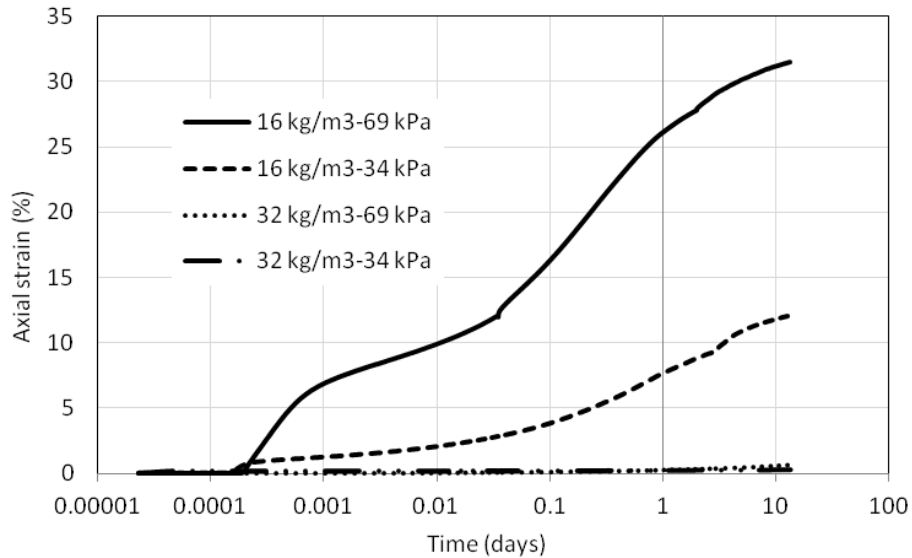
Figure 79. Isotropic creep test results (16 and 32 kg/m³)
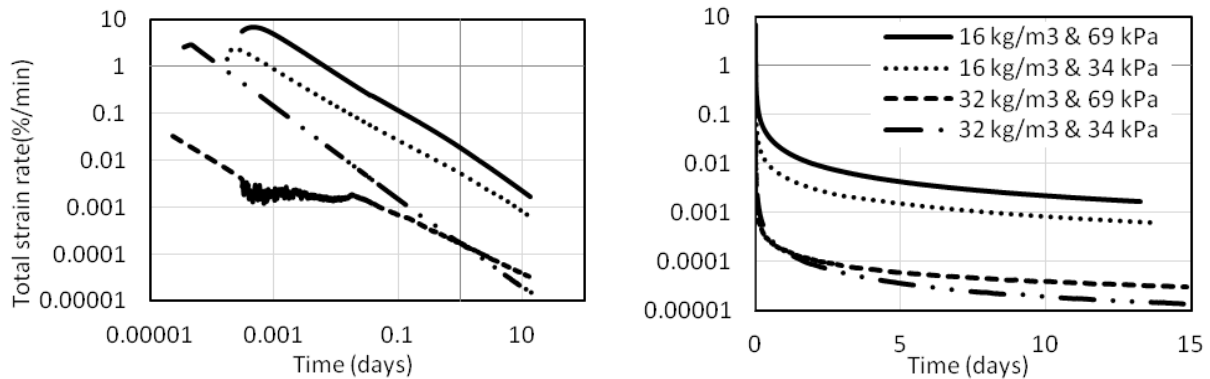
Figure 80. Axial strain rates with time (16 and 32 kg/m³)

128

Figure 81 shows axial strains for 64 and 102 mm diameter samples of 20 kg/m³ density. Both 34 and 69 kPa isotropic pressures were applied for 14 days. The 64 mm diameter samples developed 0.6 and 14 % axial strain while the 102 mm diameter samples developed 0.8 and 17 % strains. All test samples had aspect ratio of 2:1. For the relatively small contrast in the sample diameters, the effect of sample size was not as significant as differences in density and confining pressure levels.
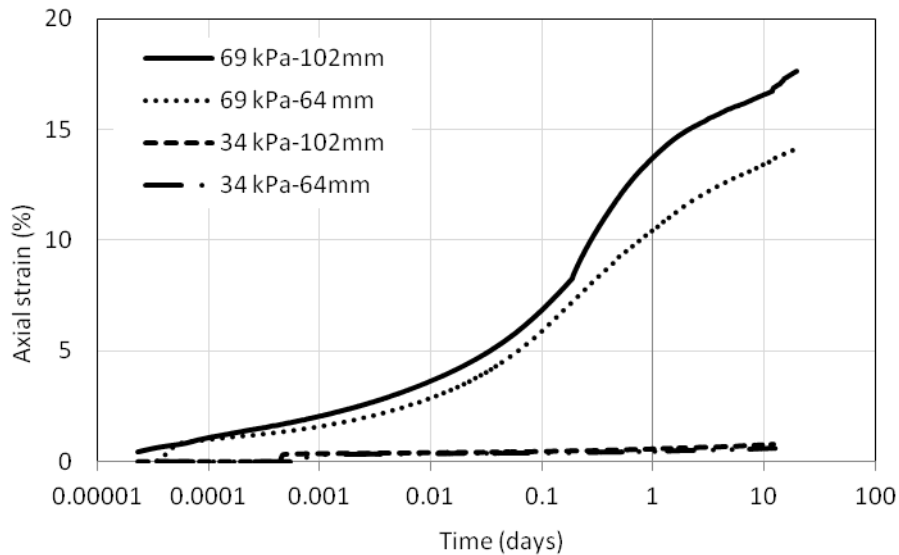
Figure 81. Sample size effect on isotropic total axial strain (20 kg/m³)

Design of EPS geofoam for creep is based on unconfined compression tests. However, occurrence of lateral deformations in confined environment may lead to movement of soil fill into the space created by such radial deformation, and hence uneven surface deformations could result. Uneven and higher deformations of EPS geofoam fill may lead to rutting and cracking related failure of the pavement system. Confining pressure of 69 kPa may develop in the field in special cases.

4.6.2 Confined and Unconfined Creep

Test sample densities, unconfined compressive strengths at 10 % axial strain as well as average axial stresses for 30 and 50 % of unconfined compressive strengths for creep loading are provided in Table 10. Creep tests were done on cylindrical samples of 64 and 102 mm nominal diameter with aspect ratios of 1:1 and 1:2 (H:D). Cube samples of 50 mm size were also used for comparison.

Table 10. Axial constant stresses used for creep tests

Density (kg/m^3)	16	20	32
Unconfined compression strength @ 10 % (kPa)	69	106	178
30 % axial stress (kPa)	21	32	53
50 % axial stress (kPa)	35	53	89

Axial deformations with time for uniaxial unconfined and confined creep tests for 20 kg/m^3 density are shown in Figure 82. For unconfined compression, Figure 82 (a), the maximum axial strain observed in 14 days was less than 2 % for axial stress of 30 % of unconfined compression strength(32 kPa). Axial strain of 4.6 % was observed in 14 days when the axial stress increased to 50 % of the unconfined compression strength (53 kPa). Strains observed from circular samples of different aspect ratio were similar and agree with that obtained from 50 mm sample. The results are reasonably in agreement with reported findings by Srirajan et al. 2001 of axial strains of less than 2 % for applied stresses less than 50 % of compressive strengths.

Figure 82 (b) represents results for creep tests with confining pressure of 34 kPa in addition to constant axial stress of 32 kPa. Axial deformations increased from about 2 % to approximately 20 % for 34 kPa confinement with axial stress of 32 kPa. Axial deformations
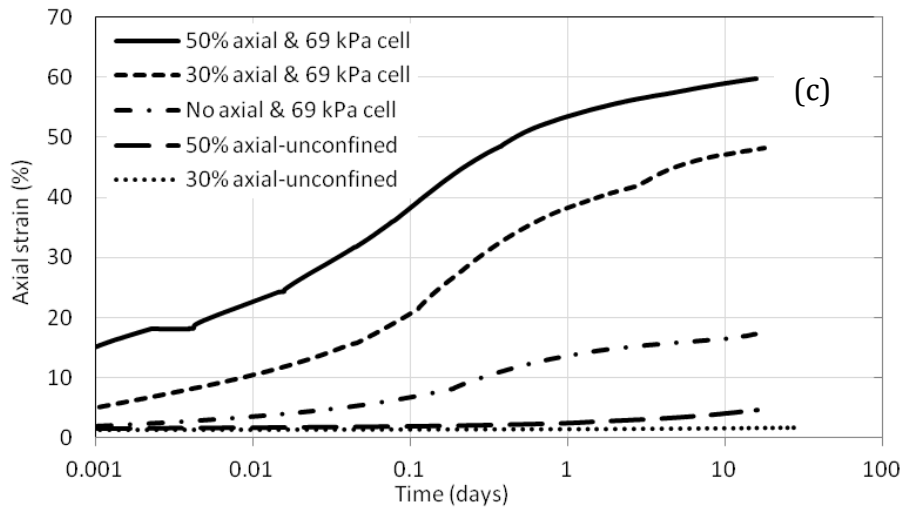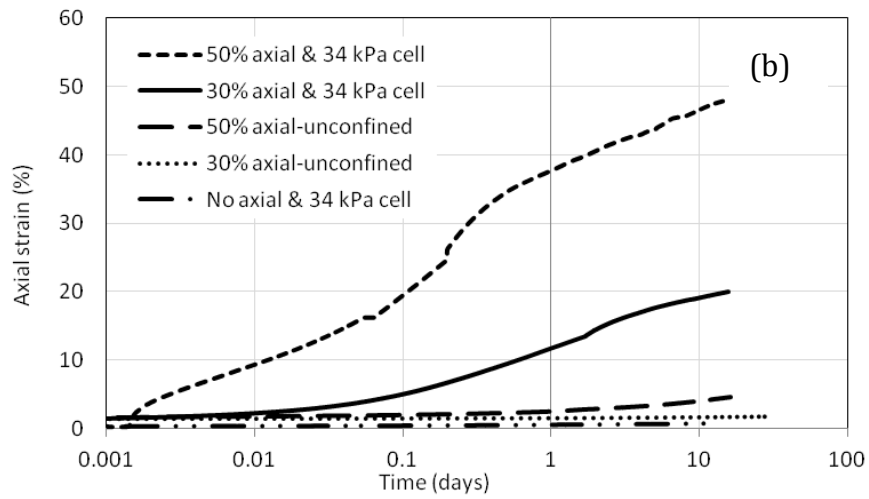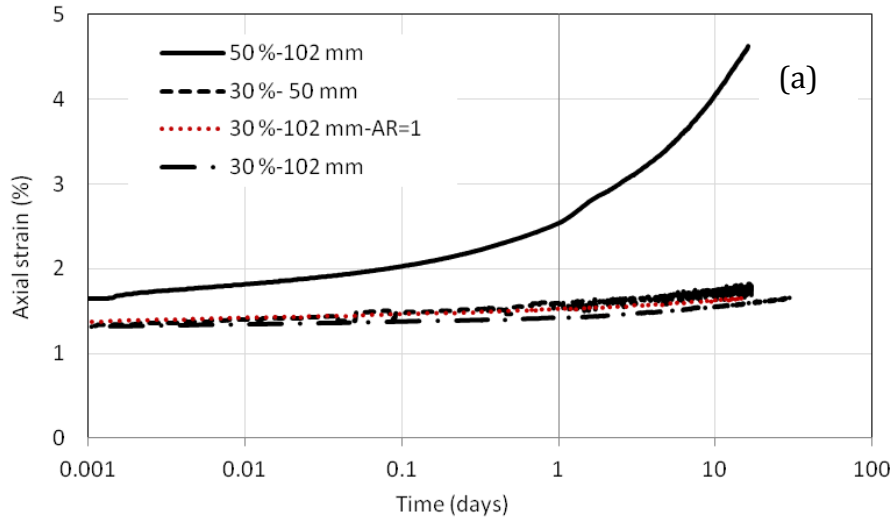
Figure 82. Axial strain vs. time for creep tests on 20 kg/m³ a) unconfined b) 34 kPa and c) 69 kPa cell pressures.

were still increasing at the end of 14 days. When confining pressure of 34 kPa was applied

with 53 kPa axial stress, 50 % of the unconfined compressive strength, about 48 % axial

deformation developed. Separately applied, axial stresses at 30 and 50 % of unconfined

compression strength at 10 % strain as well as isotropic compression at 34 kPa (50 % of
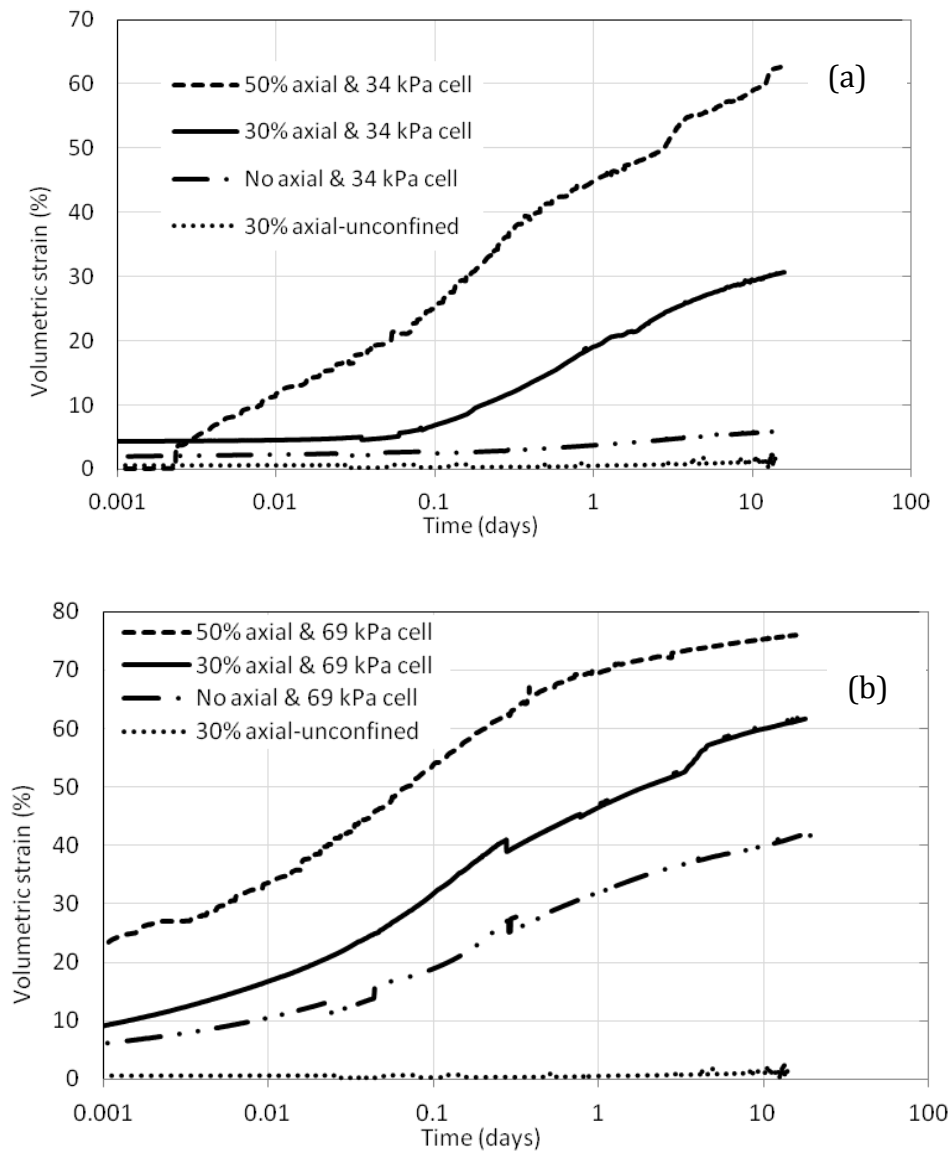
Figure 83. Volumetric strain vs. time for creep tests on 20 kg/m³ and a) 34 kPa and b) 69 kPa cell pressure

yield stress under isotropic compression) all resulted in axial strains of 5 % or less. Figure

82 (c) shows the severe influence of confining pressure on axial deformation. For 69 kPa

confinement and 30 % axial stress, axial deformation reached over 30 % in 1 day and more

than 40 % after 14 days and was continuing to increase. For 50 % axial stress and 69 kPa

confinement, over 50 % axial strain occurred in 1 day. There were no apparent creep

deformations for 30 % axial stress after 14 days loading without confining pressure.
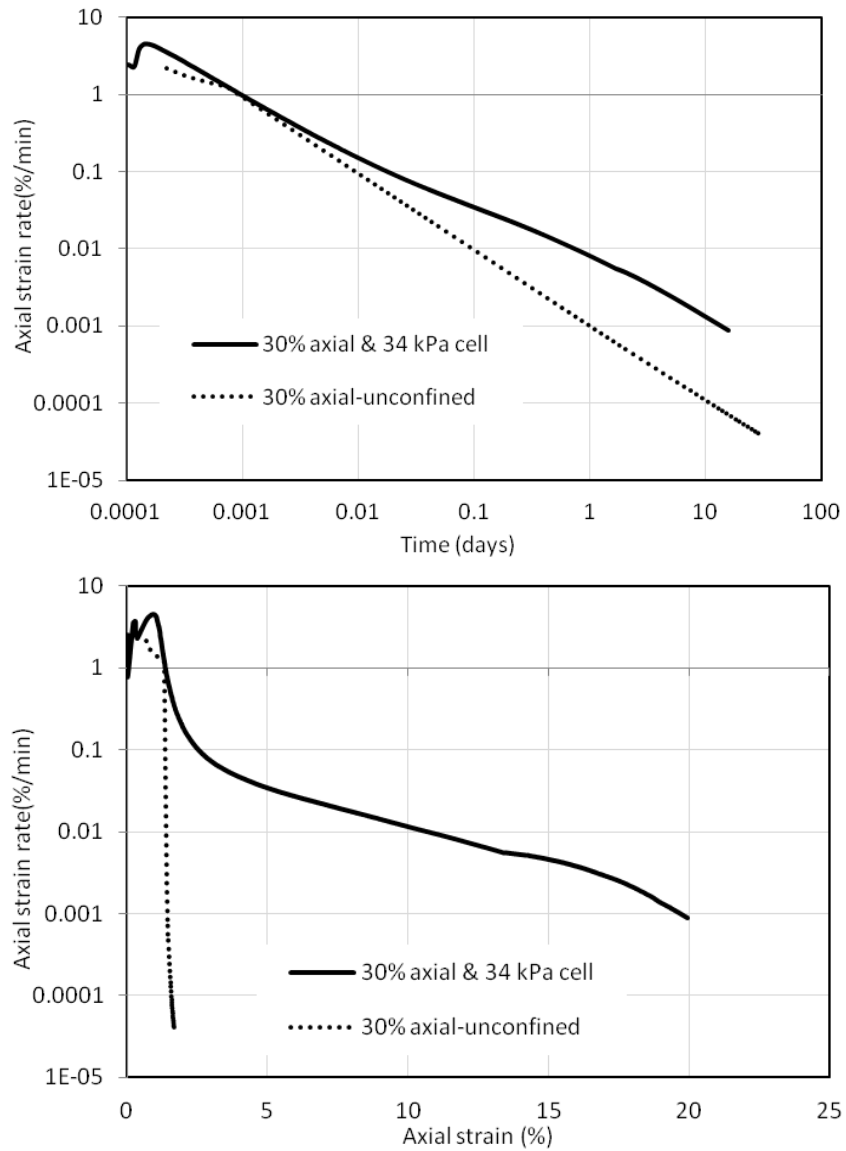
Figure 84. Strain rates and total strains (34 kPa and 20 kg/m³)

When 34 kPa confining pressure was applied with 30 % axial stress, the volumetric strain of the sample reached nearly 30 % in about 14 days and was still increasing, Figure 83 (a). For unconfined compression at the same axial stress level, the initial volumetric strain was about 2 % and further creep strain was not evident. The corresponding axial deformations for these two conditions were about 20 and 2 %, respectively.

Tests done with 69 kPa confining pressure produced large volumetric deformations, Figure 83 (b). Confining pressure of 69 kPa with 30 % axial stress resulted in volumetric strain of about 62 %. For unconfined compression at 30 % axial stress, this value was about 2 %. The respective axial strains were about 50 and 2 %. When the constant axial stress of 50 % was applied with 69 kPa confining pressure, axial strains increased to above 60 %.

Figure 85(a) shows unconfined creep deformations at respective 30 % of compressive strength axial stresses for three densities, Table 1. EPS geofoam of 32 kg/m^3 density developed 0.7 % axial strain as compared to 2.5 % for 16 kg/m^3 density in 14 days. For the same level of loading, both initial and subsequent creep strains were highest for the lowest density of 16 kg/m^3. When confining pressure of 34 kPa was applied together with 30 % axial stress, observed axial strains after 14 days jumped to about 2 and 35 % for 32 and 16kg/m^3 densities, respectively, Figure 85(b). When the confining pressure was doubled to 69 kPa, the corresponding axial strains for 32 and 16 kg/m^3 densities became approximately 16 and 56 % in 14 days, Figure 85(c).

Figure 86 shows volumetric creep strains over 14 days for cell pressures of 34 and 69 kPa but no additional axial stresses. Volumetric creep strains for 34 kPa cell pressure exceeded 40 and 25 % for 16 and 20 kg/m^3 density, respectively. For 32 kg/m^3 density, volumetric creep strains were less than 1 %. For 69 kPa cell pressure volumetric creep strains were

134
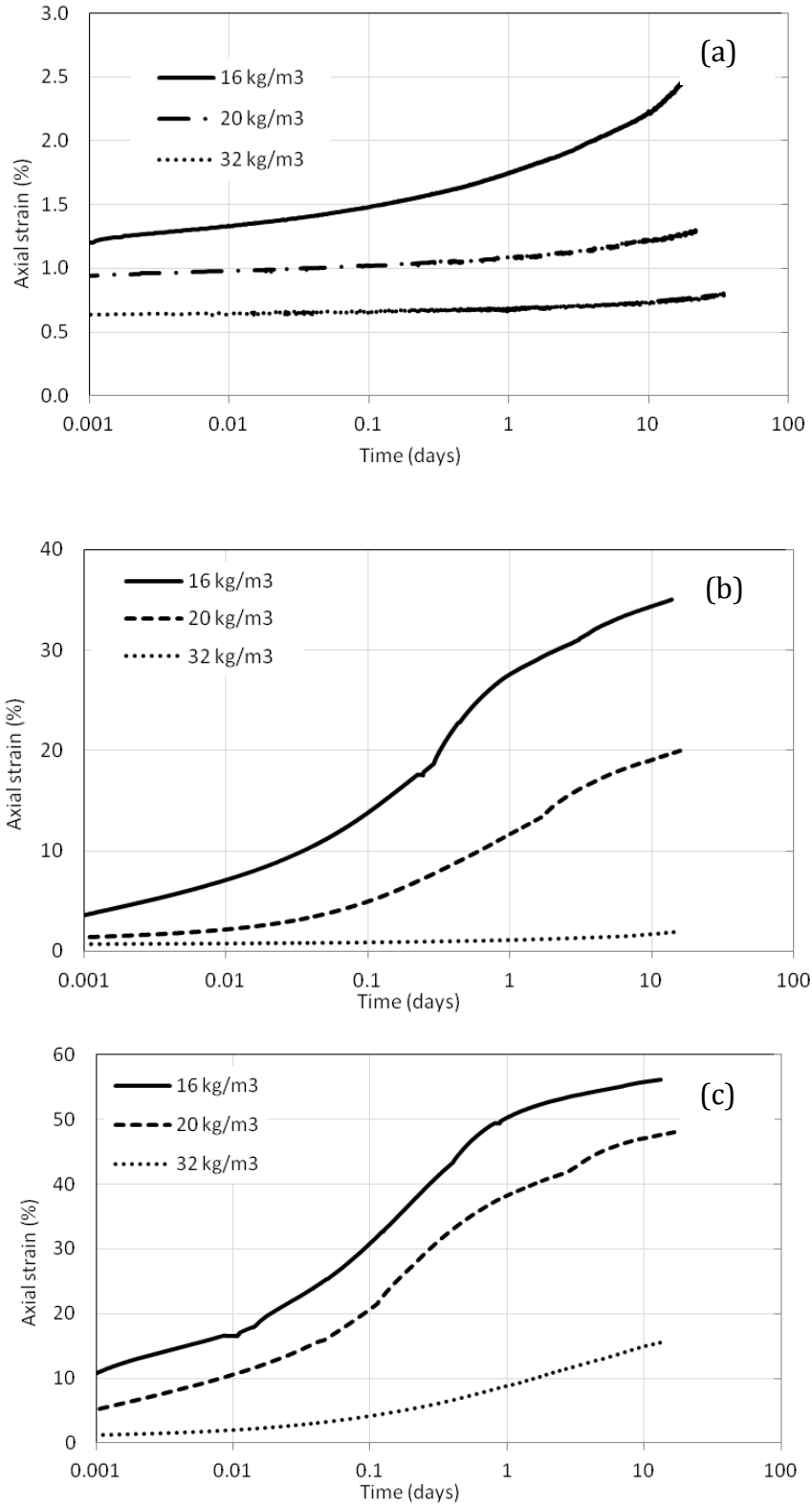
Figure 85. Unconfined and confined creep at 30 % of strength loading for 16, 20 and 32 kg/m³ densities a) unconfined b) 34 kPa and c) 69 kPa confinements.
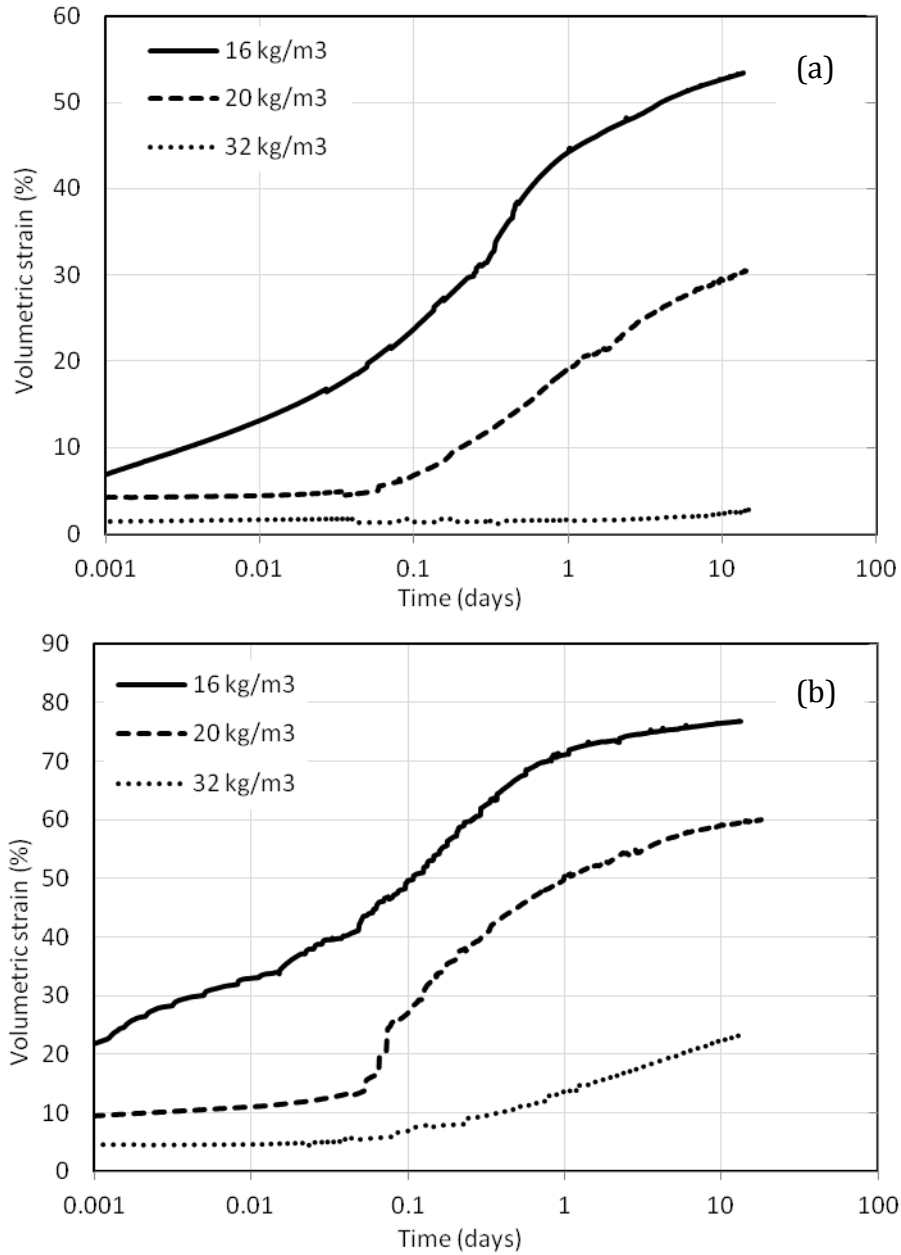
Figure 86. Volumetric strains (a) 34 kPa (b) 69 kPa confinement

50 % and greater for 16 and 20 kg/m³ densities. The volumetric creep strain for 32 kg/m³ density was more than 10 % also after 14 days. For all confined creep results, axial strains were about one third of volumetric strains in both initial and end of test stages.

Test results from this investigation indicate confining pressures can have significant effect on creep deformations of EPS geofoam. Results from tests on 20 kg/m³ density samples from 14 days of loading are summarized in Figure 87. Vertical pressures and deformations are represented in terms of major principal stresses and strains. The major principal stresses are in terms of total stresses and not effective stresses. This is because almost all of the EPS geofoam volume consists of gas (air) within relatively impervious closed cell microstructures. Deformation of the cell structure and volume change of the trapped gas result from applied total stress changes. The trend lines are isochrones for 0.001, 0.1 and 14 days of sustained loading. Each isochrone is defined by major principal stresses from both unconfined and confined creep. This is in line with findings that yield stresses for unconfined and confined compression remain approximately constant when expressed in
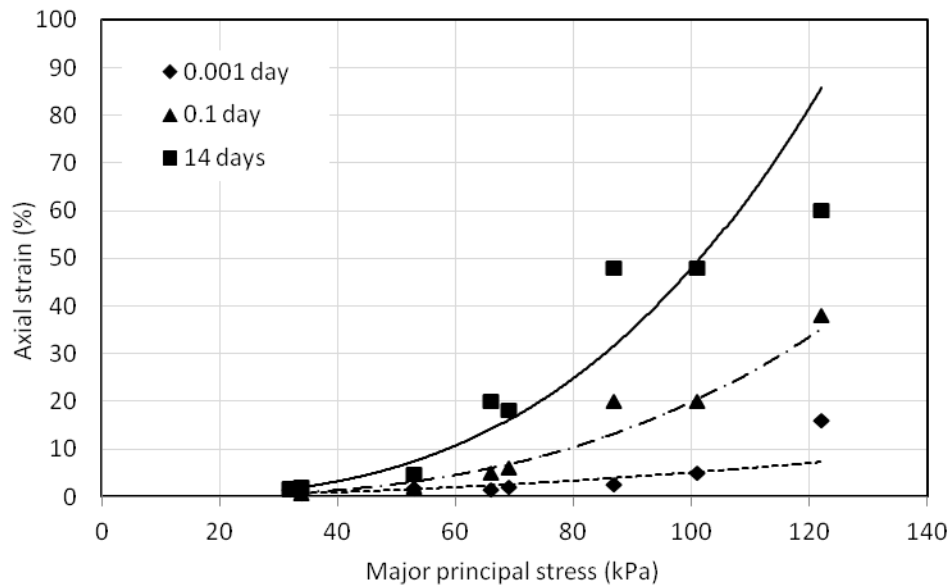
Figure 87. Equal time creep curves for unconfined and confined compression of 20 kg/m³ density.

terms of the major principal stress for one density or type of EPS geofoam(Birhan and

Negussey 2014; Wong and Leo 2006). Significant creep deformations developed beyond a

threshold major principal stress of about 35 kPa for 20 kg/m^3 density EPS geofoam in both

confined and unconfined compression loadings.

   For an allowable working stress entry on the x axis, the strain value for a particular

isochrone represents the total major strain that developed. The isochrones converge

towards a major stress near 30 kPa below which creep strains become negligible. For the

20 kg/m^3 density, this threshold stress state is close to the Norwegian criteria of 30 % of

compressive strength at 5 % strain for dead loads. Additional allowance of 10 %

compressive strength for attenuated live loads would be above the threshold but durations

of loading would be short and much less than for the lowest isochrones. Over 50 % of creep

deformations that occurred after 14 days of loading occurred in the first day. Strain rates

continued to decrease and remained in apparent primary state.

   Design with EPS geofoam is based on limiting allowable stresses to maintain creep

deformations over the service life of the project to tolerable level. Support for the design

approach has been based on unconfined compression short and long term tests. Results

reported in this investigation indicate confining pressures can significantly increase creep

deformations. Criteria for yielding and creep in unconfined and confined compression can

be related to states of total major principal stress. For the same percentage of design loads

relative to compression strengths, EPS geofoams of higher densities develop lower creep

deformations. In situations where groundwater and lateral earth pressures can produce

significant boundary total pressures, effects of confinement on EPS geofoam creep

deformations should be considered in design. Most of the creep strains would tend to occur

in the few weeks after loading. Adapting the construction sequence with complementary

monitoring can be helpful to reduce creep deformations after project completion.

4.6.3 Effect of Cyclic Stresses on Creep

Creep tests were done on EPS geofoam where additional cyclic stresses were applied after some time to study effect of cyclic stresses resulting from vehicles either during construction or operation of pavements where geofoam is used as light weight fill. A double axel truck induced an estimated average stress increase of up to 34.5 kPa or more on EPS geofoam fill employed without redistribution concrete slab. Such stress increase was considered as an increase in deviator stress when the EPF fill is dry and as cell pressure increase if there is poor drainage with higher water level. In the saturated case where the surrounding soil is not free draining and the water level is high, the pore water pressure is directly transferred to the EPF fill and is modeled by the cell pressure increase. Nevertheless, use of distribution concrete slabs significantly reduced stress increases on EPS fill.
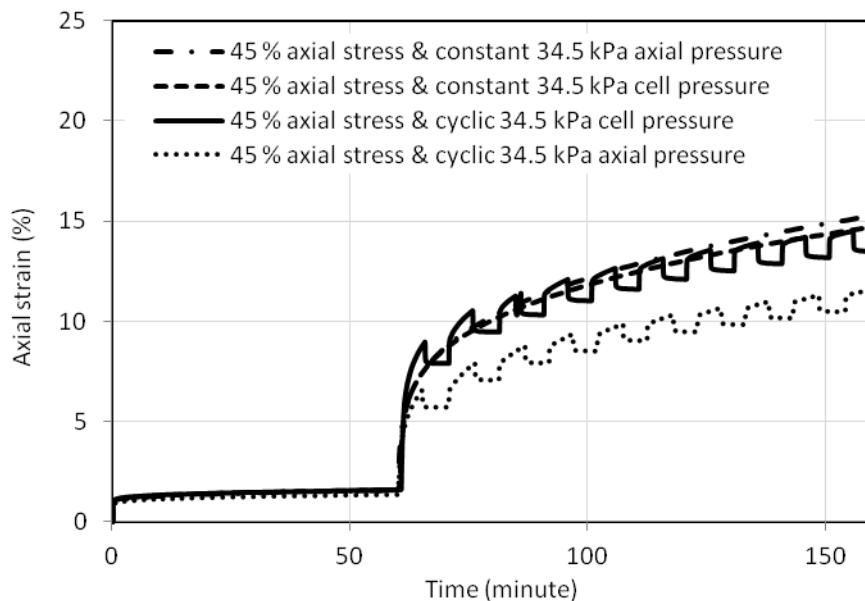
Figure 88. Axial stress of 45% and effect of increased stresses after 1 hr

Figure 88 shows results of creep tests on 20 kg/m³ and 121 mm diameter EPS geofoam samples where stresses were increased after 1 hr. Initially axial stresses of 48 kPa (1000 psf), which was 45 % of the compressive stress at 10 % axial strain, were applied in all cases shown. After 1 hr, additional stresses of 34.5 kPa were applied. The additional stresses were applied as a) constant axial stress b) constant cell pressure c) cyclic cell pressure and d) cyclic axial stress. The cycles repeated after 5 minutes assuming that one vehicle passed after the other in 5 minutes. Except the test where additional cyclic axial stress was applied (case (d)), deformation trends followed by the other three cases were reasonably similar. It can be noted that axial strain of about 2 % due to the 45 % axial stress increased abruptly to strains of up to 15 % after 160 minutes in the three tests and to about 12 % for the case where the additional stress was cyclic axial stress. Results from these tests suggest that use of concrete distribution slabs and free draining soil around EPS geofoam fill helps to reduce geofoam deformation.
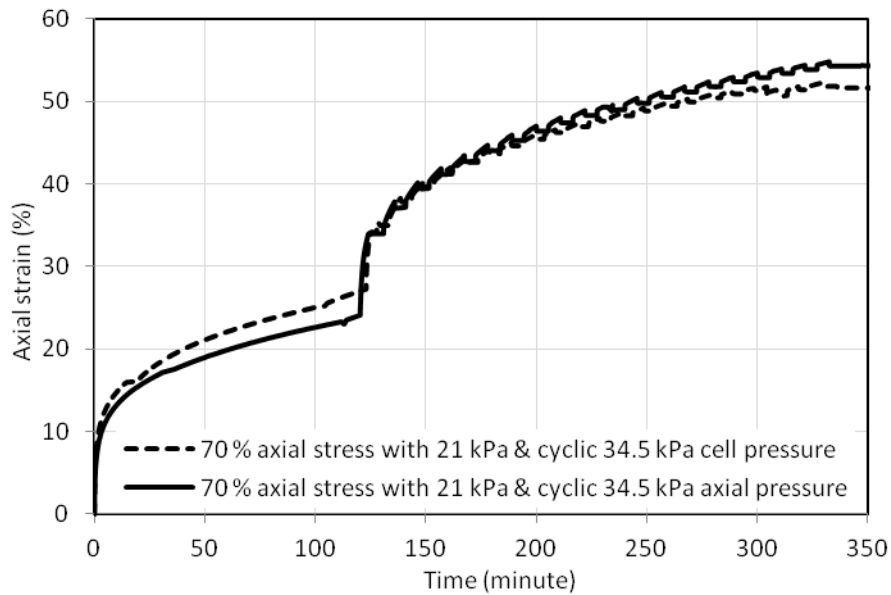
Figure 89. Axial stress of 70 % with 21 kPa and effect of increased stresses after 2 hrs

Confining pressure of 21 kPa with axial stress of 70 % of the compressive strength at 10 % axial strain was applied and deformation was observed for 2 hrs. Additional cyclic stress of 34.5 kPa was then applied either as deviator axial stress or cell pressure. Axial strain of up to 24 % was observed after 2 hrs of loading before the application of the cyclic stresses as shown in Figure 89. When the cyclic stresses were applied the axial strains reached about 52 % after about 300 minutes from start of the test. These tests were done to investigate significance of EPS geofoam design with higher axial stress loading like 70 % of the compressive strength.

The cyclic stresses resulted in cyclic strains particularly for tests which were having relatively less initial stresses. Hence, cyclic strains are more pronounced in Figure 88 than Figure 89.

4.6.4 Relaxation Tests

  In creep tests, constant loads were applied and the resulting deformations were observed. Another phenomenon that needs to be studied is relaxation. In relaxation tests, axial deformation is kept constant after some time and loads were observed in time. Relaxation tests were done on 50 mm cubes of 20 kg/m^3 EPS geofoam samples with axial stresses of 30, 50 and 70 % of the compression stress at 10 % axial strain. Axial stresses were first applied for one day and the actuator was stopped so that the axial strain was kept constant with load being monitored with time. Loads corresponding to 30, 50 and 70 % axial stresses were 193, 138 and 83 N, respectively. These loads were kept constant for one day and after one day relaxation tests started. It can be seen in Figure 90 that the loads got smaller and smaller with time. Bigger relaxations were observed for bigger loads. The test with 70 % axial stress has reduced from 193 to 120 N which was about 40 % relaxation.
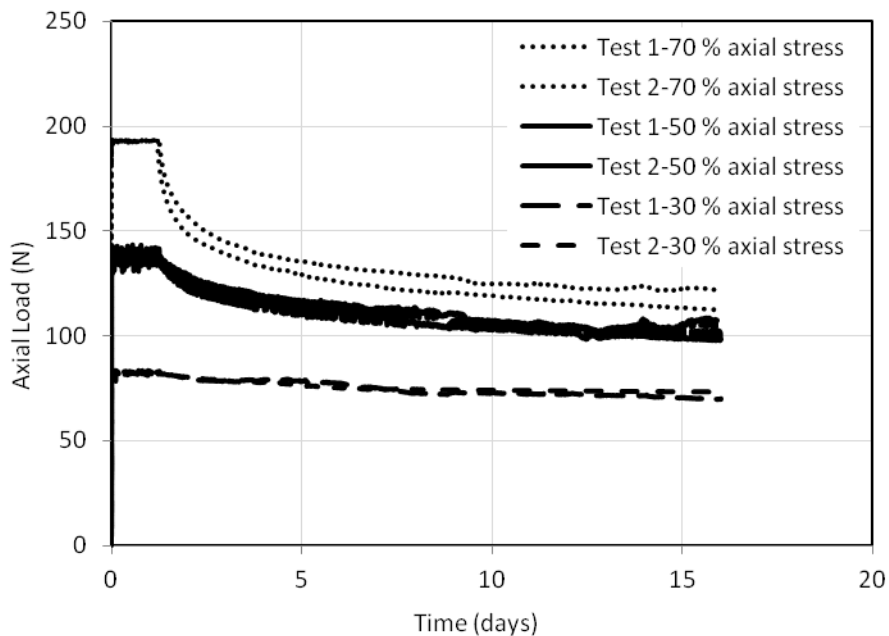
Figure 90. Load relaxation after one day loading

143

Percentage relaxations are shown Figure 91 and it can be noted that the percent

relaxations in 16 days were about 40, 25 and 13 % for axial stresses of 70, 50 and 30 %

axial stresses, respectively.
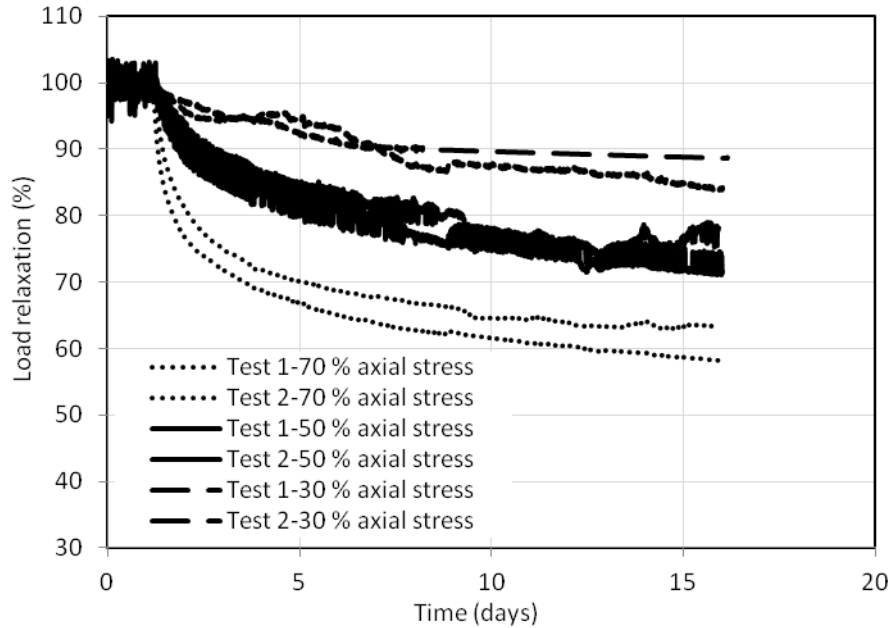
Figure 91. Percent load relaxations

Rate of relaxation was greater at the start and got smaller and smaller with time. After

two weeks of observation, the loads or stresses were relatively constant. EPS geofoam can

be used as backfill materials in bridge abutments and such relaxations may be manifested

while in service. Thus lateral load reductions of up to 40 % can be expected depending on

the initial stress levels.

4.6.5 Creep Constitutive Modeling

Time dependent behavior of EPS geofoam is affected by density, stress level, duration of loading and temperature. Creep and relaxation are time dependent properties of EPS geofoam. Creep is deformation that occurs in time under constant stress whereas relaxation is reduction in stresses with time under constant strain. In this section the creep deformation will be modeled using available constitutive models.

Constitutive Modeling of Creep of EPS Geofoam

Creep or stress-strain-time characteristic of geofoam has been modeled by different investigators. In most of these models, the total strain is in general expressed as (Horvath 1998):

$$\varepsilon = \varepsilon_o + \varepsilon_c \tag{42}$$

where ε = the total strain at some time t after stress application

ε_o = the immediate strain when the stress is applied and

ε_c = the time dependent creep strain at time t after stress application.

The stress is assumed to be applied instantaneously, and will stay constant permanently. One such creep model for EPS geofoam blocks is the General Power Law equation which uses coefficients developed by the Laboratoire Ponts et Chaussess (LCPC) is (Magnan and Serratrice 1989):

$$\varepsilon = \frac{\sigma}{E_{ti}} + 0.00209 \left(\frac{\sigma}{\sigma_y}\right)^{2.47} \left(t^{\left(-0.9\log_{10}\left[1 - \frac{\sigma}{\sigma_y}\right]\right)}\right) \tag{43}$$

Where ε = total strain at some time t after stress application in decimal (not in %)

σ = applied stress in kPa

t = time after stress application in hrs

E_{ti} = initial tangent modulus of the EPS block geofoam in kPa

σ_y = yield stress in kPa

E_{ti} and σ_y of EPS geofoam blocks were empirically related with the density, ρ (kg/m³) of

EPS geofoam blocks as follows:

$$E_{ti} = 479\,\rho - 2875 \tag{44}$$

$$\sigma_y = 6.41\rho - 35.2 \tag{45}$$

where E_{ti} and σ_y are in kPa and, ρ in kg/m³

Hence the complete *General Power Law equation of LCPC* is:

$$\varepsilon = \frac{\sigma}{479\,\rho - 2875} + 0.00209\left(\frac{\sigma}{6.41\rho - 35.2}\right)^{2.47}\left(t^{\left(-0.9\log_{10}\left[1 - \frac{\sigma}{6.41\rho - 35.2}\right]\right)}\right) \tag{46}$$

Note that the yield stress, σ_y was equivalently referred as plastic stress σ_p.

Another creep model known as the Findley equation was proposed in order to obtain the

total time dependent strain of geofoam(Findley 1960). The total creep is obtained from:

$$\varepsilon = \varepsilon_o + \varepsilon_c = \varepsilon_o + m\left(\frac{t}{t_o}\right)^{n_F} = \varepsilon'_{oF}\sinh\left(\frac{\sigma}{\sigma_{eF}}\right) + m'_F\sinh\left(\frac{\sigma}{\sigma_{mF}}\right)\left(\frac{t}{t_o}\right)^{n_F} \tag{47}$$

Where ε, ε_o, and ε_c are as defined above.

   m = a dimensionless material parameter

   n_F = a dimensionless Findley material parameter

   m_F = a dimensionless Findley material parameter

   t = time after stress application in hrs

   t_o = one hour (used to normalize time)

   ε'_{oF} = a dimensionless Findley material parameter

   σ_{eF} = a Findley material parameter with dimensions of stress

   σ_{mF} = a Findley material parameter with dimensions of stress and

σ = applied stress in kPa

The Findley equation as originally presented is only part of the above expression and given below(Findley 1960). It will be referred here as the *original Findley equation*.

$$\varepsilon = \varepsilon_o + \varepsilon_c = \varepsilon_o + m \left(\frac{t}{t_o}\right)^{n_F} \tag{48}$$

where $m = m'_F \sinh\left(\frac{\sigma}{\sigma_{mF}}\right)$

Creep tests were conducted on block molded EPS by BASF AG in Ludwigshafen, Germany during 1987 to 1989. (Horvath 1998) considered three of these tests conducted on 50 mm cube samples of 20 kg/m³ density for axial stresses of 30, 40 and 50 kPa and the following expression was proposed.

$$\varepsilon = 0.011\sinh\left(\frac{\sigma}{54.2}\right) + 0.000305\sinh\left(\frac{\sigma}{33}\right)(t)^{0.2} \tag{49}$$

where σ is in kPa and t is in hrs. This is applicable only for density of approximately 20 kg/m³, applied stress of ≤ 50 kPa and at temperature of about 23 ᵒC. This equation is referred to as *modified Findley equation* in the subsequent discussions.

Creep models discussed above will be used to predict strains and are compared with test results. EPS geofoam of 20 kg/m³ has been tested for both short term and long term compression. Compression strength of 54, 91 and 107 kPa was obtained respectively at 1, 5, and 10 % axial strains. Initial modulus and unconfined yield stress of 6.47 MPa and 96 kPa respectively were obtained from same test.

Test results for 50 mm cube samples are shown in Figure 92 along with creep model predictions. It is shown that original Findley equation [Eq. (48)] predicted the axial strains better. On the other hand, LCPC creep model's [Eq. (46)] prediction was less than observed axial strains during testing. Value of initial elastic modulus in the LCPC model is higher than

147

that obtained during testing. Test result value instead of equation. (44) was used for initial

tangent modulus and the prediction was better as shown by the curve labeled as 'LCPC-

modified'; and this is close to that of the original Findley's prediction. Similar observation

was reported previously (Horvath 1998).
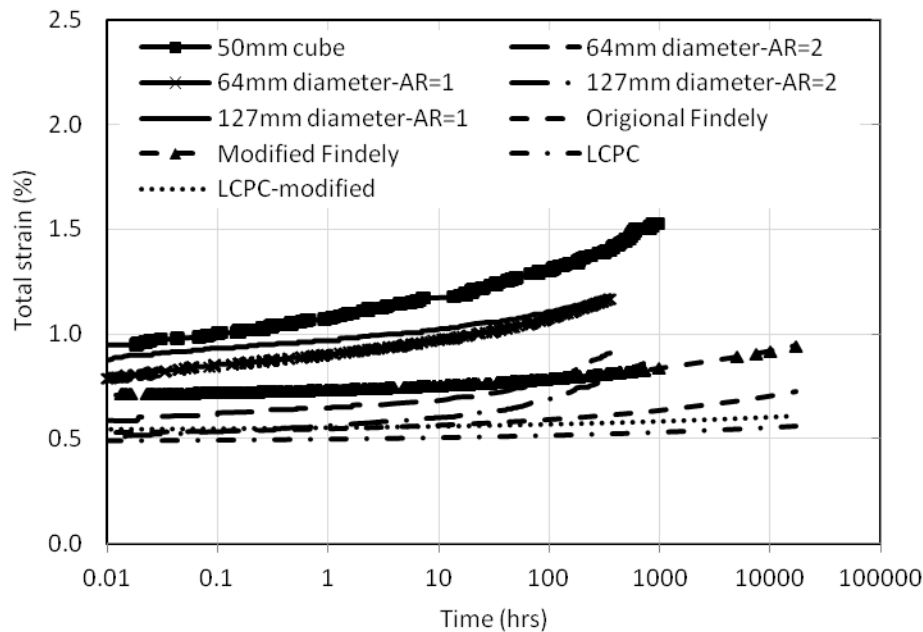
Figure 92. Creep models and test data for 30 % axial stress and 20 kg/m³

Shown also in Figure 92 is prediction using modified Findley equation [Eq. (49)]. This

also resulted in smaller strains. It can be said that all the creep models predicted strains

which are less than test results. Creep models were used to predict the axial strain at

10,000 hrs (~417days) and these values are very small even when compared to test result

values at 1,000 hrs (~42days).

Cylindrical samples of 64 and 102 mm diameters with aspect ratio of 2 (AR=2) are also

shown in Figure 92. Results from modified Findley are in both cases greater than test

results in early stages and thereafter test results exceeded predicted strains. But

148

predictions from original Findley and LCPC creep models are less than the test results. When samples with smaller aspect ratio were used (AR=1), the predictions from all creep models were less than the test results. Note that axial strain from test result on 50 mm cube sample is greater than all the others. In addition, samples with smaller aspect ratio have more axial strains.

For tests done with axial stress of 50 % of compression strength at 10 % axial stain, predictions from creep models are far from test results as shown in Figure 93. It is shown that cylindrical sample of 102 mm diameter showed axial strain of about 4 % as compared to predicted value of 1.5 % in 14 days. Note that 50 % axial stress (i.e. 53 kPa) is a little greater than half unconfined yield stress of 96 kPa.
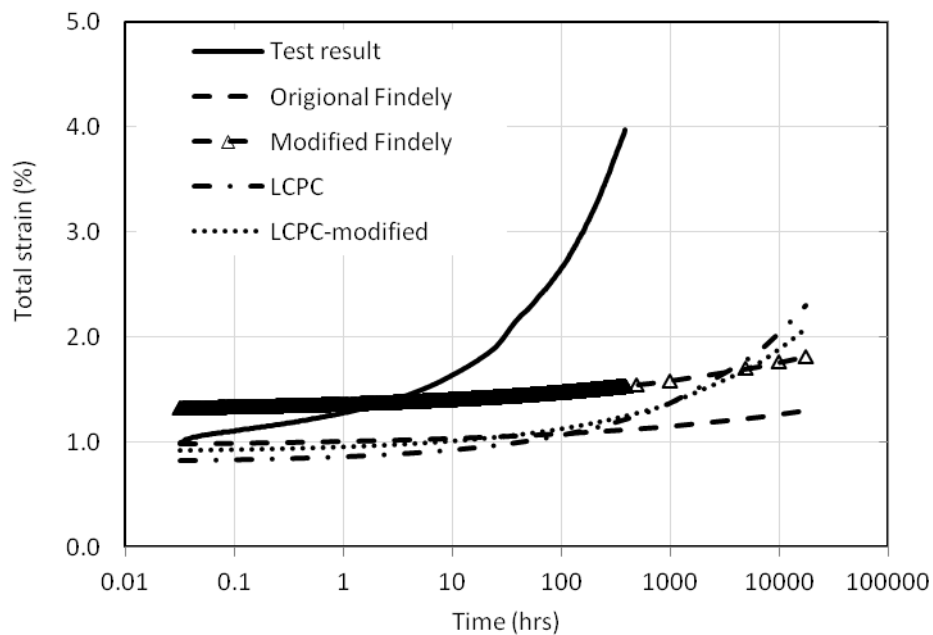
Figure 93. Creep models and test data for 50 % axial stress and 20 kg/m³

Findley parameters used above are based on test results conducted on 50 mm samples of 20 kg/m³ EPS geofoam. These parameters were determined here based on test results on

cylindrical samples of 64 and 102 mm diameter with aspect ratio of 2. The modified

Findley equation is given by

$$\varepsilon = 0.0168\sinh\left(\frac{\sigma}{100}\right) + 0.00013\sinh\left(\frac{\sigma}{18}\right)(t)^{0.24} \qquad (50)$$

where σ is in kPa and t is in hrs. This is applicable only for density of approximately

20kg/m³, applied stress of $\leq$ 53 kPa and at temperature of about 23 °C. Results of this new

equation are shown in Figure 94 by curves labeled as "Modified Findley (2)"with results

from earlier equations. Small improvement is shown for predictions with axial stress of 53

kPa. For smaller stress, the result is about the same as that from equation based on 50 mm

cube samples.
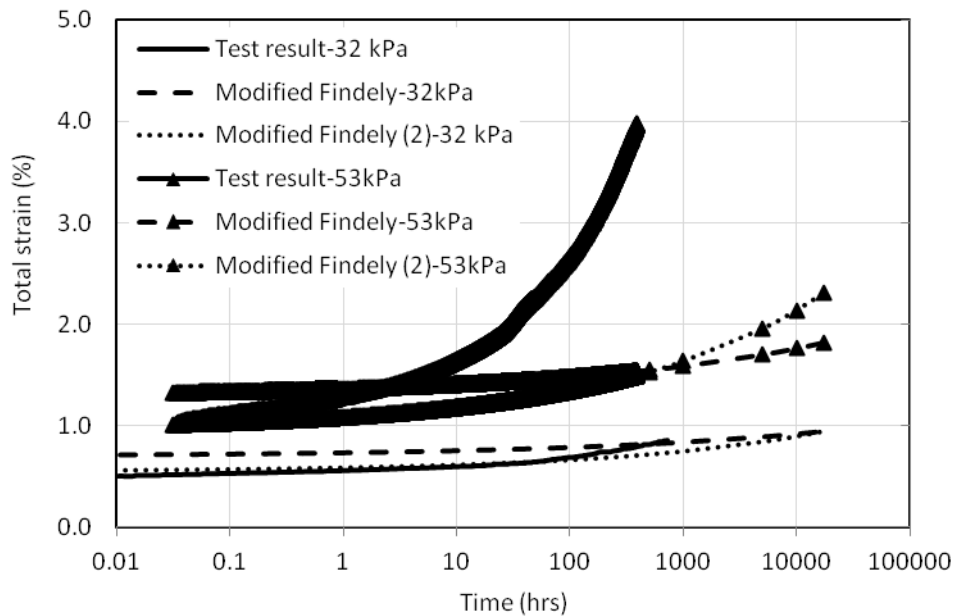
Figure 94. Modified Findley equation based on results on cylindrical samples of 20

kg/m³

Creep tests were conducted on cylindrical samples of 16 kg/m³ EPS geofoam. Creep

models were used to predict axial strains and these outputs are portrayed in Figure 95.

150

Findley parameters obtained for 50 mm cube samples of 20 kg/m³ were used in order to test their applicability for other densities. Here also the original Findley equation [Eq. (48)] predicted the axial strains better. The LCPC creep model [Eq. (46)] prediction was less than the measured axial strains. The LCPC prediction was improved by using initial modulus and yield stress values obtained from compression tests as shown by the curve labeled as 'LCPC-modified'.
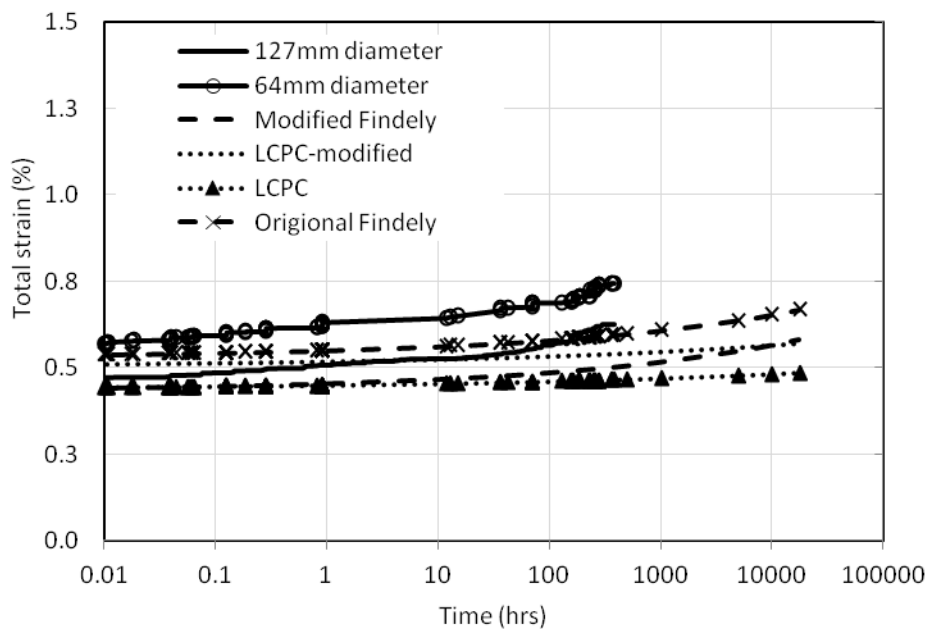
Figure 95. Creep models and test data for 30 % axial stress and 16 kg/m³

Creep models were also used for axial stress of 50 % and Figure 96 shows that all creep models predicted axial strains less than measured values during testing. It can be noted that modified LCPC model predicted better than others.
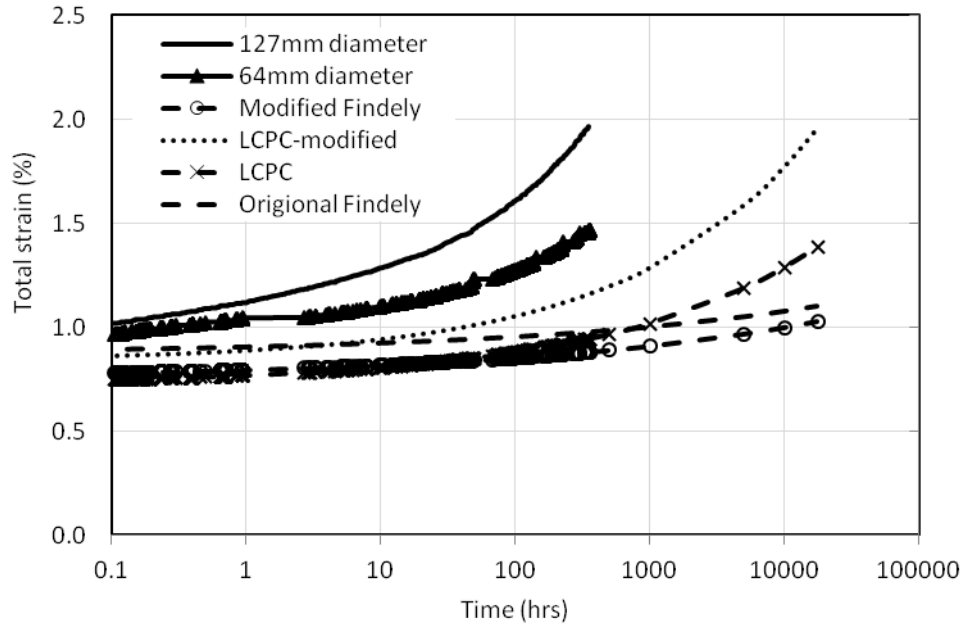
Figure 96. Creep models and test data for 50 % axial stress and 16 kg/m³

Findley parameters for 16 kg/m³ were obtained and the following modified Findley equation is provided based on data from cylindrical samples of 64 and 102 mm diameter with aspect ratio of 2.

$$\varepsilon = 0.0241\mathrm{sinh}\left(\frac{\sigma}{100}\right) + 0.00014\mathrm{sinh}\left(\frac{\sigma}{10}\right)(t)^{0.23} \tag{51}$$

where σ is in kPa and t is in hrs. This is applicable only for applied stress of ≤ 35 kPa and at temperature of about 23 °C. Modified Findley results are labeled in Figure 97 as "Modified Findley(2)". The predictions were reasonably good for both 30 and 50 % axial stresses. Available creep model are mostly for 20 kg/m³. Thus equations for other densities are provided based on 2 weeks duration of loading; nevertheless, long duration of loading must be conducted for better results.

152
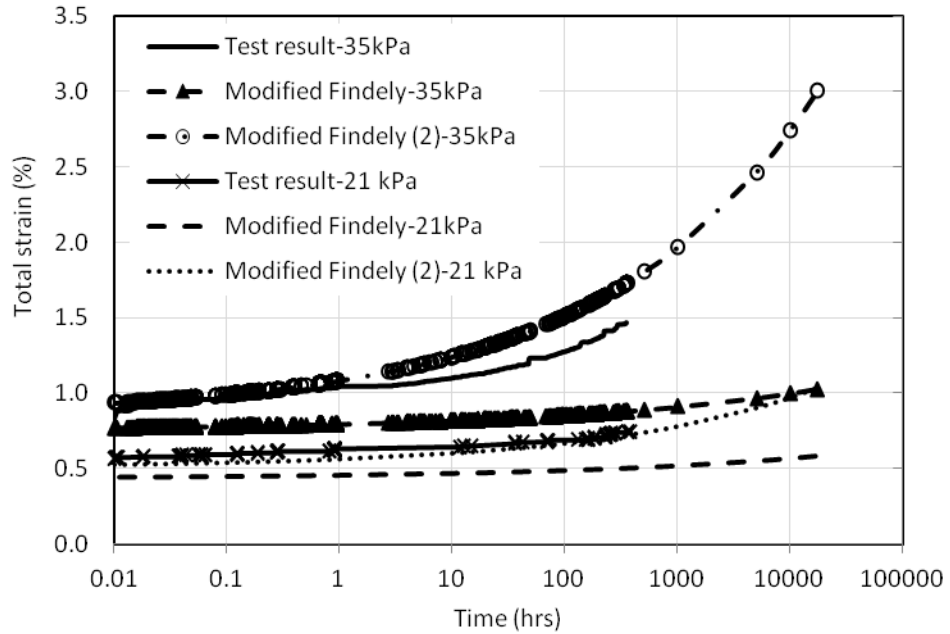
Figure 97. Modified Findley equation based on results on cylindrical samples of 16 kg/m³
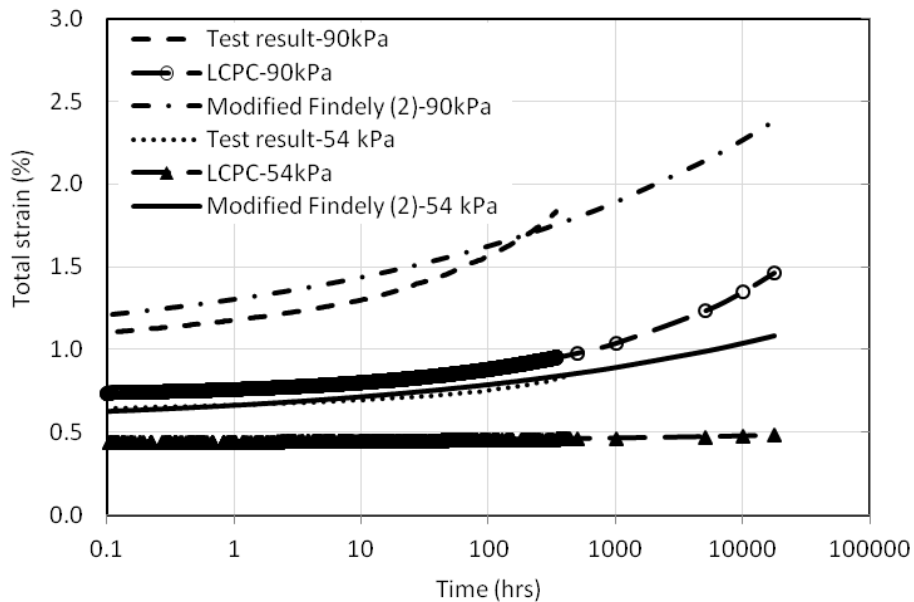
Figure 98. Modified Findley equation based on results on cylindrical samples of 32 kg/m³

153

Creep models were also employed for 32 kg/m³ and the modified Findley equation [Eq. (49)] does not work for this density. LCPC equation predicted smaller axial strains than observed as shown in Figure 98.

Parameters for Findley equation were obtained for 32 kg/m³ EPS from tests on cylindrical samples. Axial stresses of 54 and 90 kPa were applied during testing. The modified Findley is given for 32 kg/m³ EPS as:

$$\varepsilon = 0.00961\sinh\left(\frac{\sigma}{100}\right) + 0.0007\sinh\left(\frac{\sigma}{40}\right)(t)^{0.15} \qquad (52)$$

where σ is in kPa and t is in hrs. This is applicable only for applied stress of ≤ 90 kPa and at temperature of about 23 ºC. Results from this modified Findley are labeled in Figure 98 as "Modified Findley(2)". The predictions were excellent for both 30 and 50 % axial stresses. Note also that the equations were used to predicted total axial strains up to 2years (17520hrs) where as observed strains during testing were for about two weeks (336hrs).

4.7 Temperature Effects on the Behavior of EPS Geofoam

EPS geofoam can be used in areas where the temperature may rise as high as 40° C. Effect of temperature on the strength of EPS geofoam was studied by Yeo and Hsuan 2009 and Zou and Leo 2001. Generally, compressive strength was observed to decrease with increase in temperature. Duškov 1997a conducted compression tests on cylindrical EPS20 samples at temperature ranges of -8.6 to -12.9 ^{o}C and found that low temperatures have no negative impact on the mechanical behavior of EPS. (Zou and Leo 2001) studied effect of temperature on compressive strength, yield stress, initial Young's modulus, plastic tangent Young's modulus and creep behaviors. EPS geofoam of 20 kg/m^3 and 50 mm diameter with aspect ratio of 1:1 were used. Confining pressures of 0, 5, 10, 15 and 20 kPa were used for three temperatures 23 (room temperature), 35 and 45 ^{o} C. Decrease in compressive strength, yield stress, initial Young's modulus, and plastic tangent Young's modulus were observed with temperature increase for unconfined compression with axial strain rate of 10 %/min. In addition, creep test results of 30, 40 and 50 kPa stresses at room temperature and 40 ^{o} C showed that the creep response for 40 ^{o} C was more for same stress level.

Most of the studies available compared response of EPS geofoam at constant temperature. In this study, creep responses of EPS geofoam to cyclic temperatures were evaluated by conducting creep tests in a temperature controlled chamber. Coupled effects of temperature and creep were studied for different stress levels. Comparison was made to long term field observations at the Interstate 15 reconstruction project in Salt Lake City, Utah. FLAC models were run for lab and field size samples and the results were compared. Thermal induced stresses in EPS geofoam placed in constrained states were observed.

Tests with Different Temperatures

Seasonal temperature variations were observed to affect deformation magnitudes of EPS geofoam fills. Creep tests were done in a thermal chamber where the temperature can be varied in a controlled cycle. The test set up is shown in Figure 99. Load cell, LVDT and thermistor were used for measuring load, deformation and temperature respectively. The chamber has ability to cycle the temperature at set time intervals. In these tests, temperature was set to stay at 24 ^{o}C for 24 hrs and then to immediately increase to 40 ^{o}C and then kept constant for another 24 hrs. Again the temperature was immediately dropped to 24 ^{o}C and kept constant for 24 hrs followed by immediate drop to 0 ^{o}C and kept constant for 24 hrs and finally immediately rose to 24 ^{o}C. This 72 hr cycle was repeated as many times as needed as shown in Figure 100.

Figure 99. Set up of creep test inside chamber
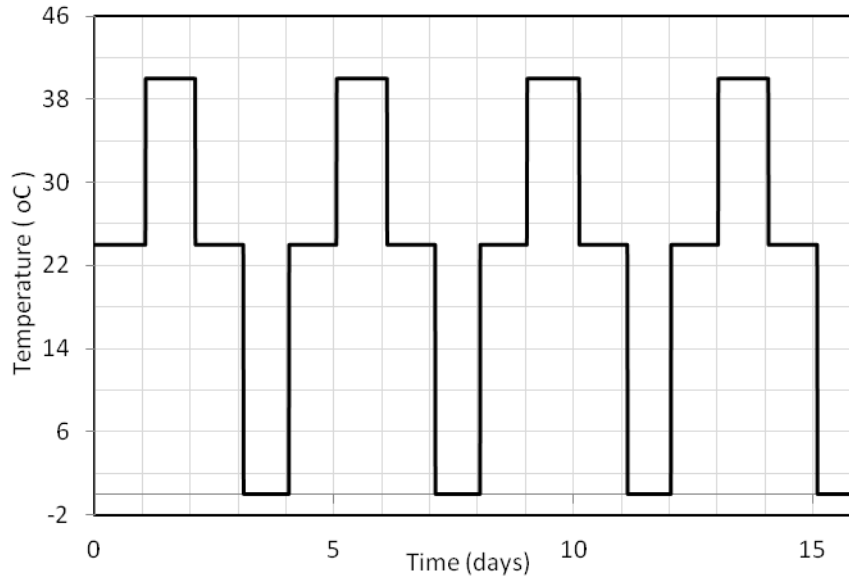
Figure 100. Typical temperature variation with time inside chamber

Creep Tests at Constant Temperatures

EPS geofoam samples of 64 mm diameter and 20 kg/m³ density were used to conduct creep tests at three different constant temperatures. The axial stresses were kept constant at 32 kPa, which is 30 % of the compression stress at 10 % axial strain. Figure 101 shows results of creep tests at room temperature (24 °C), 0 and 40 °C. Highest initial and creep strains were observed for creep tests with 40 °C. Initial strains for 0 and 24 °C were both about 0.8 % with creep strain remaining relatively constant for 0 °C and moderately increasing with time for 24 °C.
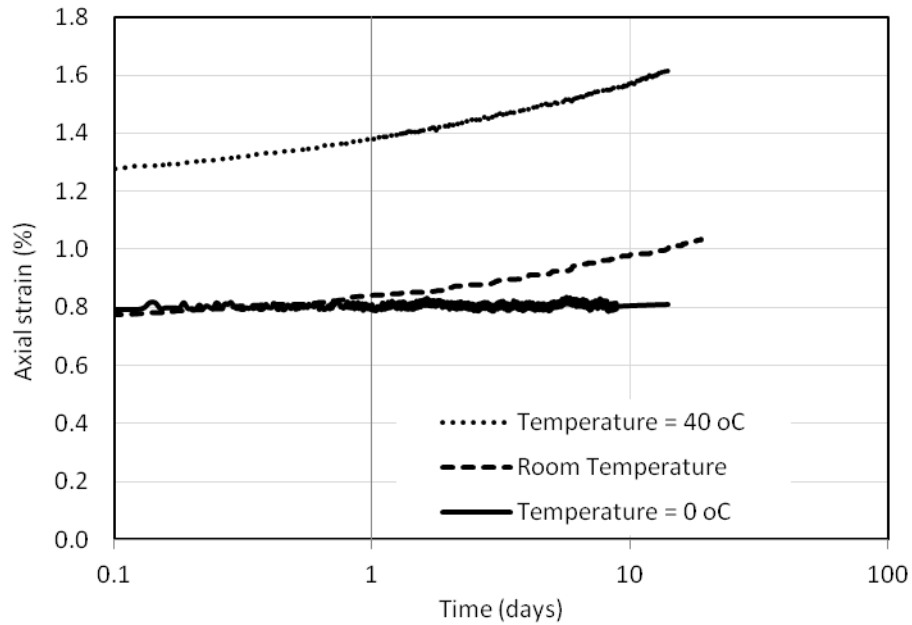
Figure 101. Creep tests at three temperatures

Figure 102 shows the stress-strain curves in unconfined compression tests at different constant temperatures. The stress-strain relations remained relatively the same for 0, 24 °C and room temperature (which was close to 24 °C). But for 40 °C temperature the stress-strain curve was below others showing that there was reduction in the initial modulus, yield stress and compressive strength. Reduced initial strain in creep tests at elevated temperature was related to lower initial modulus. Similar results were reported by Zou and Leo 2001.
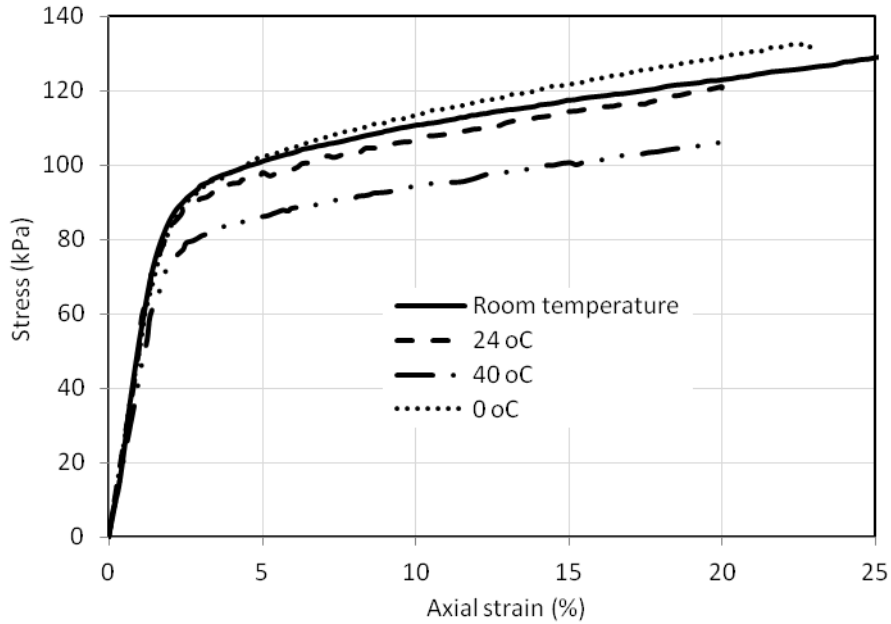
Figure 102. Unconfined compressions tests at constant temperatures

Creep Tests with Cyclic Temperature

Figure 103 shows total deformations with time for an axial stress of 32 kPa (which is 30 % of strength at 10 % strain). Creep results with cyclic temperature variation showed cyclic deformation trend when compared with creep results of constant room temperature. More total axial strain was observed when the temperature was lower and vice versa. When the temperature increased polystyrene and air inside the foam cells expanded to counterbalance deformation resulting from axial loading. Thus, axial strains due to load and expansion due to temperature cycles were out of phase. This trend was observed for small axial stresses. Tests were repeated on other samples of same density but different sample sizes. Figure 103 (b) shows repeatable trend.
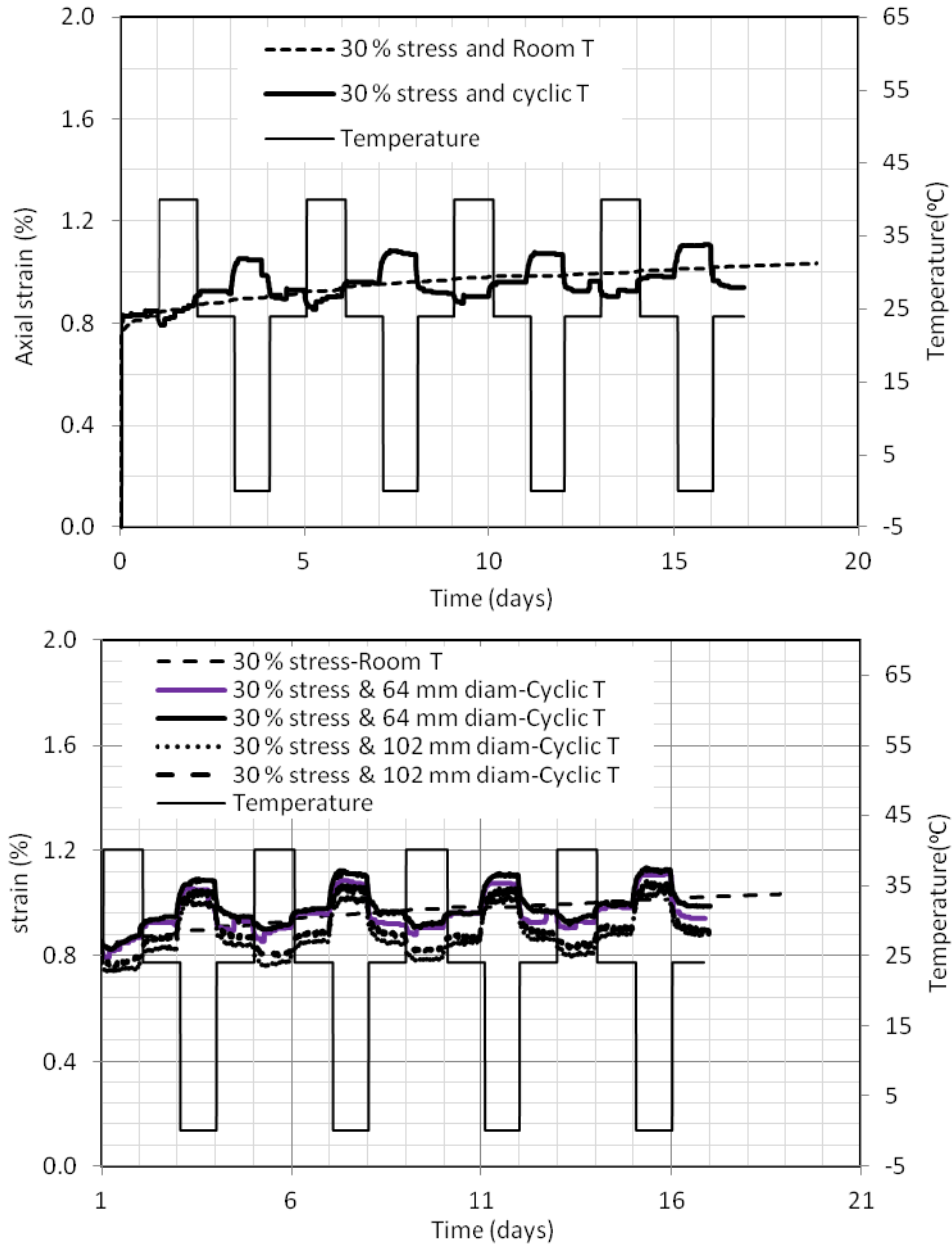
Figure 103. Axial strain with time for cyclic temperature change (32 kPa & 20 kg/m³)

Cyclic deformation trend when the axial stress was increased to 54 kPa (i.e. 50 % of strength) is shown in Figure 104. The thermal expansion of the geofoam was suppressed by large magnitude of deformation due to larger axial load. Unlike results shown in Figure

103, there is no observable depression in the plots during temperature rise. But the saddles during temperature drop stayed similar irrespective of the magnitude of the axial stresses.
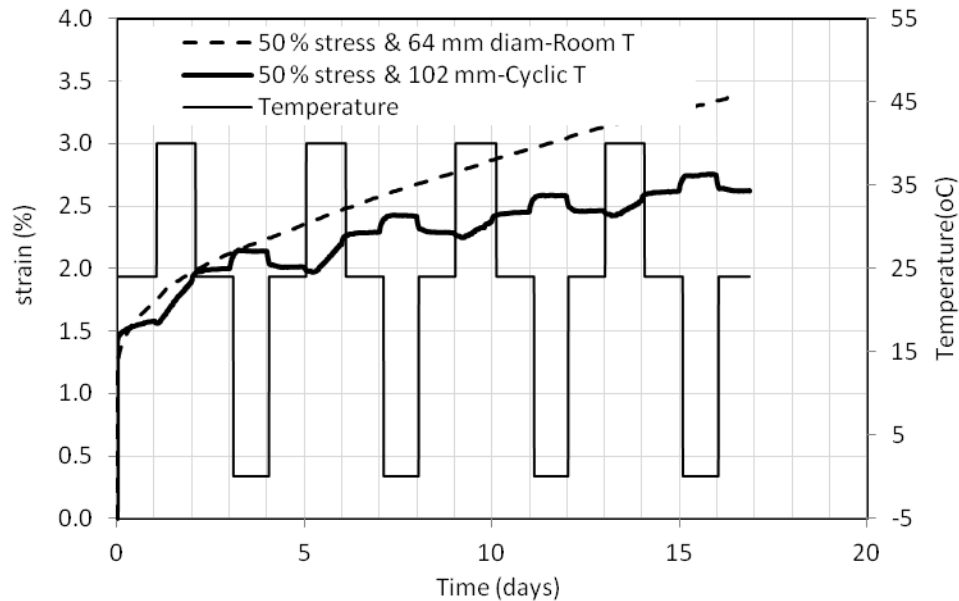
Figure 104. Axial strain with time for cyclic temperature change (54 kPa & 20 kg/m³)

Field Observation at Interstate 15

Geofoam fill performance monitoring was made at Interstate 15 Reconstruction Project in Salt Lake City, Utah (Negussey and Stuedlein 2003). Magnet extensometers were used in the 100 South geofoam embankment where magnet plates, which can move with the surrounding EPS geofoam fill, were installed along a central PVC access riser pipe. Magnet plate positions followed the fill deformations and successive changes in position with respect to an initial baseline survey represented magnitude of movement or deformation over a depth profile. Solid lines of Figure 105(a) show plots of such settlements in reference to initial baseline survey at deferent levels along the depth. Calculated seasonal thermal deformations are plotted in Figure 105(b) along with mean daily temperatures with respect to time. When seasonal thermal deformations (Figure 105(b)) are taken out

from the observed deformations (solid lines of Figure 105(a)), EPS creep deformations were obtained and are plotted as broken lines of Figure 105(a). Exclusion of thermal deformations from observed movements resulted in less undulated plots. The magnet extensometer observations made over long period clearly showed seasonal trend of cyclic deformation. Magnitude of seasonal thermal deformations was about 0.16 % and was of similar magnitude to that measured in the lab. Observed strains in 100 South geofoam embankments are shown in Figure 106. The strains plotted are results of both thermal and creep deformations. Seasonal undulations in the strains are clearly visible in this plot.
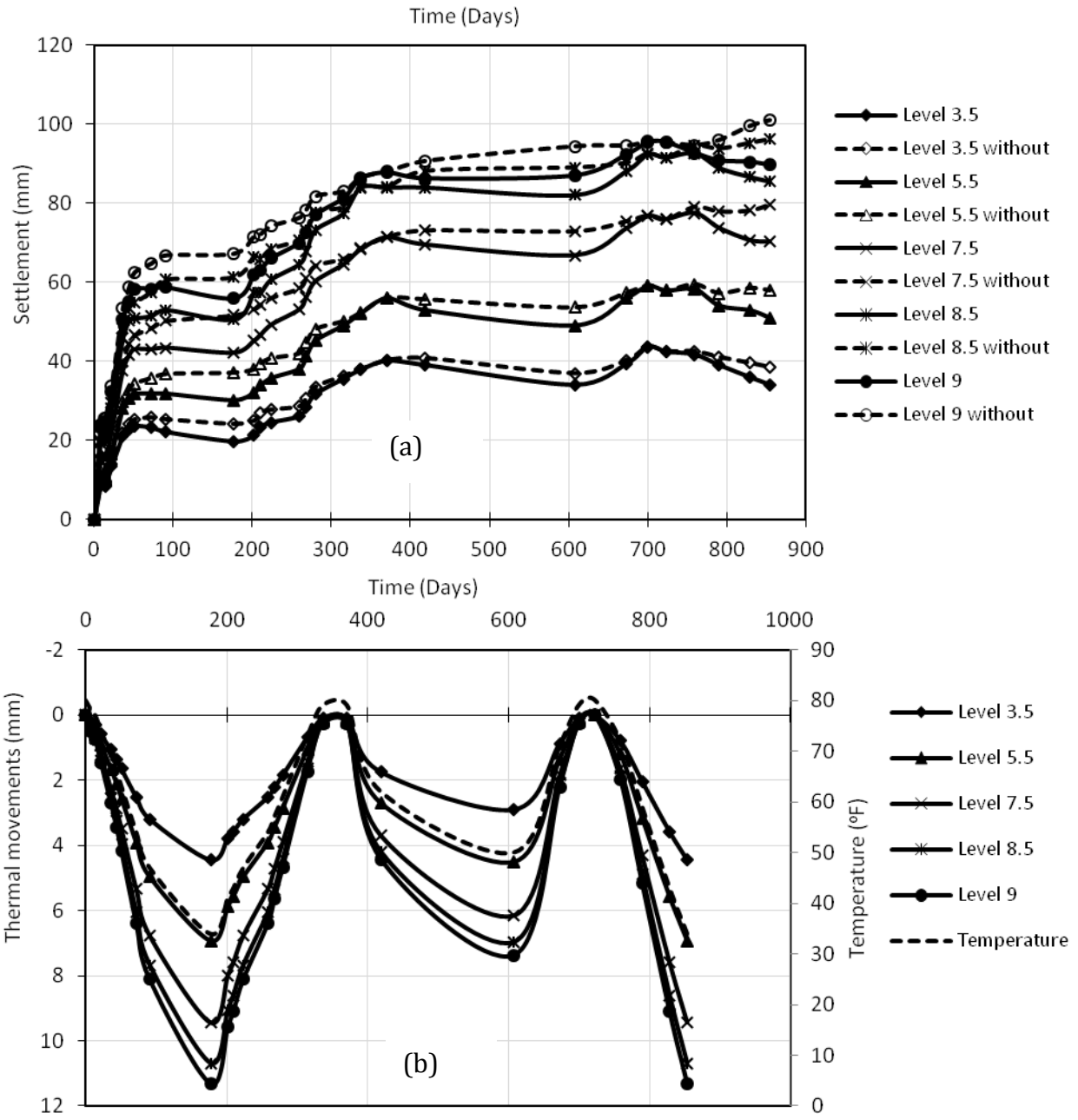
Figure 105. EPS Deformation from magnet extensometer, South array.
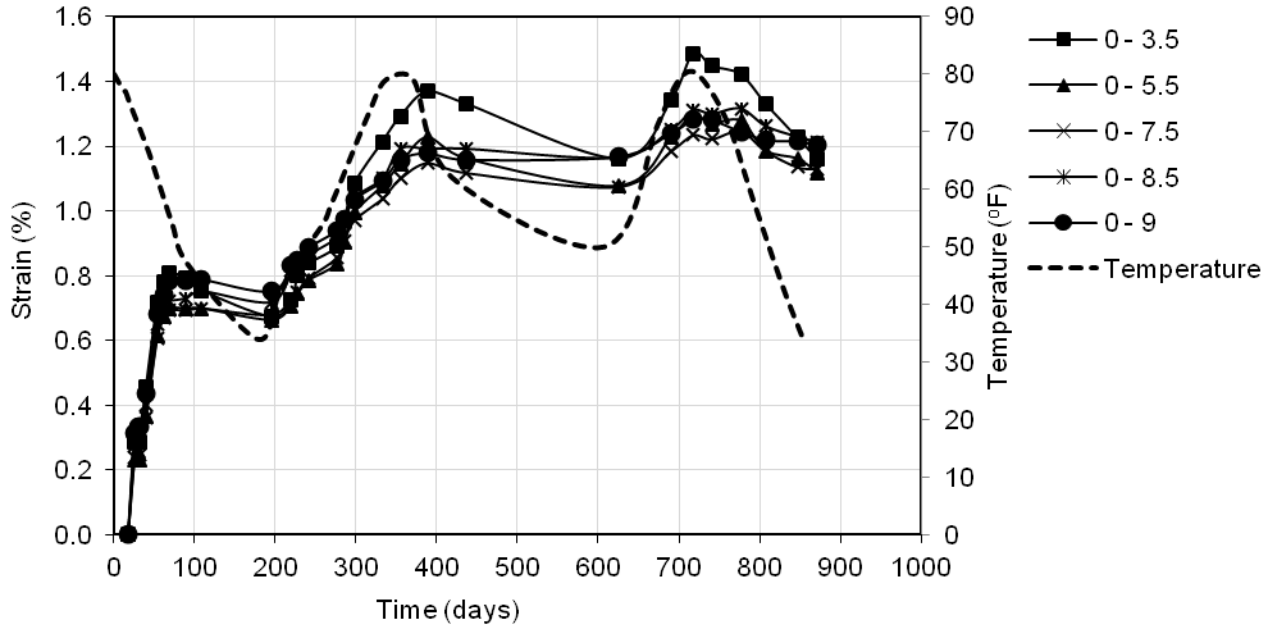
Figure 106. Strains in EPS from magnet extensometer, South array.

The deformation is observed to be out of phase with the seasonal temperature variation. This same trend was observed in creep tests with cyclic temperature variation.

FLAC Modeling

EPS geofoam samples of 64mm diameter and 127 mm high were modeled in FLAC to simulate temperature changes and time taken to reach steady state and thermal deformations. Expansion of 0.076 mm and contraction of 0.114 mm were calculated when temperature changed from 24 to 40 ºC and from 24 to 0 ºC or 0.00375% strain per ºC change. Temperature reached a steady state of 40 from 24 ºC in about 1300seconds as shown in Figure 107. Similarly 2200 sec were taken to reach 0 ºC from 24 ºC.
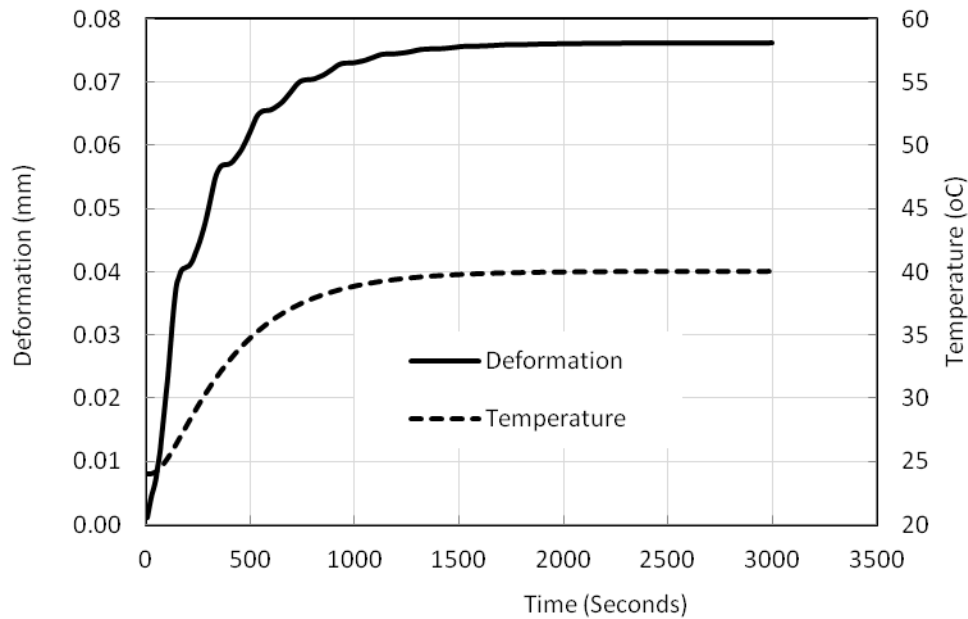
Figure 107. Time to reach steady state in a 64 mm diameter sample for temperature change from 24 to 40 °C

Time for steady state is where all points within the sample reach the steady state. Temperature distribution within the sample at the 5th minute is shown in Figure 108 when the temperature was changing from 24 to 40 °C. EPS geofoam fills in the field would be of much larger dimensions. Thus, 4.5 m by 4.5 m EPS geofoam was analyzed in FLAC in order to determine the time needed to reach steady state and the thermal deformations as a result of temperature change. About 34.7 days were needed to reach a steady state of 40 °C from 24 °C with maximum deformation of 3.02 mm. If period of cyclic temperature variation was less than 34.7 days, this deformation might not be observed. Same observations can be made in Figure 105 and Figure 106 that cyclic responses of big fills were seasonal and did not have daily cyclic periods as the 4.5 m high fill needed longer time to reach steady state to develop observable deformations in daily temperature cycles.

165
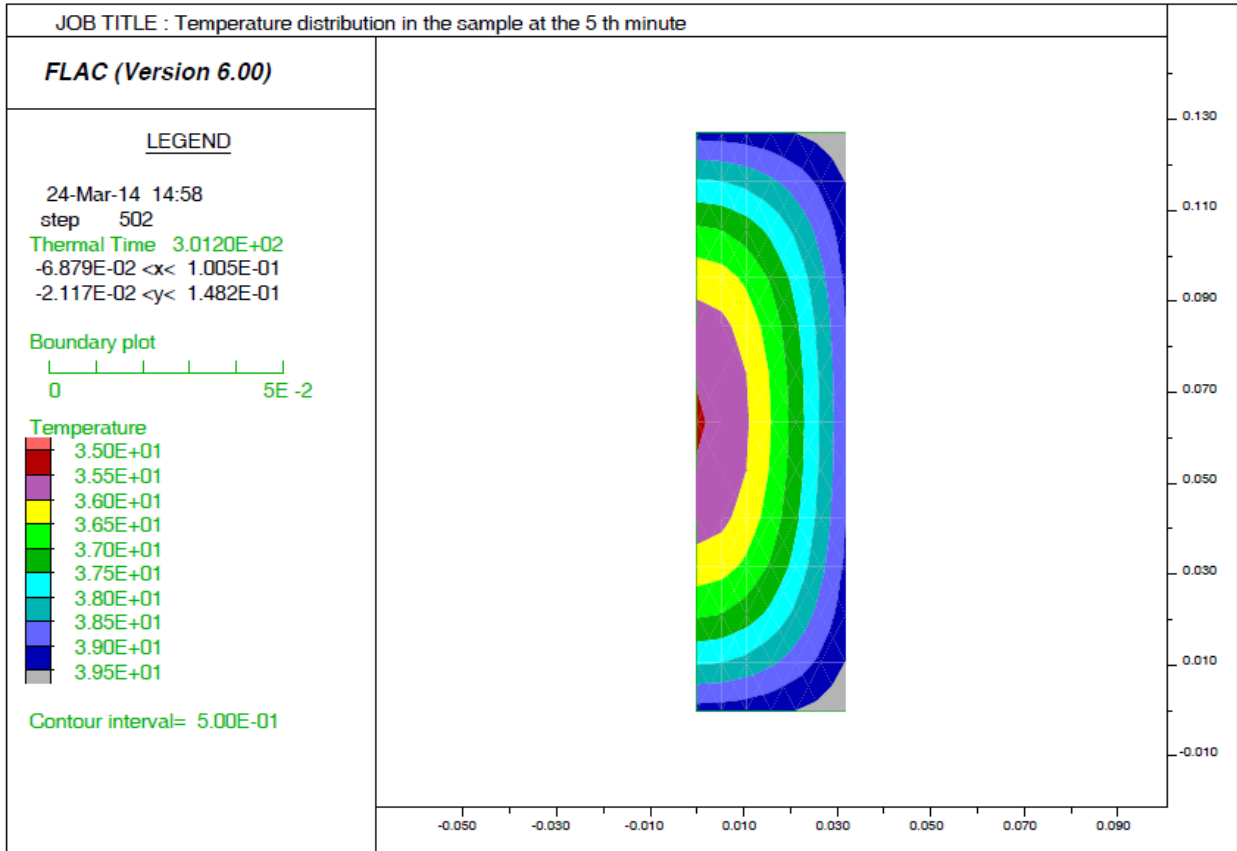
Figure 108. Temperature distribution at the 5th minute (64 mm x 127 mm)

Temperature distribution of the 4.5 m x 4.5 m EPS geofoam model at the 5th minute is shown in Figure 109. The temperature within the section ranged 24 to 25 °C as compared to 35 to 39.5 °C in the smaller section, Figure 108. On the 5th minute, 64 mm x 127 mm section deformed by about 0.122 mm (0.096% strain)as compared to about none the 4.5 m x 4.5 m section.
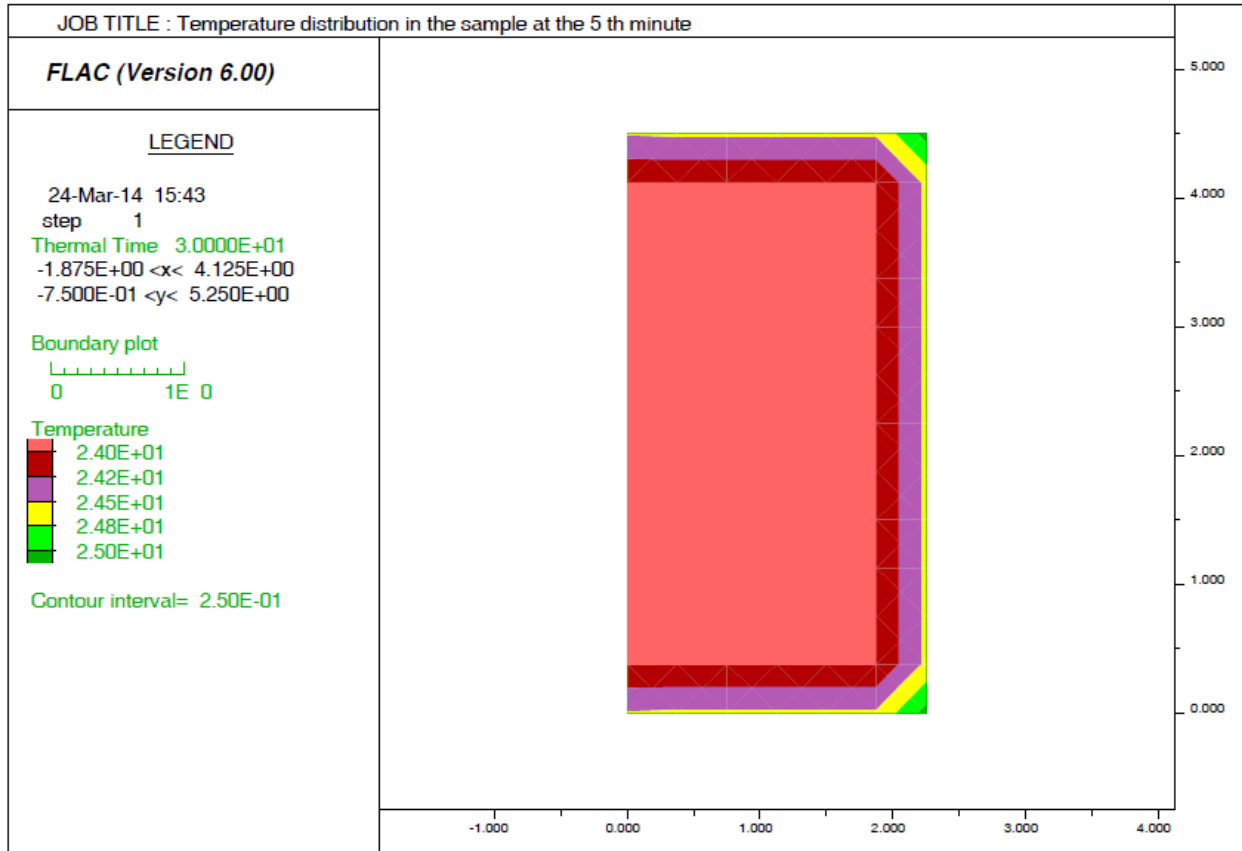
Figure 109. Temperature distribution at the 5th minute (4.5 m x 4.5m section)

Investigation of FLAC outputs suggest that the temperature lag between what was set in the chamber and that in the sample was short as compared to the 24hr cycle period set in the chamber.

EPS geofoam fills may be used in constrained areas and stresses may be induced when the temperature rises. FLAC model of 64 mm x 127 mm section was constrained at its boundaries and the temperature was increased from 10 to 35 ºC. The stresses induced were plotted as a function of time when the temperature increased as shown in Figure 110. Maximum confining stress of about 4.5 kPa was observed. Tests were also done in the temperature controlled chamber with the load measured in a constrained condition as the

temperature changed. A stress of about 4 kPa was observed for a temperature rise to 35 °C, Figure 111. Test result and FLAC predicted induced stresses were close and small.
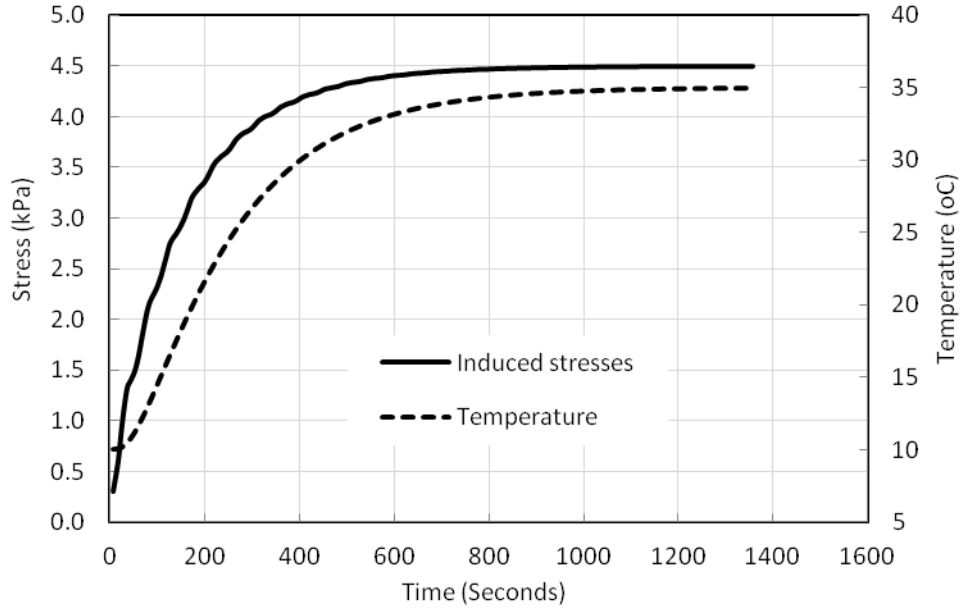
Figure 110. Induced stresses due to temperature rise (64 mm x 127 mm)
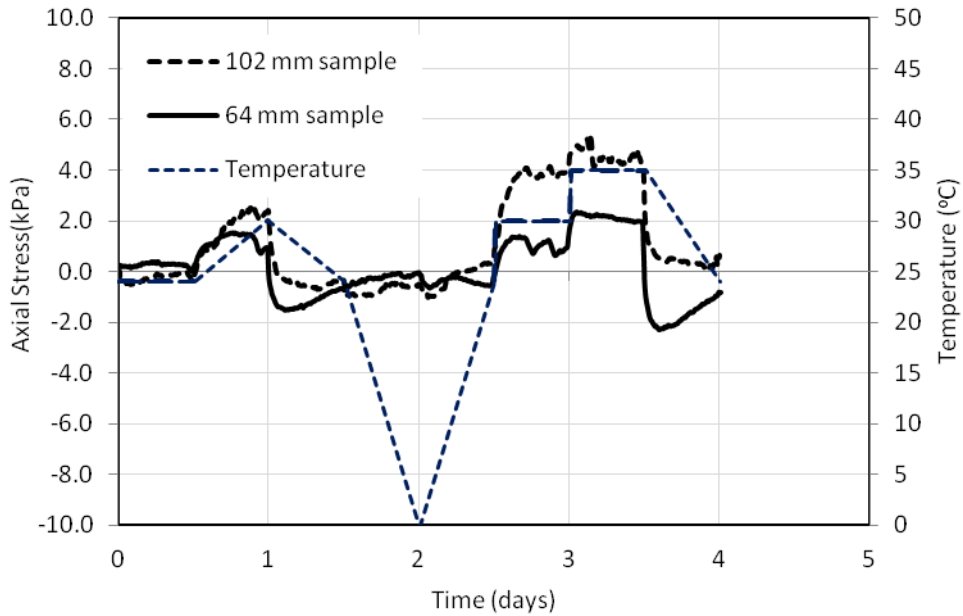
Figure 111. Measured stresses due to temperature changes

Stress-strain behavior of EPS geofoam remained relatively unaffected up to a temperature of 24 ^{o}C. Elevated temperatures affected the behavior of EPS geofoam and resulted in higher initial and creep deformations. Seasonal temperature variations produced small seasonal deformations. Stress induced in constrained EPS geofoam application due to change in temperature would also be small and can be neglected in practice due to inherent relaxation properties of EPS geofoam.

5. CONCLUSIONS AND RECOMMENDATIONS

Effects of confining pressure and temperature on the compression and creep behavior of EPS geofoam were studied and the following conclusions and recommendations were made.

1. In the elastic or working stress range, the yield stresses of low and high density EPS geofoam decreased as confining pressures increased. But under higher confining pressures, yield stresses reversed from decreasing to increasing. At one density, the critical or transition confining pressure at which yield stresses began to increase with increasing confining pressure was at a value about equal to the unconfined compression yield stress. For confining pressures over which yield stresses decreased, major principal stresses at yield remained relatively constant. The major principal stresses at yield increased with density. Yield stresses can be estimated from density and modulus of elasticity of the resin bead, allowing for both the EPS density and anticipated confining pressures. Yield conditions on the basis of major stress can account for confining stress effects.

2. The stress-strain relations for both unconfined and confined compression can be generated using density of geofoam block and resin bead properties. The results obtained are in good agreement with lab test results. The proposed method furnishes the stress-strain relations easily and can be employed in numerical modeling. It is one of the easiest models to predict the stress-strain relations in EPS geofoam.

3. Design with EPS geofoam is based on limiting allowable stresses to maintain creep deformations over the service life of the project to tolerable levels. Support for the

design approach has been based on short and long term unconfined compression tests. Results reported in this investigation indicated that confining pressures can significantly increase creep deformations. Criteria for yielding and creep in unconfined and confined compression can be related to states of total major principal stress. For the same percentage of design loads relative to compression strengths, EPS geofoams of higher densities develop lower creep deformations. In situations where groundwater and lateral earth pressures can produce significant boundary total pressures, effects of confinement on EPS geofoam creep deformations should be considered in design. Most of the creep strains would tend to occur in the few weeks after loading. Adapting the construction sequence with complementary monitoring can be helpful to reduce creep deformations after project completion.

4. EPS geofoam relaxation property was studied and the rate of relaxation was greater at the start and got smaller and smaller with time. After two weeks of observation the loads or stresses were relatively constant. EPS geofoam can be used as backfill materials in bridge abutments and such relaxations may be manifested while in service. Thus lateral load reductions of up to 40 % can be expected depending on the initial stress levels.

5. Effect of induced anisotropy on the stress-strain characteristics of EPS geofoam is not considered in the design of fills. Pre straining of EPS fills may result from operation of heavy machineries or trucks during construction. Such pre straining is shown to result in degradation of the initial elastic modulus, and hence higher magnitudes of deformation in subsequent loadings.

171

6. Hyperbolic relationship has been employed successfully for stress vs. strain representation of geofoams. The modified hyperbolic model proposed here considered the confining pressure effect and was able to predict the reduction in strength and modulus as a result of confinement increase. The three parameters-K, n and m were determined from triaxial tests performed at different confining pressures. The model results agree well with test results and can be integrated into numerical modeling.

7. Stress-strain behavior of EPS geofoam remained relatively unaffected up to a temperature of 24 °C. Elevated temperatures reduced the initial modulus and creep deformations were higher.

8. Seasonal temperature variations resulted in seasonal cycles of deformations of relatively small magnitudes. Stresses induced in constrained EPS geofoam due to changes in temperature were also small and can be neglected in practice due to inherent relaxation properties of EPS geofoam.

Studies done here to investigate the effects of confinement and temperature on behavior of EPS geofoam were not exhaustive and the following are recommended for future studies

- Longer duration creep tests for developing creep models for analysis and design of EPS geofoam

- Effect of confinement on creep characteristics should also be investigated for very big samples to account sample size effects

- Effect of cyclic confining pressures of higher magnitudes on the deformation characteristics of EPS geofoam

- Effect of cyclic stress on EPS geofoam after long time creep

- Relaxation tests for longer duration and amount of stress

- Coupled confining stress and thermal tests with modeling

- Longer duration creep tests for developing creep models for analysis and design of EPS geofoam under confinement

- Coupled effects of induced anisotropy and confining pressure on the behavior of EPS geofoam

6. REFERENCES

Aabøe, R. (1993). "Deformation and stress conditions in fills of EPS." Norwegian Public Roads Adminstration, Oslo, Norway.

Abdelrahman, G. E., Kawabe, S., Tatsuoka, F., and Tsukamoto, Y. (2008). "Rate effects on the stress-strain behaviour of EPS geofoam." *Soils and Foundations*, 48(4), 479–494.

Anasthas, N. (2001). "Young's Modulus by Bending Test and Other Properties of EPS Geofoam Related to Geotechnical Applications." Master's Thesis, Syracuse University, Syracuse, New York,USA.

Anasthas, N., Negussey, D., and Srirajan, S. (2001). "Effect of confining stress on compressive strength of EPS geofoam." *Proceedings of 3rd International Conference of EPS Geofoam*, Salt Lake City, Utha, USA.

ASTM C578. (2011). "Specification for Rigid, Cellular Polystyrene Thermal Insulation." *ASTM International, West Conshohocken, PA, USA*.

ASTM D1621. (2010). "Test Method for Compressive Properties of Rigid Cellular Plastics." *ASTM International, West Conshohocken, PA, USA*.

ASTM D1622. (2008). "Test Method for Apparent Density of Rigid Cellular Plastics." *ASTM International, West Conshohocken, PA, USA*.

ASTM D6817. (2013). "Standard Specification for Rigid Cellular Polystyrene Geofoam." *ASTM International, West Conshohocken, PA, USA*.

Athanasopoulos, G. A., Nikolopoulou, C. P., Xenaki, V. C., and Stathopoulou, V. D. (2007). "Reducing the seismic earth pressure on retaining walls by EPS geofoam buffers - numerical parametric study." *Proceedings of the Geosynthetics Conference, January 16 - 19*, Industrial Fabrics Association International, St. Paul, Minn., Washington, DC.

Athanasopoulos, G. A., Pelekis, P. C., and Xenaki, V. C. (1999). "Dynamic properties of EPS geofoam: An experimental investigation." *Geosynthetics International*, 6(9), 171–194.

Atmatzidis, D. K., Missirlis, E. G., and Chrysikos, D. A. (2001). "An investigation of EPS geofoam behaviour in compression." Salt Lake City, Utha, USA.

BASF. (1993). "Styropor foam as a lightweight construction material for road base-courses." Styropor Technical Information, Ludwigshafen, Germany.

BASF. (1998). "Styropor technical information." Ludwigshafen, Germany.

Birhan, A., and Negussey, D. (2014). "Effects of confinement on the stress strain behavior of EPS geofoam." *International Conference on Geotechnical Engineering*, Shanghai, China.

Chun, B. S., Lim, H.-S., Sagong, M., and Kim, K. (2004). "Development of a hyperbolic constitutive model for expanded polystyrene (EPS) geofoam under triaxial compression tests." *Geotextiles and Geomembranes*, 22(4), 223–237.

Chun, B.-S., Lim, H.-S., and Shin, Y.-W. (2001). "Application of constitutive model to predict the behavior of EPS-geofoam." *KSCE Journal of Civil Engineering*, 5(2), 175–183.

Van Dorp, T. (1988). "Expanded polystyrene foam as light fill and foundation material in road structures." *International Congress on Expanded Polystyrene*, Milan, Italy.

Duncan, J. M. (1980). *Strength, stress-strain and bulk modulus parameters for finite element analyses of stresses and movements in soil masses*. College of Engineering, Office of Research Services, University of California, Berkeley, Calif.

Duncan, J. M., and Chang, C.-Y. (1970). "Nonlinear Analysis of Stress and Strain in Soils." *Journal of the Soil Mechanics and Foundations Division*, 96(5), 1629–1653.

Duškov, M. (1997a). "Measurements on a flexible pavement structure with an EPS geofoam sub-base." *Geotextiles and Geomembranes*, 15(1), 5–27.

Duškov, M. (1997b). "Materials research on EPS20 and EPS15 under representative conditions in pavement structures." *Geotextiles and Geomembranes*, 15(1–3), 147–181.

Elragi, A. F. (2000). "Selected engineering properties and applications of EPS geofoam." Ph.D., State University of New York College of Environmental Science and Forestry, New York, United States.

Elragi, A., Negussey, D., and Kyanka, G. (2001). "Sample size effects on the behavior of EPS geofoam." *Geotechnical special publication*, 280–291.

Eriksson, L., and Tränk, R. (1991). "Properties of expanded polystyrene - laboratory experiments." Swedish Geotechnical Institute, Linköping, Sweden.

Findley, W. N. (1960). "Mechanism and mechanics of creep of plastics." SPE Journal, 16 (1), 57 – 65.

Findley, W. N., and Khosla, G. (1956). "An equation for tension creep of three unfilled thermoplastics." SPE Journal, 12 (12), 20 – 25.

Flaate, K. (1987). "Super light material in heavy construction." *Geotechnical news (0823 - 650X)*, 22 – 23.

FLAC V.6. (2008). "Fast Lagrangian Analysis of Continua-V.6.0.387." Itasca Consulting Group, Inc.

Frydenlund, T. E., and Aabøe, R. (1996). "Expanded polystyrene - The light weight solution." *Proceedings of International Symposium on EPS construction method (EPS TOKYO '96)*, Tokyo, Japan, 32–46.

Frydenlund, T. E., and Aabøe, R. (2001). "Long term performance and durability of EPS as a light weight filling material." *EPS Geofoam 2001, 3rd International Conference,*, Salt Lake City, Utha, USA.

Gibson, L. J., and Ashby, M. F. (1999). *Cellular Solids: Structure and Properties*. Cambridge University Press.

Greeley, T. R. (1997). "A review of Expanded Polystyrene (EPS) properties, Performance and new Applications- Insulation materials: testing and applications." *Insulation Materials- Testing and Applications*, ASTM International.

Hazarika, H. (2001). "Mitigation of seismic hazard on retaining structures – A numerical experiment." *Proceedings of the 11th International Offshore and Polar Engineering Conference*, Kyushu Sangyo University, Fukuoka, Japan, 459–464.

Hazarika, H. (2006). "Stress–strain modeling of EPS geofoam for large-strain applications." *Geotextiles and Geomembranes*, 24(2), 79–90.

Hillmann, R. (1996). "Research projects on EPS in Germany. Material behaviour and full scale model studies." *Proceedings of International Symposium on EPS construction method (EPS TOKYO '96)*.

Horvath, J. S. (1992). "New developments in geosynthetics; 'Lite' Products Come of Age", Standardization News." *ASTM*, 20(9), 50–53.

Horvath, J. S. (1994). "Expanded polystyrene (EPS) geofoam: an introduction to material behavior." *Geotextiles and Geomembranes*, 13(4), 263–280.

Horvath, J. S. (1995). "Geofoam Geosynthetic: a Monograph." Scarsdale, NY , USA.

Horvath, J. S. (1997). "The compressible inclusion function of EPS geofoam." *Geotextiles and Geomembranes*, 15(1), 77–120.

Horvath, J. S. (1998). "Mathematical modeling of the stress-strain-time behavior of geosynthetics using the Findley equation: General theory and application to EPS-Block geofoam." *New York: Civil Engineering Department*, 35.

IBC. (2006). "International Building Code-IBC."

Ishihara, K., Kurihara, T., Tatsumi, O., Mae, Y., and Abe, M. (1996). "Application of EPS construction method to a level joint on abutment." *Proceedings of International Symposium on EPS construction method (EPS TOKYO '96)*.

Koerner, R. M. (2005). *Designing with geosynthetics*. Pearson Prentice Hall, Upper Saddle River, NJ.

Kondner, R. L., and Zelasko, J. S. (1963). "Void ratio effects on the hyperbolic stress-strain response of a sand." *Laboratory Shear Testing of Soils, ASTM*, STP 361, Ottawa.

Kutara, K., Aoyama, N., Takeuchi, T., and Takechi, O. (1989). "Experiments on application of expanded polystyrene to light fill materials." *Journal of the Soil Mechanics and Foundation Division, ASCE*, 37(2), 49–54.

Leo, C. J., Kumruzzaman, M., Wong, H., and Yin, J. H. (2008). "Behavior of EPS geofoam in true triaxial compression tests." *Geotextiles and Geomembranes*, 26(2), 175–180.

Leo, C. J., Wong, H. K., and Liyanapathirana, S. (2010). "A Simple Updated Constitutive Model of EPS Geofoam." 288.

LST, EN. 826. (1998). "Thermal insulating products for building applications–Determination of compression behaviour."

Magnan, J. P., and Serratrice, J. F. (1989). "ropriétés mécaniques du polystyréne expansé pour ses applications en remblai routier ." *Bulletin Liaison Laboratoire Ponts et Chaussées (164)*, 25 – 31.

Matsuda, T., Ugai, K., and Gose, S. (1996). "Application of EPS to backfill of abutment for earth pressure reduction and impact absorption." *Proceedings of International Symposium on EPS construction method (EPS TOKYO '96)*.

Miki, G. (1996). "Ten year history of EPS method in Japan and its future challenges." *Proceedings of International Symposium on EPS construction method (EPS TOKYO '96)*, Tokyo, Japan.

Momoi, T., and Kokusyo, T. (1996). "Evaluation of Bearing Properties of EPS subgrade." *Proceedings of International Symposium on EPS construction method (EPS TOKYO '96)*, Tokyo, Japan, 94–100.

Monahan, D. J. (1993). "Weight-credit foundation construction using artificial fills (with discussion and closure)." *Transportation Research Record*, (1422).

Murphy, G. P. (1997). "The influence of geofoam creep on the performance of a compressible inclusion." *Geotextiles and geomembranes*, 15(1), 121–131.

NAHB. (2004). "Revised builder's guide to frost protected shallow foundations." National Association of Home Builders (NAHB) Research Center.

NCHRP Web Document 65. (2004). "Geofoam Applications in the Design and Construction of Highway Embankments."

Negussey, D. (1997). *Properties and applications of geofoam*. Society of the Plastics Industry, Inc., Washington, DC.

Negussey, D. (2007). "Design parameters for EPS geofoam." *Soils and Foundations*, 47(1), 161–170.

Negussey, D., Anasthas, N., and Srirajan, S. (2001). "Interface friction properties of EPS geofoam." *Proc.EPS Geofoam 2001: 3Rd International Conference*, Salt Lake City, Utha, USA.

Negussey, D., and Jahanandish, M. (1993). "Comparison of some engineering properties of expanded polystyrene with those of soils (with discussion and closure)." *Transportation Research Record*, (1418).

Negussey, D., and Srirajan, S. (2001). "Slope stabilization using EPS geofoam." *Proceedings of EPS Geofoam 3rd International Conference*, Salt Lake City, Utha, USA.

Negussey, D., and Stuedlein, A. W. (2003). "Geofoam fill performance monitoring." *Utah Dept. of Transportation, Rep. No. UT*, 3.

Negussey, D., and Sun, M. C. (1996). "Reducing lateral pressure by geofoam (EPS) substitution." *Proceedings of International Symposium on EPS construction method (EPS TOKYO '96)*, Tokyo, Japan, 202–11.

Nishi, T., Hotta, H., Kuroda, S., and Hasegawa, H. (1996). "Feedback to design based on results of field observations of EPS embankments." *Proceedings of International Symposium on EPS construction method (EPS TOKYO '96)*.

NRRL. (1992). "Expanded polystyrene used in road embankments: Design, Construction and Quality Assurance. Form 482E." Norwegian Road Research Laboratory, Oslo, Norway.

Ooe, Y., Matsuda, Y., Tada, S., and Nishikawa, J. (1996). "Earth pressure reduction for culverts using EPS." *Proceedings of International Symposium on EPS construction method (EPS TOKYO '96)*.

Padade, A. H., and Mandal, J. N. (2012). "Behavior of expanded polystyrene (EPS) geofoam under triaxial loading conditions." *Electronic Journal of Geotechnical Engineering*, 17 S, 2542–2553.

Partos, A. M., and Kazaniwsky, P. M. (1987). "Geoboard reduces lateral earth pressures." *Proceedings of geosynthetics*, 628–39.

Pelekis, P. C., Xenaki, V. C., and Athanasopoulos, G. A. (2000). "Use of EPS geofoam for seismic isolation of earth retaining structures: results of an FEM study." *Proceedings of the 2nd European Geosynthetics Conference*, Bologna, Italy.

Preber, T., Bang, S., Chung, Y., and Cho, Y. (1994). "Behavior of expanded polystyrene blocks." *Transportation Research Record*, (1462).

Sanders, R. L. (1996). "United Kingdom design and construction experience with EPS." *Proceedings of International Symposium on EPS construction method (EPS TOKYO '96)*, Tokyo, Japan, 236–46.

Sanders, RL, Seedhouse, and RL. (1994). "The use of polystyrene for embankment construction." *The use of polystyrene for embankment construction*, 1(1), 1–55.

Sheeley, M. (2000). "Slope Stabilization utilizing geofoam." Master's Thesis, Syracuse University, Syracuse, New York,USA.

Sheeley, M., and Negussey, D. (2001). "An investigation of geofoam interface strength behavior." *Soft Ground Technology*, American Society of Civil Engineers, 292–303.

Srirajan, S., Negussey, D., and Anasthas, N. (2001). "Creep behavior of EPS geofoam." *Proceedings of EPS Geofoam 3rd International Conference*, Salt Lake City, Utha, USA.

Stewart, S., Hugh S., L., and Charles C., L. (1994). "Settlement of large mat on deep compressible soil." *Proceedings of the Conference on Vertical and Horizontal Deformations of Foundations and Embankments*, V-1, n-40, ASCE, 842 – 859.

Sun, M. C. (1997). "Engineering behavior of expanded polystyrene geofoam and lateral pressure reduction in substructures." Master's Thesis, Syracuse University, Syracuse, New York,USA.

Suzuki, Y., Nishimura, A., and Kuno, T. (1996). "Design and construction of road embankment on steep hill isde by EPS." *Proceedings of International Symposium on EPS construction method (EPS TOKYO '96)*.

Takahara, T., and Miura, K. (1998). "Mechanical Characterstics of EPS block fill and its simulation by DEM and FEM." *Soils and Foundations*, 38(1).

Trandafir, A. C., Bartlett, S. F., and Lingwall, B. N. (2010). "Behavior of EPS geofoam in stress-controlled cyclic uniaxial tests." *Geotextiles and Geomembranes*, 28(6), 514–524.

Trautwein. (2004). "True Path-Automated stress path system for triaxial testing." Trautwein Soil Testing Equipment Co.

Upright, W. (1989). "Fighting frost heave with polystyrene insulation." *Public Works*, 120(8), 81–82.

Vaslestad, J., Johansen, T. H., and Holm, W. (1993). "Load reduction on rigid culverts beneath high fills: Long term behavior." *Transportation Research Record*, (1415).

Wong, H. K., and Leo, C. J. (2007). "A constitutive model for EPS geofoam–experimental investigation and theoretical development." 533.

Wong, H., and Leo, C. J. (2006). "A simple elastoplastic hardening constitutive model for EPS geofoam." *Geotextiles and Geomembranes*, 24(5), 299–310.

Yamanaka, O., Onuki, T., Katsurada, H., Kitada, I., Kashima, K., Takamoto, A., and Maruoka, M. (1996). "Use of vertical wall type EPS elevated filling (H=15m) for bridge abutment backfill." *Proceedings of International Symposium on EPS construction method (EPS TOKYO '96)*, Tokyo, Japan, 224–33.

Yeh, S.-T., and Gilmore, J. B. (1992). "Application of EPS for slide correction." ASCE, 1444–1456.

Yeo, S.-S., and Hsuan, Y. G. (2009). "Effects of temperature and stress on the short- and long-term compressive behavior of expanded polystyrene." *Geosynthetics International*, 16(5), 374–383.

Zarnani, S., and Bathurst, R. J. (2007). "Experimental investigation of EPS geofoam seismic buffers using shaking table tests." *Geosynthetics International*, 14(3), 165–177.

Zarnani, S., and Bathurst, R. J. (2009). "Numerical parametric study of expanded polystyrene (EPS) geofoam seismic buffers." *Canadian Geotechnical Journal*, 46(3), 318–338.

Zou, Y., and Leo, C. J. (1998). "Laboratory studies on the engineering properties of expanded polystyrene (EPS) material for geotechnical applications." *Proceedings of the 2nd International Conference on Ground Improvement Techniques*, 7–9.

Zou, Y., and Leo, C. J. (2001). "Compressive Behaviour of EPS Geofoam at Elevated Temperatures." School of Engineering and Industrial Design, University of Western Sydney.

Vita

Name: Amsalu Gashaye Birhan

Place of Birth: Gojjam, Ethiopia

Education:

Name and Location	Dates	Degree
Addis Ababa University, Addis Ababa, Ethiopia,	2003-2005	M.Sc. (Geotechnical Eng'g)
Addis Ababa University, Addis Ababa, Ethiopia,	1996-2000	B.Sc. (Civil Engineering)

Employment:

Name and Location	Dates	Job Title
Syracuse University, Syracuse, NY	2009-2014	Teaching Assistant
Addis Ababa University, Addis Ababa, Ethiopia	2007-2009	Lecturer
Bahir Dar University, Bahir Dar, Ethiopia	2000-2007	Lecturer